DIGITAL DEPOSITION OF ULTRATHIN Pd FILMS ON WELL-DEFINED Pt(111)

ELECTRODES VIA SURFACE-LIMITED REDOX REPLACEMENT REACTION:

AN ELECTRON SPECTROSCOPY-ELECTROCHEMISTRY STUDY

A Dissertation

by

MOHAMMAD AKHTAR HOSSAIN

Submitted to the Office of Graduate Studies of
Texas A&M University
in partial fulfillment of the requirements for the degree of

DOCTOR OF PHILOSOPHY

December 2010

Major Subject: Chemistry

Digital Deposition of Ultrathin Pd Films on Well-Defined Pt(111)

Electrodes via Surface-Limited Redox Replacement Reaction:

An Electron Spectroscopy-Electrochemistry Study

DIGITAL DEPOSITION OF ULTRATHIN Pd FILMS ON WELL-DEFINED Pt(111)

ELECTRODES VIA SURFACE-LIMITED REDOX REPLACEMENT REACTION:

AN ELECTRON SPECTROSCOPY-ELECTROCHEMISTRY STUDY

A Dissertation

by

MOHAMMAD AKHTAR HOSSAIN

Submitted to the Office of Graduate Studies of
Texas A&M University
in partial fulfillment of the requirements for the degree of

DOCTOR OF PHILOSOPHY

Approved by:

Chair of Committee,	Manuel P. Soriaga
Committee Members,	Gyula Vigh
	Lawrence S. Brown
	Bing Guo
Head of Department,	David H. Russell

December 2010

Major Subject: Chemistry

ABSTRACT

Digital Deposition of Ultrathin Pd Films on Well-Defined Pt(111)

Electrodes via Surface-Limited Redox Replacement Reaction:

An Electron Spectroscopy-Electrochemistry Study. (December 2010)

Mohammad Akhtar Hossain, B.S., M.S.; University of Dhaka

M.S., Lamar University

Chair of Advisory Committee: Dr. Manuel P. Soriaga

In this study, ultrathin (submonolayer to eight-monolayer) Pd films were deposited one layer at a time on well-defined Pt(111) surfaces via a process known as surface-limited redox replacement reaction (SLR^3). In this digital-deposition method, one monolayer of a nonnoble metal (Cu) is deposited on a noble metal (Pt) by underpotential deposition (UPD). When the UPD adlayer is exposed to cations of less reactive metals (Pd^{2+}), it is oxidatively stripped and reductively displaced by the more inert metal. The positive difference between the equilibrium potential of the noble metal in contact with its solvated cations and the equilibrium potential of the UPD adlayer is the driving force behind SLR^3. The Pd films were characterized by Auger electron spectroscopy (AES), low-energy electron diffraction (LEED), and electrochemistry. The LEED patterns indicated (1×1) surface structure of the deposited films. No residual Cu was detected by AES in the Pd films. The Pd ultrathin films on Pt(111) showed H_{UPD} adsorption/desorption peaks which are not observed in bulk Pd. These peaks were

observed even at 8 monolayer thick films. The interfacial structure and electrochemical properties of SLR^3-prepared films were compared with those prepared by controlled-potential deposition (CPD). There is a linear correlation between Cu deposition charge (i.e., Pd deposition charge) and I-catalyzed Pd dissolution charge. Electrochemical and LEED results suggest that SLR^3 prepared films are smooth (if not slightly smoother) compared to those prepared by CPD. SLR^3 thus appears to be capable of preparing atomically smooth ultrathin films on Pt(111) surfaces without any additional thermal or electrochemical annealing.

DEDICATION

To the loving memory of my father Mohammad Mosharof Hossain

ACKNOWLEDGMENTS

My graduate studies at Texas A&M University have been very exciting and rewarding. It helped me grow both as a person and as a scientist. During the course of this journey, I met a number of excellent persons who inspired and helped me achieve my dreams.

First and foremost, my heartiest thanks and gratitude go to Dr. Manuel P. Soriaga, my advisor and chair of committee, for his constant enthusiasm, guidance, and encouragement throughout my graduate career. I learned so much from him, both in and out of the laboratory, about science, and life in general. His unparallel dedication to science has been a source of inspiration.

I would like to thank my committee members, Dr. Gyula Vigh, Dr. Lawrence S. Brown, Dr. Bing Guo, and Dr. Dong Hee Son for all the instructive comments and advice provided throughout the course of my graduate studies.

I would also like to thank my former committee members, Dr. Marvin W. Rowe and Dr. Donald G. Naugle for their encouragement and advice over the years.

I would like to thank Dr. Marian Hyman for her constructive suggestions. I am highly indebted to her for allowing me to use a few instruments while ours were being repaired.

I would like to acknowledge and thank the former and current members of Dr. Soriaga's research group. Special thanks and regards are due to Dr. Yeon Su Park and Dr. Jack H. Baricuatro for their encouragement and mentoring during the early part of

my graduate career. I would like to thank Dr. Xiaole Chen and Dr. Jean Sanabria for their help and inspiration.

I am highly indebted to Dr. Ding Li, Juan Cruz Jr., Kyle Cummins, and Alnald Javier, for their help on many occasions to carry out repair and maintenance procedures of the UHV systems. Their kindness and generosity went far beyond the call of duty. A special thanks to Kyle for his assistance in conducting the experiments. I am thankful to Raj Karr, Miguel Cruz-Quiñons, Laura Granda Marulanda, James Cantu, Stephen Fordham, and Joshua Fonzy who aided in this project in many ways.

I would like to thank the support personnel in the Electronics Shop, Glass Shop, and Machine Shop in the Department of Chemistry for their help and assistance with troubleshooting and repair of various instruments. I would also like to thank the personnel in the Physics Electronics Shop for their service.

The financial assistance from the Department of Chemistry during my graduate studies is gratefully acknowledged. This research was financially supported by the Welch Foundation.

I would like to thank all my family members, specially my mother, sister, brother, brother-in-law, sister-in-law, nephew and niece for their unending love, patience, and inspiration. Without their sacrifice and understanding my journey through graduate school would not have been possible.

Finally, I would like to thank all my friends and colleagues and the department faculty and staff for making my stay at Texas A&M University a truly rich and remarkable experience.

ACRONYMS

AES	Auger Electron Spectroscopy
CPD	Controlled-Potential Deposition
CV	Cyclic Voltammetry/Voltammogram
EC	Electrochemistry
LEED	Low-Energy Electron Spectroscopy
ORR	Oxygen Reduction Reaction
PZC	Potential of Zero Charge
PZFC	Potential of Zero Free Charge
PZTC	Potential of Zero Total Charge
SEM	Scanning Electron Microscopy
SLR^3	Surface-Limited Redox Replacement Reaction
STM	Scanning Tunneling Microscopy
TPD	Temperature Programmed Desorption
UHV	Ultra-High Vacuum
UPD	Underpotential Deposition
XPS	X-Ray Photoelectron Spectroscopy

TABLE OF CONTENTS

LIST OF FIGURES

LIST OF TABLES

1. INTRODUCTION

There is a continuing scientific and technological interest in precious or noble metals due to their unique physical and chemical properties [1-6]. They show outstanding resistance to corrosion, optimal catalytic activity, and high catalytic selectivity [3,6-10]. Noble metals are used in a wide variety of applications, such as industrial catalysis, electrocatalysis, batteries, corrosion protection, and in electronics industry [2,11]. As electrocatalysts, noble metals have been utilized in a variety of ways, such as bulk electrodes, thin films, bimetallic systems, nano-structures [12], and supported nano-clusters or particles.

Historically, most of the electrochemical studies on noble metals have been carried out with polycrystalline electrodes. The characterization of such electrodes is, however, difficult due to the presence of a variety of small domains with different crystal facets and edges that are exposed to the electrolyte [13]. The different crystalline facets show different properties (e.g., potential of zero charge [13] or work function [14-18]) and reactivity [19-23]. Consequently, the electrochemical behavior observed at polycrystalline electrodes corresponds to an average or mixture of that for the crystal planes and sites   present [13]. On the other hand, well-defined or single crystal surfaces are more reproducible compared to polycrystalline, alloy, or co-deposited

_____

This dissertation follows the style of the Journal of Electroanalytical Chemistry.

systems [24]. The motivation to gain an atomic and molecular level understanding of the processes that take place at solid-liquid interface has led to a plethora of studies with single-crystal electrodes having clean and well-ordered surfaces [13,25-27].

1.1 Ultrathin noble metal films on well-defined surfaces

Ultrathin transition and noble metal films on single crystals have attained considerable interest for more than a few decades due to their exceptional catalytic, electrocatalytic, electronic, and magnetic properties [28-31]. Thin films that have thicknesses varying from one atomic layer up to ten monolayers are generally referred to as ultrathin films [30]. Among these thin films, the *noble metals* deposited on *noble-metal* substrates are of fundamental interest because the resulting bimetallic systems blend the electrocatalytic properties of the individual metals concerned. A few key concepts have been suggested [32] to account for the higher activity of bimetallic catalysts: (a) each individual component in a bimetallic system may promote different elementary reaction steps (theory of "bi-functional mechanism" [33]), (b) electronic effects resulting from the interaction of the two metals involved [34], and (c) specific arrangements of surface atoms which act as active sites [35]. Since the deposition of noble metals onto noble metals is irreversible, they are stable in solution in a wide range of potentials in terms of both surface composition and adlayer ordering [36]. As a result, ultrathin noble metal films shows exceptional chemical properties that are not displayed by their bulk counterparts [28,30,37,38]. For instance, the bulk gold surfaces are inert

towards dissociative adsorption of hydrogen due to a high-energy activation barrier [39]. Epitaxially grown ultrathin films of Au on Ir [40] surfaces, however, show dissociative adsorption of hydrogen, which has been confirmed by temperature programmed desorption (TPD) and nuclear reaction analysis (NRA) [37,38]. The chemical reactivity of the supported noble metal films has been suggested to depend on the electronic and geometric structures of the surface (such as lattice constant, crystallographic orientation, and morphologies) [37]. It has been shown that the d-band center of a metal surface plays a significant role in its chemical reactivity. The d-band center can be defined as the weighted average of the projections of the total metal density of states onto d-orbitals centered on each atom in the respective surface layers [41]. According to Hammer and Nórskov [39,42], as the d-band moves downward away from the Fermi level (E_F), the energy of the highest occupied electronic state at 0 K, the surface tends to be less active. It has been found that the center of the filled d-band for bulk Au lies far below the E_F in such as way that the antibonding state formed between the σ_g state of H_2 and the d states of Au is placed below E_F in the transition state. Therefore, the activation barrier for hydrogen dissociation on ultrathin Au films deposited on Ir surface would be higher and would not cause the dissociation of hydrogen molecules. The experimental results, on the other hand, clearly indicated dissociative chemisorption of hydrogen on pseudomorphic monolayer of Au on Ir{111} surfaces [37]. This deviation from the expected behavior projected by the theory [39,42] has been suggested to have resulted due to local surface features (e.g., defects, steps or kinks, or those emanating from strain effects), rather than an extended nature of the surface electron.

As a second example, the dissociation of methane takes place on surfaces of either Ni or Ru, the later being the more active of the two [31]. When a pseudomorphic layer of Ni is grown on Ru, however, the reactivity of the ultrathin overlayer surpasses that of any of the individual components. The lattice constant of Ru is larger than that of Ni. Because of the lattice mismatch, the pseudomorphic Ni films on Ru are expected to be under strains. Ruban and coworkers [43] have demonstrated that when a small metal atom is placed into the lattice of a larger one, either as an impurity or overlayer, the neighbors are farther apart and the d-band width at the atom becomes smaller than at the surface of the elemental atom. This in turn causes an upward shift of the d-band center in order to preserve the same d-band filling locally. As a result, Ni overlayer on Ru is more active than pure nickel. This finding is in agreement with the prediction made by density functional theory (DFT) calculations [42]. Similar catalytic enhancement has also been reported for the dissociation of methane on Co overlayer deposited on Cu although Cu is unreactive towards the dissociation reaction at temperatures below 600 K [31].

In addition to gas phase reactions, noble metal ultrathin films have been utilized as electrocatalysts for a number of reactions, such as oxygen reduction reaction (ORR) [44-46], hydrogen oxidation [44,47], carbon monoxide electrooxidation [48,49], methanol oxidation [50], and ethanol electrooxidation [51,52].

 It has been found that noble metal (such as Pt and Pd) monolayer deposited on to a second noble metal surface (such as Pd(111), Ir(111), Ru(0001), and Au(111)) shows enhanced electrocatalytic activity towards ORR. For instance, when a monolayer of Pt is deposited on carbon-supported Pd nanoparticles it shows 5 to 8 times higher Pt mass-

specific activity [53,54] than that of a commercial carbon-supported Pt electrocatalyst [45]. In addition, Pt monolayer modified Pd(111) electrodes or Pd nanoparticles enhance the kinetics of ORR significantly compared to either Pt(111) surfaces or Pt nanoparticles.

Chrzanowski and Wieckowski [50] have studied the effect of the modification of low index Pt single crystals by controlled amounts of electrodeposited Ru on methanol oxidation. It has been reported that Pt(111) surfaces covered by 0.2 monolayer of Ru showed an order magnitude higher electrocatalytic activity towards methanol oxidation compared to commercial Pt/Ru catalysts [50].

Hazzazai and coworkers [51] have studied the electrooxidation of ethanol on Au/Pd{hkl} electrodes in alkaline media and found that submonolayer (0.5 – 0.6 ML) Au-covered electrodes displayed higher activity than that of Pt pure electrodes. In a differential electrochemical mass spectrometry (DEMS) investigation, Fujiwara et al. [52] observed a synergistic effect of Ru and Pt on the electrode surface for electrooxidation of ethanol. The optimum composition of the bi-metallic electrodes was found to vary between $Pt_{0.67}Ru_{0.33}$ (at 5 °C) and $Pt_{0.85}Ru_{0.15}$ (at temperatures 25 – 40 °C) to ensure the total oxidation of ethanol [52].

The aforementioned studies clearly demonstrate the catalytic and electrocatalytic applications of noble metal ultrathin films. It a nutshell, it may not be an overstatement that noble metals are indeed the driving force behind the industrial production of commodities that supports our modern life style. Nonetheless, the supply of noble metals, such as Pt and Ru, is limited. In order to increase efficiency and long-term

stability while reducing costs, the quest continues for new materials that may be alternative to current Pt-based catalysts and electrocatalysts. In this effort, there have been many studies to delineate the unique and elegant properties of the ultrathin noble metal adlayers, including Pd films, supported on noble metal substrates [28,29,37,38,55-58].

1.2 Pd films on platinum

Pd films on noble metal surfaces have drawn a lot of attention due to their unique properties [28,59-62] and catalytic activities for a number of reactions, such as oxidation of small molecules (methanol, formic acid, carbon monoxide, etc.) and ORR [46,63]. Pd ultrathin films on various noble metals such as Pt [21,40,64,65], Au [61,63,66-70], Ir, Ru, and Rh have been investigated [46,60]. Among these bimetallic systems, the Pd-Pt pair shows distinctive properties. For example, they have identical lattice parameters, similar atomic radii, comparable lattice energy but different cohesive energy [71]. Moreover, Pd has lower surface energy than that of Pt. Consequently, favorable deposition of Pd on Pt with minimal lattice strain is expected [72]. Therefore, this system has been extensively studied [40,55,64,73-88] due to prospects of catalysis enhancement [75].

Early studies of Pd films on Pt surfaces were aimed to investigate the influence of the underlying polycrystalline substrate on the electrosorption properties of the Pd thin films [89]. In a seminal work, Attard and Bannister [90] studied the electrochemical

properties of spontaneously deposited Pd films on Pt(111) electrodes. The voltammetric features of the Pt surface modified by irreversibly adsorbed submonolayer and monolayer Pd showed reversible hydrogen adsorption/desorption peaks which were not observed for bulk Pd electrodes. Following this discovery, Clavilier and coworkers [65] observed a second hydrogen adsorption peak at a slightly more positive potential than that of the first one. Since then, Pd films have been deposited on various Pt single crystal substrates such as Pt(111) [21,65,74,90], Pt(100) [21,91,92], Pt(110) [21,92], and Pt(001) [81]. Among them, Pd films on Pt(111) [36,40,55,64,75,77,78,80,93-97] have been widely studied as a model system to investigate well-defined adlayers.

One of the major advantages of Pd ultrathin films is that they do not suffer from the limitation of perturbations due to hydrogen absorption which is known to interfere with the characterization of bulk Pd electrodes [97-102]. It has been reported that the hydrogen absorption on Pd ultrathin films are kinetically hindered [63,97]. Secondly, Pd ultrathin films show superior electrocatalytic activity compared to bulk Pd. For example, Baldauf and Kolb [103] have found that when a 2-3 monolayer (ML) pseudomorphic Pd films on Pt(*hkl*) show much higher electrocatalytic activity towards formic acid oxidation as compared to those grown on Au(*hkl*) or even for bulk Pd(*hkl*) electrodes. These Pd films also showed high tolerance against poisoning by CO adsorption [103].

A key thermodynamic parameter in the characterization of an electrochemical interface is the potential of zero charge (PZC) which can be defined as the potential at which the surface charge is zero [36]. Frumkin and Petrii [104] have further distinguished PZCs as potential of zero total charge (PZTC) and potential of zero free

charge (PZFC). PZTC is available thermodynamically parameter whereas PZFC is the relevant magnitude for microscopic models, equivalent to PZC determined for mercury and coinage metals (Au, Ag, Cu) [105]. Both of these are structure sensitive properties. PZFC of a metal in contact with the electrolyte is related to the work function of the metal in vacuum and affects all aspects of electrocatalysis and electron transfer [59]. It has been reported that there is a 90 mV shift of PZFC for a pseudomorphic Pd monolayer on Pt(111) as compared to bulk Pd(111) electrodes [59]. This dramatic change in PZFC may have been brought about by the alteration of the electronic properties of the Pd adlayers by platinum substrate [59].

The structure and interfacial properties of ultrathin Pd films (up to 4 ML) on Pt(111) has been studied by electron spectroscopy and electrochemistry [106]. The Pd coverage was determined by I_{ads}-catalyzed dissolution of the Pd films. At coverages ≤ 2 ML, the I adlayer displayed either a Pt(111)-(l×l)Pd-(3×3)-I or a mixed (3×3) and ($\sqrt{3}×\sqrt{3}$) LEED patterns. At Pd coverages > 2 ML, the LEED pattern indicated Pt(111)-(l×l)Pd-($\sqrt{3}×\sqrt{3}$)-I structure for the chemisorbed iodine layer, which is identical for I-coated bulk Pd(111). This is an indication of thin film-to-bulk transition if chemisorbed iodine is used as a surface-sensitive probe. It was found that Br_{ads}-catalyzed dissolution led to digital etching (i.e., dissolution of one layer at a time) of the Pd films electrodeposited on Pt(111) surfaces while bulk Br^- caused complete dissolution in a single step. In case of Br_{ads}-catalyzed dissolution of Pd in bromide free solution, Br gets desorbed with the oxidation of Pd to $Pd^{2+}_{(aq)}$. In the presence of bulk Br^-, however, Pd

dissolution proceeds unabated due to the formation of $PdBr_4^{2-}_{(aq)}$, which is a water-soluble complex.

Arenz et al. [107] have studied the adsorption and kinetics of CO on well-characterized Pd films on Pt(111) in alkaline solution by Fourier transform infrared spectroscopy (FTIR). No coupling between $Pt-CO_{ad}$ and $Pd-CO_{ad}$ molecules was observed for Pt(111)-xPd electrodes as shown by FTIR spectra. This indicates that CO catalysis on Pt and Pd surface sites occurs independently. In other words, the Pt(111)-xPd electrode does not behave like a pseudo metal electrode. On the other hand, Pd monolayer modified Pt(111) displayed CO absorption peak which was characteristic of CO molecules adsorbed on the bridge sites on Pd surfaces. The oxidation of CO on Pd modified Pt(111) surface was considerably slower as compared to Pt(111). It has been reported that the CO oxidation is dependent upon the coverage as well as the strength of the OH adsorption on the metal surface. The hydroxyl group is strongly adsorbed on the highly oxophilic Pd atoms and thus might be responsible for the slower CO oxidation kinetics. The same research group also studied the effect of specific adsorption of anions such as chloride, a trace impurity in perchloric acid, on the electrochemical behavior of ultrathin Pd films on Pt(111) [108]. The adsorbed chloride anions have been found to interact strongly with Pd and compete with the underpotential deposition of hydrogen (H_{UPD}) and hydroxyl adsorption (OH_{ad}).

Hoyer, Kibler and Kolb [95] investigated the Pd electrodeposition on Pt(111) by cyclic voltammetry and *in situ* scanning tunneling microscopy (STM). $PdCl_2$ and $PdSO_4$ were used as precursors for Pd deposition. The starting point for both cases is the

formation of pseudomorphic Pd monolayer. The Pd deposition has been found to be influenced by the anions present. In the chloride containing solution, a Pd monolayer is formed at underpotential. On the other hand, the Pd deposition is kinetically hindered in chloride-free solution to such an extent that the deposition peak is shifted negative of the equilibrium potential. A layer-by-layer growth is observed for Pd bulk deposition in chloride containing solution. When Pd is deposited from chloride free solution, however, the film growth continues in 3D fashion after the first monolayer. For the former films, voltammetric peaks associated with H_{UPD} are observed up to four monolayers whereas for the later they are observed even for films equivalent of ten monolayers.

Recently, Duncan and Lasia [97] have studied the electrochemical behavior of Pd films on Pt(111) having coverage from 1 to 20 ML by cyclic voltammetry and impedance spectroscopy. They have observed that the hydrogen adsorption/desorption on Pd deposits on Pt(111) is more reversible as compared to those on Au(111). The thermodynamics and kinetics of hydrogen adsorption are strongly influenced by the metal support at all Pd coverages under study. It was observed that the charge transfer resistance of 1 ML Pd was smaller than that of the thicker films (2 − 20 ML) supported on Pt(111), which is contrary to the observation made on Pd films deposited on Au(111). This may imply that the hydrogen adsorption on monolayer Pd is much faster compared to thicker films supported on Pt(111).

1.3 Electrodeposition of ultrathin films

In order to tailor the properties of a metal surface, foreign adatoms or molecules are deposited onto the surface either in a ultra-high vacuum (UHV) system (by molecular beam epitaxy (MBE), physical or chemical vapor deposition) or in an electrochemical environment (either by electroless or spontaneous deposition, or by electrodeposition) [24,109]. Evaporative methodologies (thermal or vacuum) usually involve the following steps [110]: (a) generation of vapor by boiling or subliming a source material, (b) the transfer of vapor from the source to the sample substrate, and (c) the condensation of vapor to a solid film on the substrate. The deposition methodologies involving UHV are deceptively simple in principle. The implementation, however, requires a great deal of knowledge and expertise of a wide variety of fields, such as vacuum technology, materials science, and electrical and mechanical engineering. In addition, thorough understanding of elements of thermodynamics, kinetic theory of gases, surface mobility, and condensation phenomena are needed. A few practical issues to be considered are: (a) source-container interaction, (b) high cost of UHV system installation and maintenance, (c) precise control of the substrate movement, (d) geometric consideration, and (e) need for process monitoring and control. Another disadvantage of UHV based thin film deposition methodologies is that often time the deposited films are annealed at high temperatures which may lead to diffusion of the adatoms to the substrate subsurface or alloy formation [48]. The deposited films, however, are not annealed if alloy formation or surface segregation is to be prevented.

Therefore, the modification of surfaces by electrochemical means is highly attractive because of their simplicity, reliability, and low cost. Electrodeposition is of considerable interest not only in fundamental studies but also in many industrial applications such as in catalysis, corrosion prevention, electronics, and sensors [109]. Electrodeposition offers a great deal of flexibility to control the structure of the deposited adlayer by careful manipulation of several parameters, such as potential/current, electrolyte, metal ion concentration, nature of the additive or surfactant, and the structure of the substrate. By varying the applied deposition potential, a thermodynamically unfavorable deposition process can be turned into a thermodynamically favorable one with relative ease. There are, however, a few issues that complicate this simplistic approach. Sometimes, the noble metal deposition might be kinetically hindered even though it is thermodynamically favorable [24]. The presence of complexing agents or ligands, such as halides, in solution affects the thermodynamics and kinetics of the electrodeposition of the desired metal. The existence of any lattice mismatch between the admetal and the substrate and any possibility of a chemical reaction between the two warrant further deliberation. The quantification of the electrodeposited substance can be achieved readily by measuring the faradaic charge during electrodeposition. This type of calculation, however, could lead to errors if the efficiency of the faradaic process is less than 100%. In such cases, an alternative method (such as spectroscopic or gravimetric) needs to be employed. The electrodeposited metal films sometimes lack uniform coverage and smoothness when the admetal starts to nucleate at steps, kinks, or other defect sites [24].

1.4 Digital deposition via surface-limited redox replacement reactions

Thin film growth modes are usually divided into three types, such as Frank-van der Merwe or layer-by-layer (2D) growth, Volmer-Webber or 3D-cluster growth, and Stranski-Krastanov (SK) mode where a transition from 2D to 3D growth is observed [111,112]. A multilayer variant of Frank-van der Merwe mode is known as step-flow which takes place at an appropriate step density and deposition flux. In 2D growth mode (either monolayer or multilayer), the adlayer follows the substrate structure, i.e., epitaxial. These are depicted in Fig. 1. The growth of uniform epitaxial ultrathin and thin films is one of the main goals of electrochemistry due to their continuity and distinctive properties, such as reduced ohmic resistivity and electromigration [112]. Although the bulk electrodeposition is reasonably well-understood, the preparation and control of atomically flat ultrathin films still remain as a big challenge and may pose as a significant drawback to many industrial and technologically important fields, such as nano-structure synthesis, electrocatalysis, magnetic materials, and formation of ultra-large scale integrated circuits (ULSI), where uniform coverage is highly desired [113]. The aforementioned limitations that are commonly encountered in electrodeposition can, however, be circumvented by several ways: (a) electroless deposition (spontaneous or forced electrodeposition) or (b) by employing underpotential deposition (UPD) of a sacrificial nonnoble metal [24].
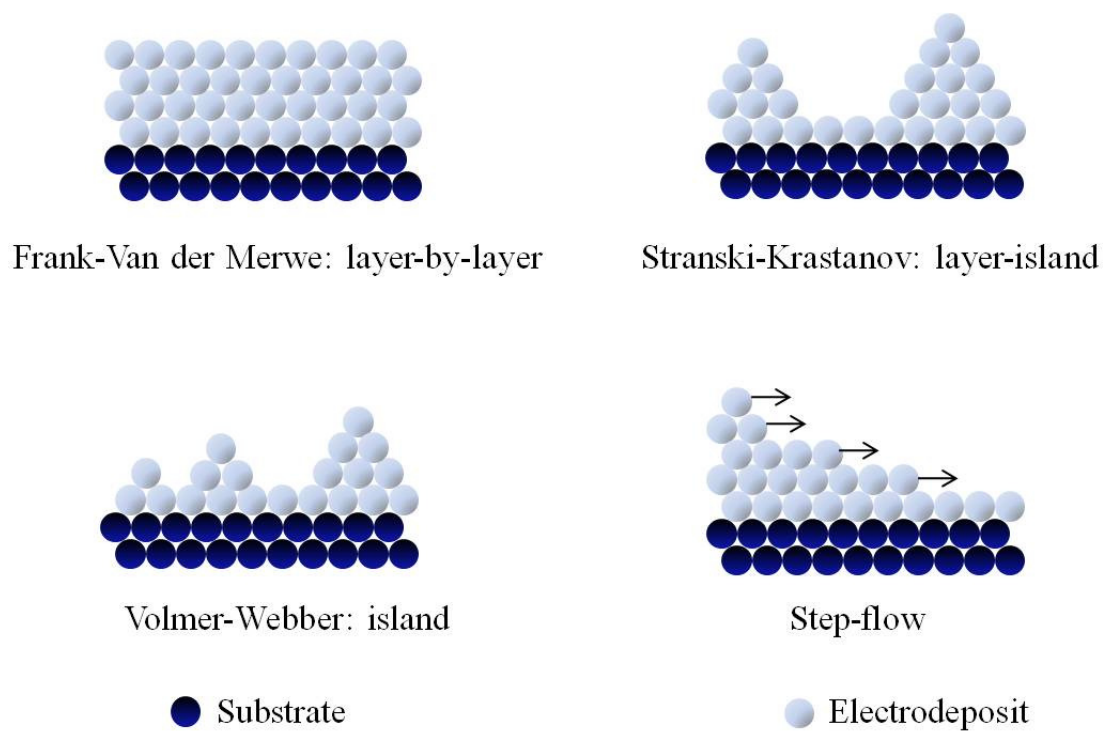
Frank-Van der Merwe: layer-by-layer

Stranski-Krastanov: layer-island

Volmer-Webber: island

Step-flow

● Substrate   ○ Electrodeposit

Fig. 1. A schematic illustration of thin-film growth modes.

UPD is a phenomenon where an atomic layer of one metal deposits onto another, at a potential positive of that required to deposit on itself [114]. It is observed when the bonding (or the affinity) of an adsorbate, A, to a substrate, S, is stronger than that of A to A [115]. Underpotential deposition has been extensively studied for more than 50 years [116-120]. UPD produces well-ordered atomic layers on well-ordered metal substrates. The monolayer deposition of metal ions in UPD, however, is greatly influenced by anion-specific adsorption [121].

It should be underscored that UPD is a common phenomenon that takes place in cathodic as well as anodic processes [122]. For instance, UPD of oxygen occurs at potential well-negative of the reversible potential of oxygen in anodic evolution [115,122,123].

UPD can be described by underpotential shift (ΔU_P), a concept first introduced by Kolb and coworkers [117,118]. The underpotential shift is defined as the difference in the UPD peak potential when a metal (e.g. Cu) is oxidatively stripped from a foreign metal (e.g., Pd) and the peak potential of electrodissolution of the atom (Cu) from its own bulk. This can be explained further by considering the thermodynamic conditions $\Delta G_I^{\circ} < 0$ and $|\Delta G_I^{\circ}| > |\Delta G_{II}^{\circ}|$ for the following processes [115]:

$$A + M \overset{\Delta G_I^{\circ}}{\Longleftrightarrow} M{-}A \tag{1}$$

$$A + A \overset{\Delta G_{II}^{\circ}}{\Longleftrightarrow} A{-}A \tag{2}$$

leading to a shift of the equilibrium potential E_{II}° (corresponding to eq. (2)) into higher values (corresponding to eq. (1)):

$$\Delta U_P = E_I^\circ - E_{II}^\circ \tag{3}$$

Strong correlations exist between the underpotential shift and the difference in the thermodynamic and physical quantities such as chemical potential, electronegativity [115], work function, and binding energy of the adsorbate metal and substrate [122]. Kolb and colleagues [117,118] observed a linear correlation between underpotential shift and the differences in work function in their studies of 20 metal pairs. Mathematically, it can be represented by the following equation:

$$\Delta U_P = 0.5\Delta\phi \tag{4}$$

Here, $\Delta\phi$ is the difference in work function of the metals involved. In a theoretical study, Trasatti [124] obtained the following relationship between underpotential shift and difference in work function assuming that the bonding character between substrate and adsorbate is completely ionic when the adsorbate coverage is approximated to zero:

$$\Delta U_P = \frac{1}{e}\Delta\phi \tag{5}$$

Later, the underpotential shift was redefined by Leiva [119] as the difference of the equilibrium potential of the adsorbate/substrate system, at a given adsorbate coverage, measured with respect to an electrode of the adsorbate bulk metal M, both in equilibrium with the same solution containing dissolved ions of the type M^{Z+}. The modified definition of underpotential shift has been denoted as $\Delta\phi_{upd}(\Theta)$ since it is dependent upon the coverage. Sanchez and Leiva also predicated a linear relationship between the underpotential shift and difference in binding energy between atoms in the pure adsorbate metal, A, and that energy between adsorbed atom of A and substrate, S [125].

Spontaneous deposition of Pd on Pt(111) produces only submonolayer films [90]. UPD of noble metals such as Au and Pt is not feasible due to their slow kinetics [113]. Examples of atomic level study on epitaxial growth of noble metals beyond monolayer thicknesses are rare. Attempts to form atomic layer epitaxy of noble metals leads to the formation of aggregates and clusters rather than epitaxial films due to high cohesive energy of the noble metals [113,126,127].

Sieradzki and coworkers have developed electrodeposition protocols known as defect-mediated growth (DMG) [128] and surfactant-mediated growth (SMG) [129], which showed very promising results to produce smooth and epitaxial growth of noble metal films. In DMG, the desired metal (e.g., Ag) is codeposited with a reversibly deposited mediator metal (such as Pb^{2+} or Cu^{2+}). By cycling of the appropriate electrochemical potentials, the mediator is periodically deposited and removed from the surface. Consequently, defects are produced on the surface and serve as nucleation sites for island growth. Each cycle produces new nuclei on the surface which is added to the existing islands left behind in previous cycles. Eventually, a monolayer is complete when the growing 2D islands merge together. On the other hand, SMG involves the predeposition of a submonolayer of a surfactant metal such as Pb^{2+}. The surfactant layer floats on the top of the depositing metal owing to fast interlayer diffusion and thus aids the 2D growth of the desired metal. By and large, the defects or surfactants either increase the nucleation density on the surface and/or decrease the edge barrier for the interlayer diffusion of adatoms, which favors the flat layer-by-layer growth [130]. These methods have been successfully used to produce metal deposits of considerable

thickness (up to 100 ML) [112,131]. Examples include Ag/Au(111) [128,129], Ag/Ag(111) [128], and Cu/Au(111) [131]. These protocols, however, suffer from a few limitations and inconveniences. Both of these techniques are tunable over a number of parameters such as metal ion concentrations, scan rate, potential excursion limits, and submonolayer coverage that are mutually dependent and thus are hard to balance. In addition, the control of thickness via measurements of charge is difficult due to interferences from side reactions and double-layer charging. The double-layer charging currents, particularly in DMG, are sometimes comparable to or even higher than the deposition current levels. Lastly, although very small, the possibility of incorporation of a mediator into the metal deposit cannot be ruled out completely [112].

Finally, Brankovic, Wang, and Adzic [132] introduced a novel method to carry out atomic layer deposition of *noble metal* films onto *noble metal* surfaces via a process called surface-limited redox replacement reaction (SLR[3]). This method is also referred to as galvanic displacement [45,133,134]. SLR[3] or galvanic displacement exploits the unique property of UPD to form uniform and well-defined adlayers for growing noble metal ultrathin films or adlayers. In this approach, a sacrificial less noble metal (e.g., Pb or Cu) is first deposited on a noble metal (such as Au) by UPD. Subsequently, ions of more noble metal (e.g., Pt^{4+} or Pd^{2+}) spontaneously oxidize the sacrificial adlayer and get themselves reduced and deposited on to the substrate at open circuit potential (OCP). The "building block" reaction cycle may be repeated multiple times to produce ultrathin films of desired thickness. The positive potential difference between the equilibrium potential of the noble metal in contact with its solvated ions and the equilibrium

potential of the sacrificial or mediator admetal is the driving force of the spontaneous deposition of noble metals in SLR^3 ([132] and references therein). One important criterion of the sacrificial or mediator adlayer is that it has to be reactive compared to the noble metal substrate [128,132]. A noteworthy feature of the SLR^3 method is that the metal deposition is a surface controlled reaction where the total amount of deposited metals is governed by the stoichiometry of the redox reaction. Hence, the reproducibility of the substrate morphology is ensured.

As an illustration of the capability and versatility of SLR^3, Brankovic and co-workers [132] deposited three different noble metals (Pt, Pd, and Ag) on Au(111) electrodes by using Cu$_{UPD}$ as the sacrificial template. Due to the difference in valencies of the metal cations involved, the removal of Cu adlayer by the noble metal ions resulted in submonolayer Pt, a monolayer Pd, and two monolayers of Ag. STM images revealed that the noble metal adlayers did not show any preferential deposition along the step edges of the Au(111) substrate [132].

In SLR^3, one atomic layer of a noble metal is deposited at a time. Hence, it may be termed as *digital deposition* which is the opposite of *digital etching* which is the removal one atomic layer at a time [135-137]. In essence, SLR^3 is the electrochemical equivalent of atomic layer epitaxy (ALE) [113,138].

In the last few years, there have been a number of studies [112,113,126,128,129,132,138-156] to prepare uniform and atomically smooth ultrathin noble metal films (e.g., Pt [44,113,132,141,144], Pd [157], Ag [128,132], Ru [151], Hg [153], and Au [158]), with thicknesses varying from a few monolayers to hundreds of

monolayers, for a wide variety of combinations of the substrates (e.g., polycrystalline [159] and Au(111) [132,143-146], Au nanoparticles [44,149], Cu(111) [140], Ag(111) [140], Pd(111) [160,161], and Ru/Si(100) [162]) and sacrificial templates (e.g., Pb [112,126,128,144,146,151,152], Cu [113,126,144,156], Ag [141], Tl [112], Cd [153], Co [157], and Ni [159,163]).

Stickney et al. [113] have studied Pt nanofilm deposition on I-coated Au(111) via redox replacement of Cu. A single replacement of Cu with Pt^{4+} cations results in the formation of incomplete monolayer of Pt although no preferential adsorption at step edges were observed. This finding is in agreement with that of Brankovic and coworkers [132]. The use of I_{ads} as a surfactant facilitated the formation of uniform films.

Mrozek and collaborators [126] have investigated Pt and Pd ultrathin films deposited onto roughened Au via redox replacement of Cu or Pb monolayer. In that study, CO and ethylene were used as probes to investigate the uniformity of the films by surface enhanced Raman spectroscopy (SERS). It has been found that a single replacement of Cu adlayer by Pt(II) cations produced remarkably uniform (i.e., pinhole-free) film which is confirmed by the absence of characteristic SERS features owing to ethylene adsorption on Au.

Huang and coworkers [141] have demonstrated that nanostructured Pt films prepared by SLR[3] have enhanced catalytic activity towards oxygen reduction.

Sasaki et al. [44] also have observed higher catalytic activity for submonolayer of Pt electrodeposited on Ru and Au nanoparticles and Au(111) via redox replacement of Cu UPD layer. The prepared bimetallic electrocatalyst showed 3-4 times higher activity

towards hydrogen oxidation as compared to the commercially available catalysts. Vukmirovic et al. also reported significantly large catalytic activity of Pt monolayer deposited on Pd(111) via galvanic displacement of UPD Cu [160].

Thambidurai and colleagues [150] have employed an automated flow system to grow Cu nanofilms on Au(111) via 500 cycles of galvanic displacement of Pb. The replacement efficiency was calculated to be 93%. The replacement efficiency (RE) [145] can be expressed as:

$$\% \, RE \;=\; \frac{[(total \; Cu \; Q) - (initial \; Cu \; UPD \; Q)]}{\sum Pb \; UPD \; Q} \;\times\; 100 \tag{6}$$

The causes for an efficiency less than 100% have been speculated to be due to side reactions such as ORR [150]. The morphology of 200 cycle Cu films was investigated by SEM and optical microscope. The resulting Cu films obtained by galvanic displacement of Pb deposited at -440 mV were uniform and in registry with the Au(111) substrate, whereas those obtained for Pb deposited at -448 mV were rough [150]. Electron microprobe analysis did not detect any Pd in the Cu films. Similarly, when Ru ultrathin films deposited on Au via SLR[3] no indication of 3D growth mode was observed [151]. Vasilic and Dimitrov [112] have successfully deposited 35 ML Ag on Au(111) via SLR[3] using Pb sacrificial adlayer. The resulting films were investigated by cyclic voltammetry and scanning tunneling microscopy (STM). A flat and uniform morphology was maintained throughout the whole deposition cycles. X-ray photoelectron spectroscopy (XPS) did not detect any residual Pb in the deposited films.

SLR[3] or galvanic displacement has been successfully employed to produce monolayer electrocatalysts. Adzic and coworkers have synthesized monolayer Pt ORR

electrocatalyst shells on Pd [133], Pd$_3$Co [164], PdPb, PdFe, PdPt [165], Pd$_2$Co/C [166], AuNi$_{0.5}$Fe [167], and PdCo/C [168] cores via galvanic displacement of a UPD adlayer of a sacrificial metal. It has been found that the Pt$_{ML}$ placed on Pd and Pd alloys having core-shell structures have approximately 4 to 5 times higher mass activity towards ORR compared to those of massive state-of-the-art Pt catalysts [166].

Recently, Sasaki et al. [133] have reported a scale-up synthesis methodology based on galvanic displacement of Cu$_{UPD}$ to produce gram-quantities of Pt monolayer electrocatalysts that are well suited for real fuel cell tests/operations. These electrocatalysts have been characterized by angle annular dark field (HAADF) scanning electron transmission microscopy (STEM), energy-dispersive X-ray spectrometry (EDS), electron energy-loss spectroscopy (EELS), and *in situ* extended X-ray absorption fine structure (EXAF). The Pt$_{ML}$ shell on Pd core show considerably higher electrocatalytic activity for ORR than that of DOE target by 2015.

Another remarkable significance of galvanic displacement method is its ability to deposit epitaxial metal films even for systems with large lattice mismatch such Cu/Au(111), which has a lattice mismatch of 11% [131]. Epitaxial growth of metal films on such systems by conventional electrodeposition method is not possible.

Our research group has been interested in the interfacial structure and properties of ultrathin Pd films on platinum surfaces, particularly Pt(111), due to possible emergence of properties which are otherwise nonexistent in the pure state of each individual element [96,169,170]. Previously in our laboratory, submonolayer to 8 ML Pd films were electrodeposited via controlled potential deposition (CPD) and potential

sweep deposition (PSD) [171]. To the best of our knowledge, there is no study yet of Pd ultrathin films deposited on Pt surfaces via SLR^3. Of particular interest is the probable appearance of unique properties of ultrathin Pd films on Pt(111) surfaces produced via SLR^3 which are not displayed by films prepared by other methods such as vapor deposition or controlled-potential deposition.

1.5 Objective

The objective of this study is to compare the interfacial structure and electrochemistry of ultrathin Pd films prepared by surface-limited redox replacement reaction and controlled potential deposition (CPD) [171] on well-defined Pt(111) electrodes.

2. EXPERIMENTAL

2.1 Integration of UHV-EC techniques in the investigation of interfacial properties of ultrathin metal films

There has been a longstanding interest in the *solid-liquid* interface [26,172-175] due to its critical role in various phenomena such as corrosion [176-187], adsorption, electrodeposition, electrocatalysis, and biomolecular recognition [188,189]. Conventional electrochemical techniques, such as cyclic voltammetry (CV), amperometry, chronocoulometry, impedance, transient measurements or capacitance measurements have been employed routinely to study the aforementioned processes. The electrochemical methodologies offer a few attractive advantages [173,190]:

(a) electrochemical techniques are well-suited to study and manipulation of surface redox processes,

(b) surfaces can be easily modified by simple immersion into electrolyte solution at controlled potentials,

(c) the chemical reactivity of the surface can be altered easily by tuning the solvent, supporting electrolyte, potential and pH,

(d) adsorbed layers and metal films prepared on electrodes in solution are generally more ordered and closer to equilibrium than those prepared in vacuum conditions,

(e) corrosive, unstable or non-volatile reagents can be handled with relative ease compared with ultra-high vacuum (UHV) based methodologies,

(f) the presence of solvent and electrolytes can render the electrode surface passive enough to minimize the catalytic fragmentation of the starting materials,

(g) electrochemical methods are very sensitive to changes in surface composition and structure.

Although these *in situ* techniques are invaluable, they are based on the determination of the macroscopic properties (e.g., current, capacitance or impedance) [173,191]. It is, however, highly desirable to gain atomic- and molecular-level information on the properties of the interface between an electrode surface and an electrolyte solution [25,27]. Consequently, fundamental studies of the interfaces that involve solid electrodes require the use of surfaces with uniform composition and structure (i.e., single-crystal surfaces). Moreover, it is essential to gain insight on the detailed structural and compositional analysis of the important intermediates, and subsequently to indentify and quantify reaction product distributions [25].

Over the past four decades, there have been revolutionary advances in modern surface spectroscopic techniques that led to the understanding of various atomic- and molecular-level structural, dynamical (e.g., energy transfer between incident and product molecules, mobility of the adsorbed species along surfaces during catalytic reactions), compositional, and thermodynamic properties (e.g., adsorbate coverage dependent heats of adsorption, adsorbate induced surface ordering, and surface segregation) of the

surface [192]. In the current study, electron spectroscopic techniques (Auger electron spectroscopy (AES) and low-energy electron diffraction (LEED)) and electrochemical (cyclic voltammetry (CV) and coulometry) methods have been utilized to investigate the interfacial properties and electrochemical reactivity of ultrathin Pd films on Pt(111) surfaces.

2.2 Electron spectroscopic techniques

The electron spectroscopic techniques utilized in this study involves the use of a beam of electrons as the surface sensitive probes. At low kinetic energies (10 – 150 eV), the mean free path of the electrons in a solid is in the order of 4 to 20 Å, as shown in Fig. 2 [25]. These electrons penetrate only the top few layers of a solid sample and are highly surface sensitive. Therefore, electron spectroscopic techniques that employ low energy electrons as probes and signals are the most suitable to investigate the surface properties of a solid [193].

2.3 AES

Auger electron spectroscopy is the most widely used surface analysis technique, highly sensitive (capable of detection even when the coverage is less than a monolayer), and suitable to study the composition of solid and liquid surfaces. An energetic beam of
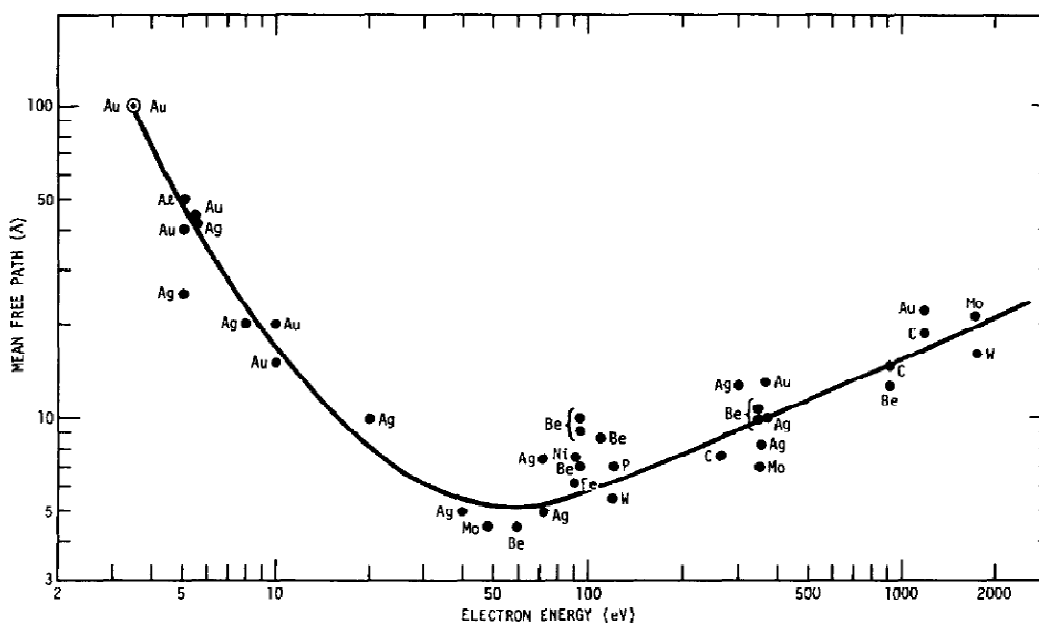
Fig. 2. "Universal curve." Electron mean free path as a function of electron kinetic energy [25].

electrons, photons or ion bombardment may cause AES transitions. The Auger process is depicted in Fig. 3. When an energetic beam of electrons having kinetic energies between 1 to 5 keV impinges upon a material, the electrons that have binding energies less than the incident beam, may be ejected from the inner atomic level leaving behind a "hole," and thus a single ionized excited atom is created. The electron vacancy or hole can then be filled again by deexcitation of electrons from other energy states. The energy released by this electron transition can still be transferred to another electron either in the same atom or of a different atom via electrostatic interaction. If the binding energy of this third electron is less than the energy transferred to it in the previous step, it will be ejected into the vacuum, and a doubly charged ion is formed. The last electron that is ejected due to the deexcitation process is called an Auger electron. The energy of an Auger electron is a function of the energy level separations in the atom. Since at least three electrons are involved in the generation of Auger electrons H and He cannot be detected by AES. The kinetic energy of the Auger electron, E_A, can be expressed as

$$E_A = E_K - E_{L_I} - E_{L_{II}} - e\Phi_{SP} \qquad (7)$$

where E_K, E_{L_I} and $E_{L_{II}}$ are the electron binding energies at the respective electronic levels, e is the electronic charge, and Φ_{SP} is the work function of the spectrometer. The kinetic energies of the Auger electrons are independent of that of the incident beam and are characteristic of their parent atoms only.   Since the Auger signal from the specimen under study is continuously superimposed on a large background of secondary electrons, which are produced from the inelastic scattering of the incident electron beam, the signal-to-noise ratio can be improved by collecting the spectrum in the derivative mode.
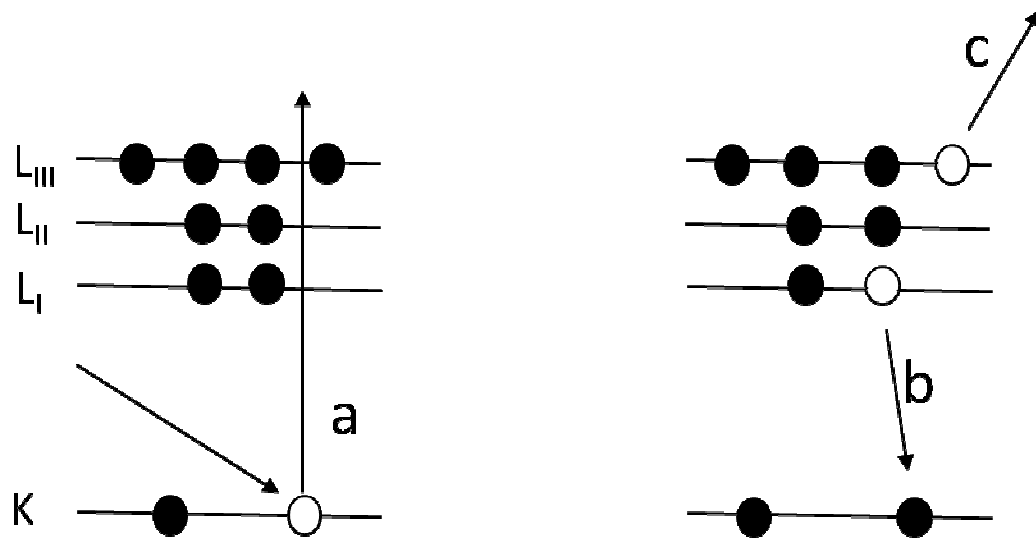
Fig. 3. Auger electron process. (a) A core level electron is ejected. (b) Electron decays to fill the vacancy. (c) An Auger electron is released with a kinetic energy is related to the relative energies of K, L_I and L_{III} energy levels.

In this mode, the sensitivity of AES is increased significantly (less than 0.1% of a monolayer). AES can be used for quantitative elemental analysis. The measured signal is, however, is influenced by the inelastic mean free path, the atomic concentration, and the atomic concentration distribution. The mole fraction of an adsorbate, x_A, in a binary system can be obtained from AES data based on the following equation [194]:

$$x_A = \frac{I_A/S_A}{I_A/S_A + I_B/S_B} \qquad (8)$$

where, I_A and I_B are the intensities of the peaks related to the adsorbate and substrate, respectively, and S_A and S_B are the corresponding relative sensitivity factors. When more than two components are present the denominator must be replaced by the sum over all components. If the spectrum is recorded in the differentiated mode the peak-to-peak distance is used instead of peak intensities.

A set of Perkin Elmer AES systems (Perkin Elmer, Eden Prairie, MN), which included PE 10-155 Cylindrical-Auger Electron Optics, PE 11-500A Auger Control System, PE 20-075 Electron Multiplier Supply, PE 11-010 Electron Gun Control, and EG&G model 5101 Lock-In-Amplifier (Princeton Applied Research), was used for the surface elemental analysis of the single-crystal electrode.

The AES optics consists of a cylindrical mirror analyzer (CMA) for electron energy discrimination, a coaxial normal-incidence electron gun, and a variable gain electron multiplier detector. In order to record an AES spectrum in the derivative mode, a small AC voltage having a frequency about 12 kHz and an amplitude of 0 to 10 V is superimposed with the DC voltage that is applied to the outer cylinder of the CMA

(Fig. 4). This AC signal is then decoupled from the high electron multiplier voltage and detected by a lock-in-amplifier. The CMA has an energy resolution of 0.6%. The resolution capability of CMA determines the width of the bandpass window of the detected electrons. The bandpass was scanned at 4 eV/s. Typical electron gun voltage employed was 1.5 kV. The beam current was adjusted to 1 μA above the background. The low beam current was used to minimize any electron beam induced surface damage.

2.4 LEED

Low-energy electron diffraction is one of the most widely used techniques used in surface science studies of single crystals. It is a highly surface-sensitive technique and can provide information regarding the long range order of periodic surface structures. It can provide valuable information even on partially disordered surfaces and where a complete and elaborate structural analysis is not carried out. In this study, LEED data were acquired with a PE 15-120 LEED Optics and PE 11-020 LEED Electronics system (Perkin-Elmer, Eden Prairie, MN).
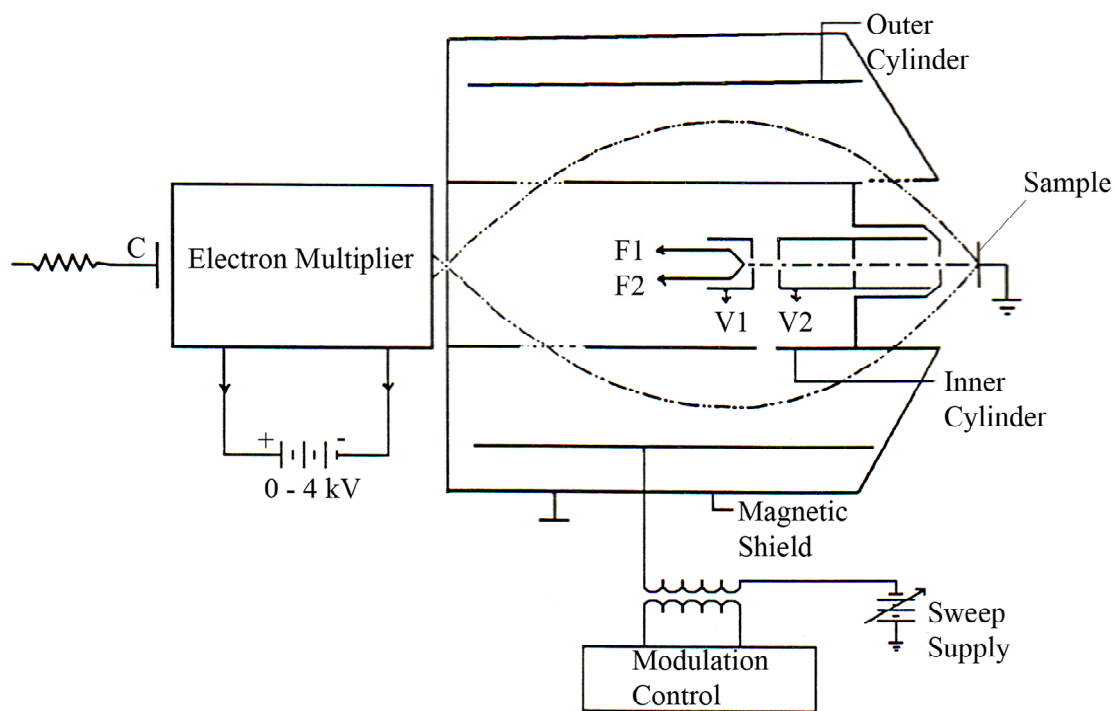
Fig. 4. Schematic cross-section of a cylindrical mirror analyzer.

Fig. 5 shows a schematic diagram of the LEED optics system. The optics consists of an electron gun and a display system. The electron gun provides a monoenergetic electron beam of 10 to 150 eV kinetic energy to the sample surface. The display system is composed of a four-grid retarding field analyzer (RFA) and a concentric phosphor-coated collector screen. The RFA allows only elastically diffracted electrons to be detected at the collector screen. The first grid (G1) is grounded to act as a shield between the negatively biased second (G2) and third grids (G3). These grids block out inelastically diffracted electrons. The elastically diffracted electrons pass through another shielding grid (G4) and are accelerated by a large potential (2 − 5 kV) onto a phosphor-coated collector screen.

LEED, like any other diffraction methods, depends on the use of the elastic scattering of monochromatic beams of incident electrons (or other particles). When a low-energy monochromatic beam of electron is directed at the sample surface the incident beam is scattered off a one dimensional array of metal ion cores, and the scattered beams can interfere constructively or destructively. The elastically diffracted electron beams pass through RFA and produces a pattern of the bright spots on a phosphor-coated screen. The pattern shown by the spots varies with the periodicity of the surface lattice and can offer information about interfacial structure of the sample.
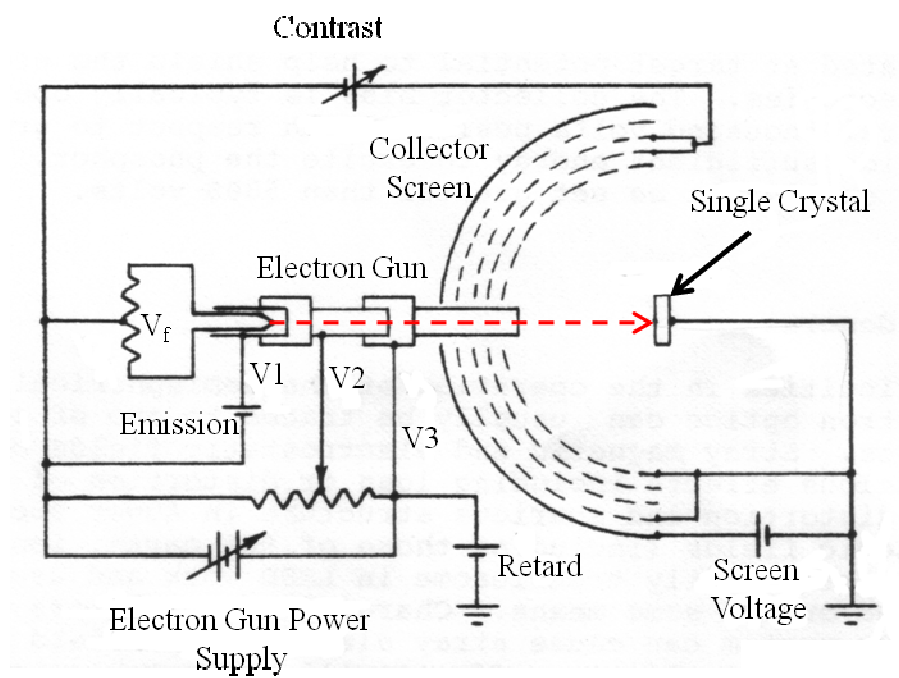
Fig. 5. Schematic diagram of the LEED optics.

The diffraction pattern is related to the atomic distance of the sample surface according to the following equation:

$$\sin(\theta) = n\lambda/a \tag{9}$$

where θ is the angle between the surface normal and the diffracted electron, n is the number of diffracted electron beams, λ is the wavelength of the diffracted electron, and a is the atomic spacing of the solid. This equation shows that the spacing of the diffraction spots is inversely related to the spacing of the atoms in the surface lattice. Consequently, the LEED pattern is in reciprocal space with respect to the surface lattice and need to be converted to real space to obtain geometrical information about the unit cell. The real space lattice can be reconstructed from the LEED pattern using the following vector relationships:

$$\vec{a}^* = \frac{\vec{b} \times \vec{z}}{\vec{a} \cdot \vec{b} \times \vec{z}} \tag{10}$$

$$\vec{b}^* = \frac{\vec{z} \times \vec{a}}{\vec{a} \cdot \vec{b} \times \vec{z}} \tag{11}$$

where $\vec{a}^*$ and $\vec{b}^*$ are denoted as the reciprocal unit cell vectors, $\vec{a}$ and $\vec{b}$ the real space unit cell vectors, and $\vec{z}$ is the surface normal.

At first, the crystal-surface unit mesh was assigned by visual inspection of the diffraction spots. Subsequently, the LEED patterns were compared with those obtained from calculations [195]. In this study, Wood's notation [196] was used to describe the structural information derived from the LEED patterns. The images were recorded with a digital camera (Canon PowerShot S410). The camera was used in the manual

programming mode and the following settings were used to photograph the LEED pattern unless indicated otherwise: ISO = 50, exposure = 15 s. The beam current was typically limited to 2 µA above the background.

2.5 Electrochemistry

Electrochemical experiments were carried out using a CV-27 Voltammograph (Bioanalytical Systems, West Lafayette, IN). In this conventional three-electrode potentiostat, the potential was applied between a working electrode and a reference electrode, and the resulting current flowed through an auxiliary electrode (a piece of Pt wire). A Ag/AgCl (1 mM NaCl) electrode was used as the reference electrode. The current or charge (the integration of current) was recorded using an analogue to digital data acquisition device (DI-158 UP, DATAQ Instruments) interfaced with a PC via a USB port.

2.6 Voltammetry

In voltammetry, a widely used conventional electrochemical technique, current is recorded as a function of applied potential. During linear sweep voltammetry (LSV), the electrode potential is changed from an initial (E_i) to a final value (E_f) at a constant rate where $E_i \neq E_f,$ whereas in cyclic voltammetry (CV), the applied potential is scanned from E_i to E_f and then returned to E_i at the same rate.

2.7 Coulometry

In coulometry, the potential is stepped from one value, at which no faradaic process takes place, to another at which a faradaic process occurs and the electrolytic charge associated with an electron transfer is measured over a predetermined time. This technique is useful to determine the surface packing density (Γ, nmol/cm^2) for an adsorbed electroactive species using Faraday's law:

$$Q - Q_b = nFA\Gamma \tag{12}$$

where Q is total charge of the electrochemical process, Q_b is the background charge obtained in the absence of adsorbate, F is Faraday's constant, A is the area of the electrode, and n is the number of electrons involved in the reaction.

2.8 UHV-EC system

The UHV-EC system employed in this investigation was based on a commercial all stainless steel UHV chamber (Perkin-Elmer, Eden Prairie, MN). A photograph of the instrument is shown in Fig. 6. The main chamber of this system consists of three major compartments: (i) an electrochemistry (EC) chamber, (ii) a gate-valve (MDC Vacuum Products, Hayward, CA) isolable surface analysis chamber, and (iii) a poppet valve-isolable ion pump well. The single-crystal electrode was transferred by means of an X-Y-Z manipulator (Varian, Lexington, MA) mounted on a linear positioning table

(LinTech, Los Angeles, CA). This design allowed sample transfer and manipulation under a controlled environment.

The EC chamber has a gate-valve (MDC Vacuum Products) isolable electrochemical cell port through which an electrochemical cell assembly can be inserted. The surface analysis chamber used for the preparation and analysis of the sample electrode is equipped with the modules for LEED, AES, and temperature-programmed desorption-mass spectrometry (TPD-MS) instrumentation (UTI 100c, UTI). Two variable leak valves (Varian, Lexington, MA) allowed the introduction of ultra-high purity gases. A custom-built ion gun was used for Ar^+-sputtering to clean the electrode surfaces. With the use of a XYZ manipulator the electrode could be placed in front of each instrument for characterization. Initial pumping of the chamber from ambient pressure down to 10^{-3} torr was achieved by liquid nitrogen-cooled sorption pumps. A
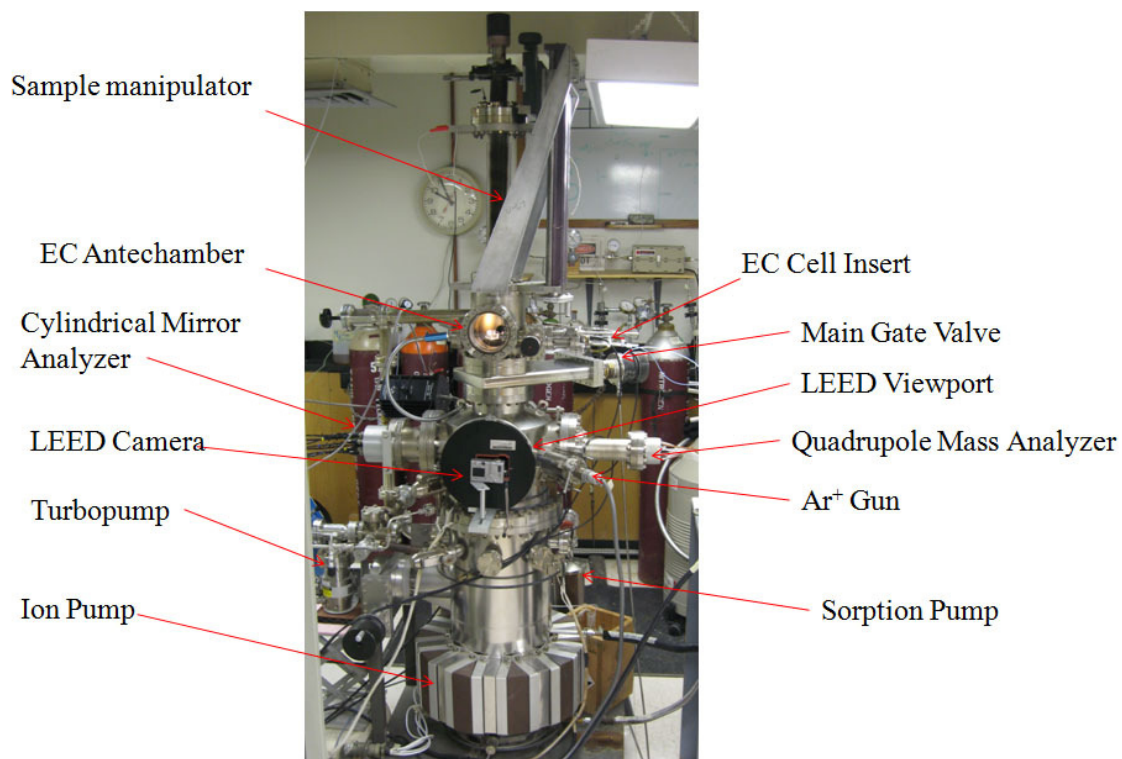
Fig. 6. Photograph of UHV-EC system.

turbomolecular pump (Balzers TPU 060, Hudson, NH) was used to lower the pressure down to 10^{-6} torr. The final pumping stage consisted of using an ion pump (Perkin-Elmer TNBX Series 1000, Eden Prairie, MN) and a cryogenically cooled titanium sublimation pump. The UHV-EC system was periodically baked at 150 – 200 °C for up to 99 hours to maintain a base pressure of 10^{-9} torr. Mass spectra were also recorded periodically to check the residual gases in the UHV system.

A single-crystal Pt(111) disc electrode (99.999% purity, 7.5 mm (diameter) and 1.0 mm (thickness), Aremco Products, Ossining, NY) was used for UHV-EC experiments. The disc electrode was oriented to within ±0.5° of the (111) plane and metallurgically polished to a mirror finish. Two pieces of Pt wires of 0.5 mm thickness (99.99% purity, Aldrich) were spot-welded to the edges of the disc to provide electrical contact and mechanical support. Two Pt-10% Rh/Pt thermocouple wires (Omega Engineering, Stanford, CT) were spot-welded to the top edge of the disc for temperature monitoring and feedback control of a crystal temperature controller (Omega Engineering). The calculated geometric electrode area of the electrode was 1.1192 cm^2.

Electrochemistry experiments in the UHV-EC system were performed using a custom-built two-compartment glass cell, a Ag/AgCl (1 mM NaCl) reference electrode (also custom built), and a Pt-wire counter electrode. In order to minimize Cl$^-$ contamination of the working electrode a low concentration of Cl$^-$ in the reference electrode was used. Fig. 7 shows a photograph of EC experiment setup.
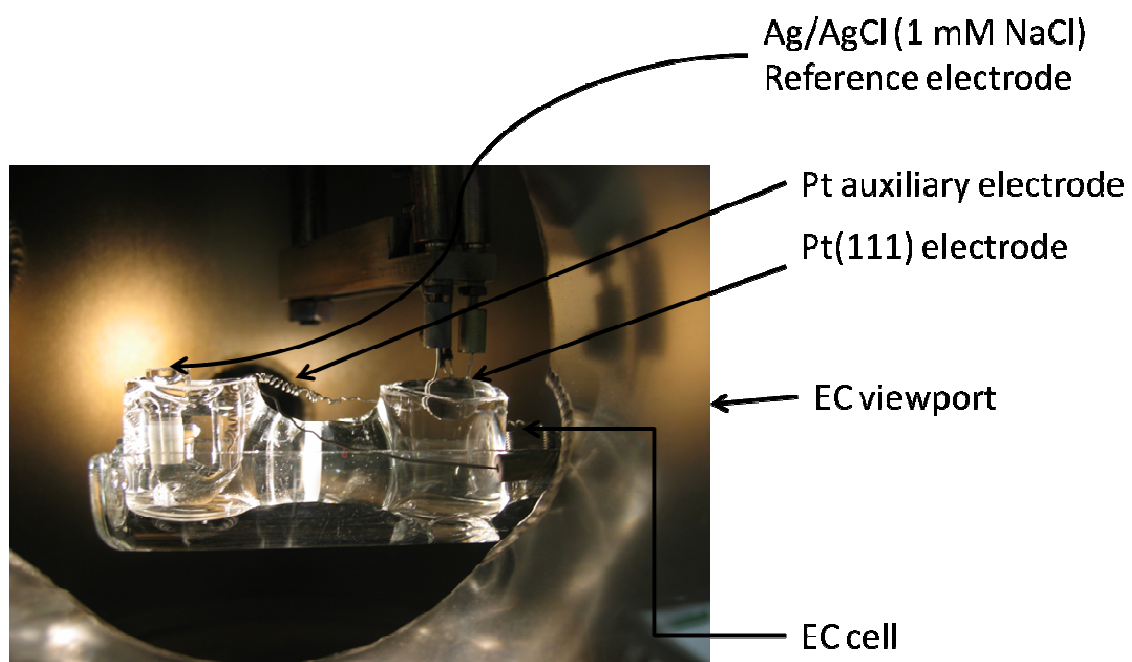
Fig. 7. EC experiment setup.

2.9 Experimental protocols

All solutions were prepared using 18.2 Ω Millipore water (Millipore Systems, Houston, TX). This water delivery system consists of a prefilter, two ion exchangers, a trap to remove trace organics, a UV lamp to get rid of any microbes, and a 0.2 micron particulate filter. All glassware was cleaned using hot chromic acid (3% $K_2Cr_2O_7$ dissolved in 10 M H_2SO_4). The following high-purity reagents were used to prepare all solutions: fuming H_2SO_4 (Aldrich, Milwaukee, WI), $PdSO_4$ (Aldrich), NaI (Curtin Matheson Scientific, Houston, TX), NaCl (Johnson Mathey), $CuSO_4$ (Aldrich), and $K_2Cr_2O_7$ (EM Science, Gibbstown, NJ). High purity gases, specifically nitrogen (99.999% purity, BOTCO, Bryan, TX), argon (BOTCO), and oxygen (BOTCO) were used in the experiments. Prior to any EC experiment, the all solutions were purged with high purity nitrogen for at least 20 minutes.

A typical set of experiments were carried out in the following way: at first the crystal was cleaned by Ar^+ sputtering for 20 - 30 min (P_{Ar} = 2.2 × 10^{-4} torr, beam current = 10 μA). Following Ar^+ sputtering, all the filaments of the optics and ion gauges were degassed in UHV. Then the crystal was heated in O_2 (PO_2 = 3.0 × 10^{-4} torr) at 650 °C for 5 minutes. Once the crystal was cooled down to 300 °C, the system was pumped down by using a turbo pump to about 10^{-6} torr. The thermal oxidation was carried out a few more times (PO_2 = 3.0 × 10^{-4} torr, 650 °C, for 5 min 2 cycles; PO_2 = 3.0 × 10^{-4} torr, 750 °C, for 3 min, 3 cycles). During Ar^+ sputtering and thermal oxidation in oxygen the ion pump was de-energized. At the last step, the crystal was flash annealed to 800 °C under

ultra-high vacuum (UHV) while operating the liquid nitrogen cooled titanium sublimation pump. The AES and LEED filaments were also degassed during this last step. The cleanliness and surface order was checked by AES and LEED, respectively. Ar^+ sputtering, thermal annealing in oxygen, and thermal annealing in UHV cycles were continued until the desired cleanliness and order were achieved and verified by AES and LEED.

In this study, digital deposition of Pd ultrathin films on Pt(111) electrode was carried out via surface-limited redox replacement reaction using Cu_{UPD} adlayer as a sacrificial template. The UPD of Cu on a number of noble metal substrates such as Au, Pt, Ru, and Pd has been studied extensively as a model system. It is fortuitous that Cu show distinctive UPD features for both Pt and Pd surfaces. Hence, Cu was chosen as a sacrificial template to deposit atomic layers of Pd films on Pt(111) via surface-limited redox replacement reaction. Fig. 8 describes pictorially the process of deposition of Pd adlayers on Pt(111), one layer at a time, i.e., digitally, via SLR[3] (after Brankovic et al. [132]). The steps involved are:

1. Deposition of Cu on Pt(111) via UPD according to the reaction

$$Cu^{2+}_{(aq)} + 2e^- \rightarrow Cu_{(s)} \tag{13}$$

2. Emersion and rinsing of the Cu/Pt(111) with pure electrolyte (typically 5 times) at UPD potential (ca. -0.054 V).

3. The Cu-modified electrode is then immersed in 0.5 mM PdSO4 in 100 mM sulfuric acid at OCP for 3 min following the procedure of Brankovic
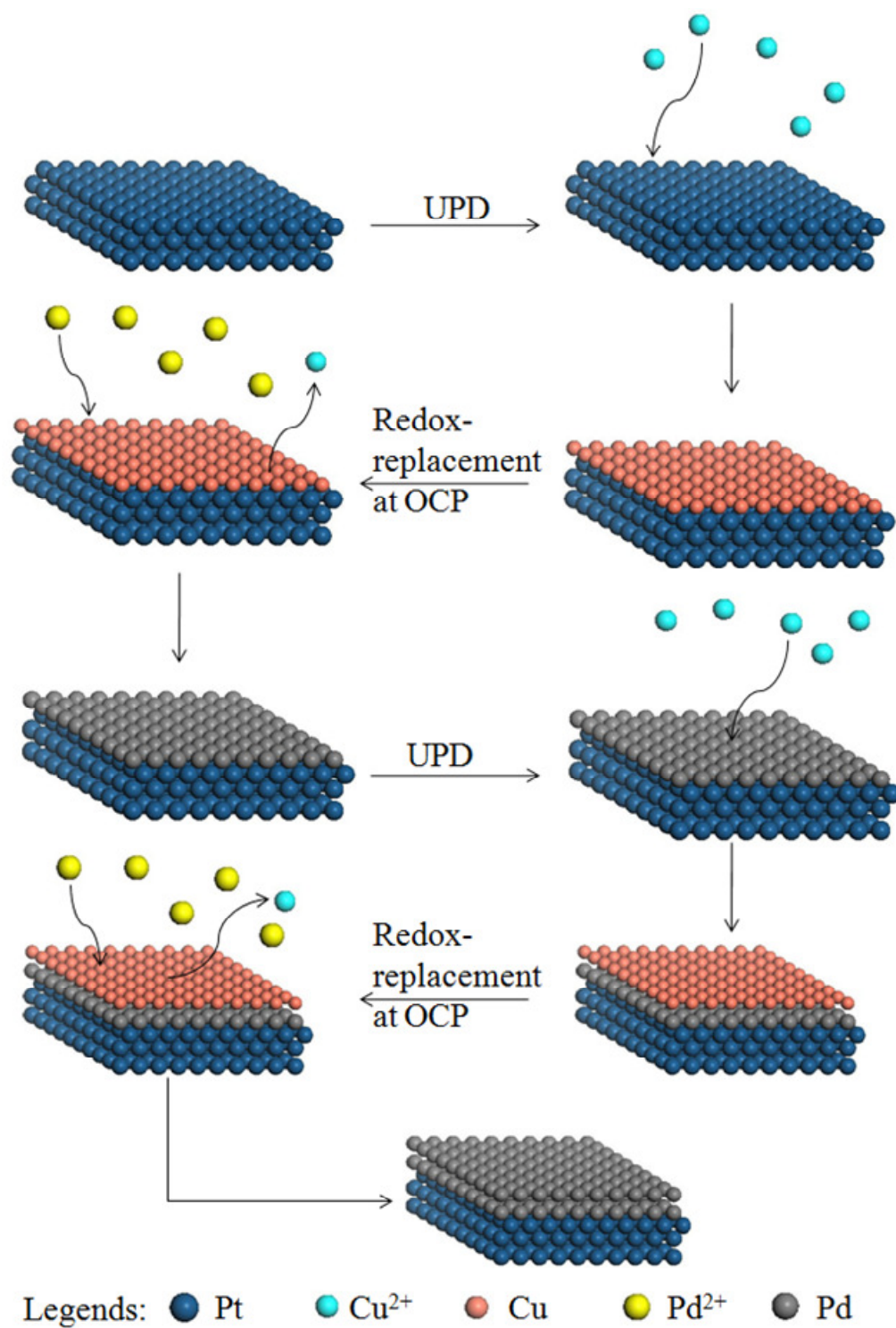
Fig. 8. Schematic representation of surface limited-redox replacement reaction.

et al. [132]. Potential control is removed just before the immersion of the Cu-coated electrode into the Pd^{2+} containing solution to avoid direct electrodeposition of Pd. At this step, Pd^{2+} cations oxidize the Cu ad-atoms and are themselves get reduced and deposited on the Pt(111) surface. This process is irreversible.

4. The Pd/Pt(111) electrode is rinsed with pure electrolyte solution at OCP (5 times). This is the end of 1st SLR[3] cycle.

$$Pd^{2+}_{(aq)} + Cu_{(s)} \rightarrow Pd_{(s)} + Cu^{2+}_{(aq)} \quad\quad\quad (14)$$
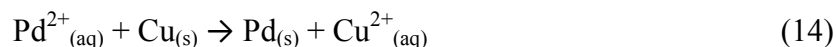
5. Deposition of Cu on Pd/Pt(111) electrode via UPD.

6. Emersion and rinsing of Cu/Pd/Pt(111) with blank (5 times) at UPD potential.

7. Replacement of Cu from Cu/Pd/Pt(111) by Pd^{2+} cations in 0.5 $PdSO_4$ in 100 mM sulfuric acid at OCP.

8. Rinsing of Pd modified Pt(111) with blank at OCP. This is the end of 2nd cycle of SLR[3].

Following the above steps, 2 ML Pd is now deposited on the Pt(111) electrode via two cycles of SLR[3]. These steps can be repeated to prepare Pd films of desired thickness.

The interfacial structure and electrochemical properties of thus prepared films were then compared to those of the electrodeposited films, more specifically, Pd ultrathin films prepared by potentiostep or controlled-potential deposition. The methodology of the preparation of the electrodeposited films have been described elsewhere [96,171]. Table 1 lists the experiments to be performed and the criteria for

comparing the Pd films prepared by SLR^3 and controlled-potential deposition (hereon, referred to as CPD) [171]. The LEED spot intensities for SLR^3 and CPD Pd films were compared by analyzing the digital images by Origin Pro 8.5 software (Origin Lab).

Table 1

Experiments to be performed.

Method	Θ_{Pd}	CV (H_{UPD})	AES	LEED	I_{ads}-Cat Stripping
CPD	0.5	●	●	●	0.5 mV/s
SLR^3	0.5	●	●	●	2 mV/s
CPD	1	●	●	●	0.5 mV/s
SLR^3	1	●	●	●	0.5 mV/s
CPD	2	●	●	●	0.5 mV/s
SLR^3	2	●	●	●	2 mV/s
CPD	4	●	●	●	0.5 mV/s
SLR^3	4	●	●	●	0.5 mV/s
CPD	8	●	●	●	0.5 mV/s
SLR^3	8	●	●	●	0.5 mV/s

3. RESULTS AND DISCUSSION

In this study submonolayer to eight monolayers Pd films were electrodeposited on Pt(111) electrodes via galvanic displacement of Cu UPD layer. The interfacial structure and electrochemical properties were investigated by electron spectroscopic (AES and LEED) and EC techniques. The AES and (1×1) LEED pattern for a clean and well-ordered Pt(111) electrode are shown in Figs. 9 and 10, respectively.

For electrochemistry experiments, the first step was to record the cyclic voltammogram of Pt(111) in blank or pure electrolyte (100 mM H_2SO_4). The potential scan was always started from OCP towards the negative potential unless mentioned otherwise. Fig. 11 shows the CV of a clean and well-ordered Pt(111) electrode in sulfuric acid solution. The sharp "butterfly" peaks at -0.052 V are good indications of large ordered domains of (111) surfaces which are essentially defect free [40,197]. These are due to desorption/adsorption of bisulfate anions for cathodic and anodic sweep, respectively [40,78]. The broad peaks between -0.45 and -0.22 V are considered to be due to hydrogen adsorption/desorption not accompanied by concurrent adsorption/desorption of anion [72]. These voltammetric features are consistent with those found in the literature [40,65,197,198]. Fig. 12 shows the steady-stead voltammogram of the Pt(111) in sulfuric acid when the potential was scanned between 1.00 V and -0.542 V at 10 mV/s. At steady-state, the peak at -0.412 V and -0.260 V matched those reported by Hubbard et al. for a parallelopiped Pt(111) electrode [199].
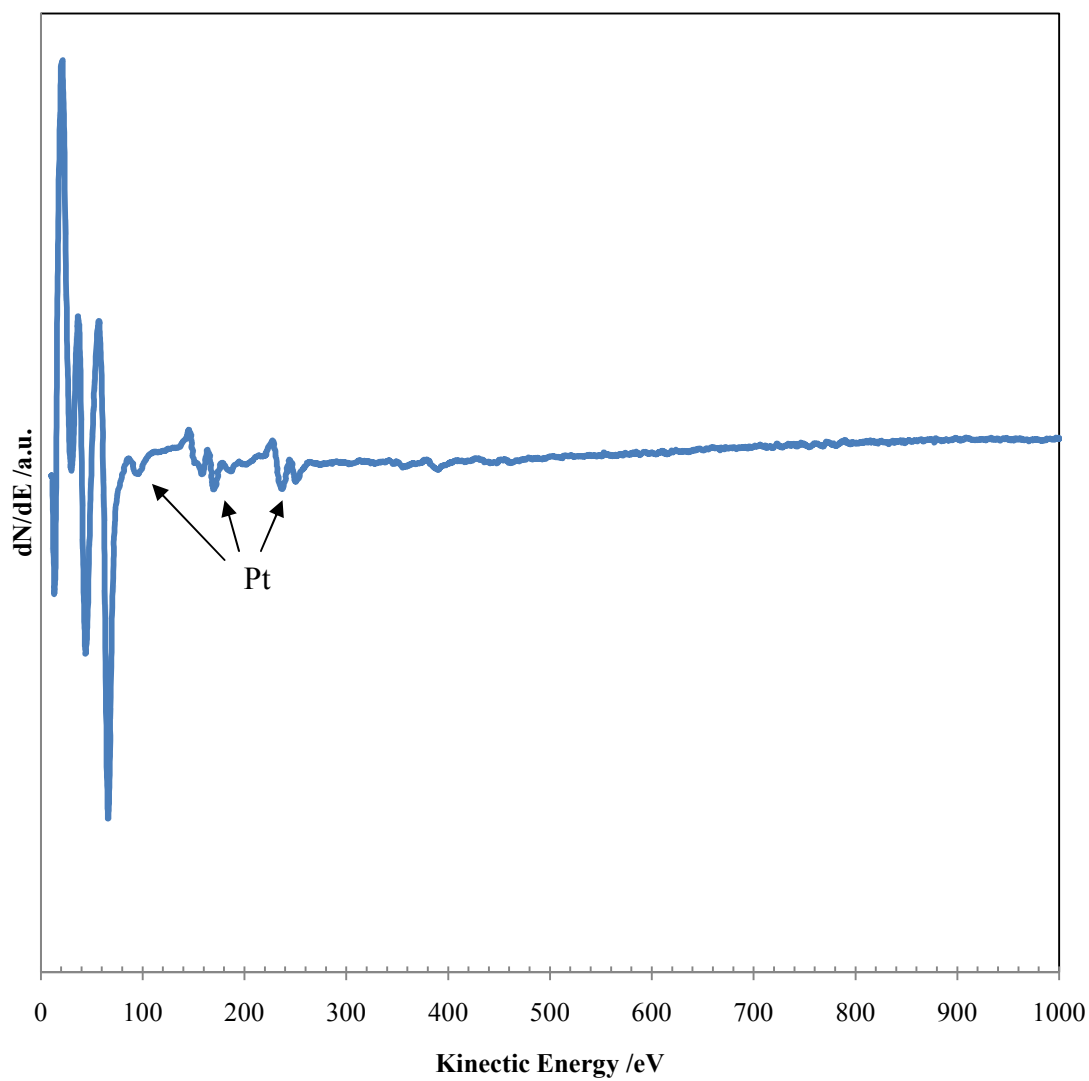
Fig. 9. The AES spectrum of a clean Pt(111) electrode. Beam energy = 1.5 keV, Ip = 1 μA.
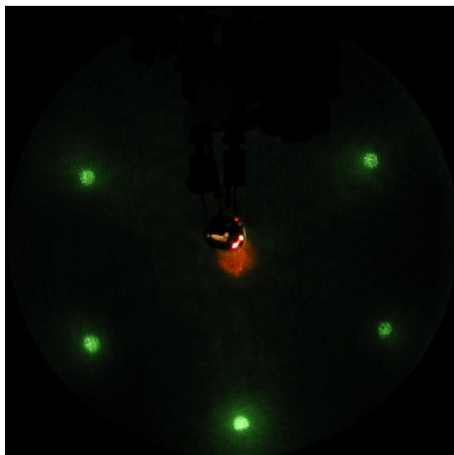
Fig. 10. LEED pattern of a clean Pt(111) electrode. Beam energy = 62 eV, I_P = 2 µA.
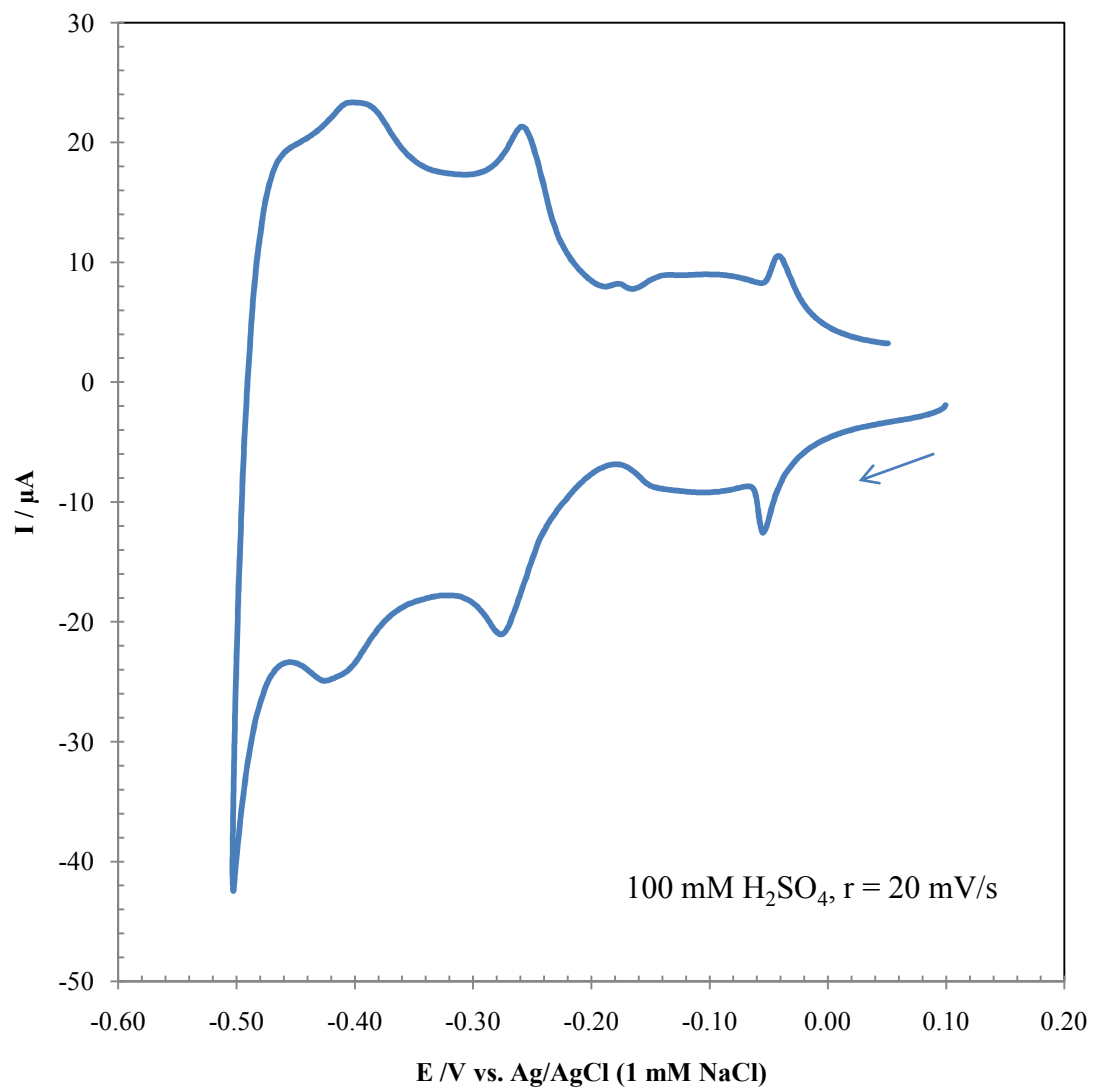
Fig. 11. A cyclic voltammogram of a clean and well-ordered Pt(111) electrode.
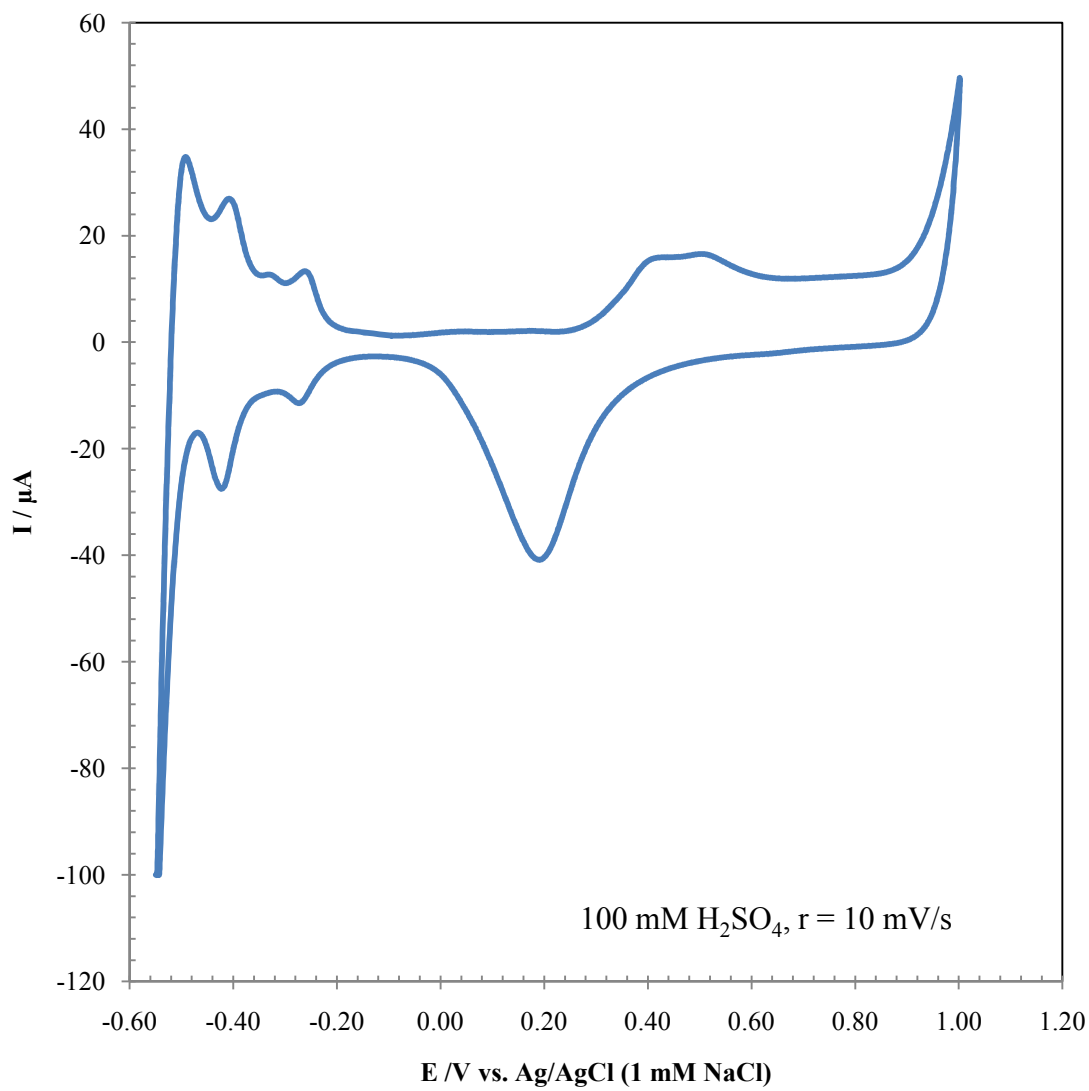
Fig. 12. Steady-state cyclic voltammogram of Pt(111) (after 20 cycles).

This is another indication of well-ordered Pt(111) surfaces employed in the current study.

A CV of Pt(111) in 1 mM $CuSO_4$ in 100 mM H_2SO_4 is shown in Fig. 13. As expected [40,200-202], a doublet of Cu_{UPD} adsorption/desorption peaks were observed for Pt(111). The shape of the Cu UPD peaks on Pt(111) has been found to be dependent upon the concentration of sulfuric acid and true crystallographic orientation [197]. As the concentration of sulfuric acid increases the UPD peaks become broader. In fact, the UPD desorption peaks merges together in 0.5 M H_2SO_4 [197]. It is worth mentioning that the under potential adsorption/desorption of Cu do not alter the surface structure of Pt(111) [197]. Cu UPD on Pt(111) is also known to depend on the anions present [40,201]. In pure sulfuric acid, the initial adsorption of Cu on Pt(111) produces a mixed, nearly coplanar, honeycomb structure of Cu/sulfate. Cu coverage accounts for about ⅔ ML while the rest is occupied by sulfate anions [203]. It has also been reported that the Cu_{UPD} peak potentials depend on the scan rate. At higher scan rates, the cathodic and anodic peaks shift in the negative and positive directions, respectively. This implies that the Cu_{UPD} on Pt(111) in sulfuric acid is a slow process [114].

Fig. 14 displays the AES spectrum of the Cu-coated Pt(111) surface, when the electrode was emersed at -0.054 V (Fig. 13). Peaks at 105, 920, and 940 eV indicate the presence of Cu on the Pt surface (Fig. 14). These peaks are non-existent for clean Pt surfaces (Fig. 9). It should be noted that the electrodes were rinsed with 100 mM H_2SO_4 acid instead of 0.1 mM electrolyte solution at the end of the EC experiments. Consequently, the electrode surfaces would have an emersed layer of electrolyte [25].
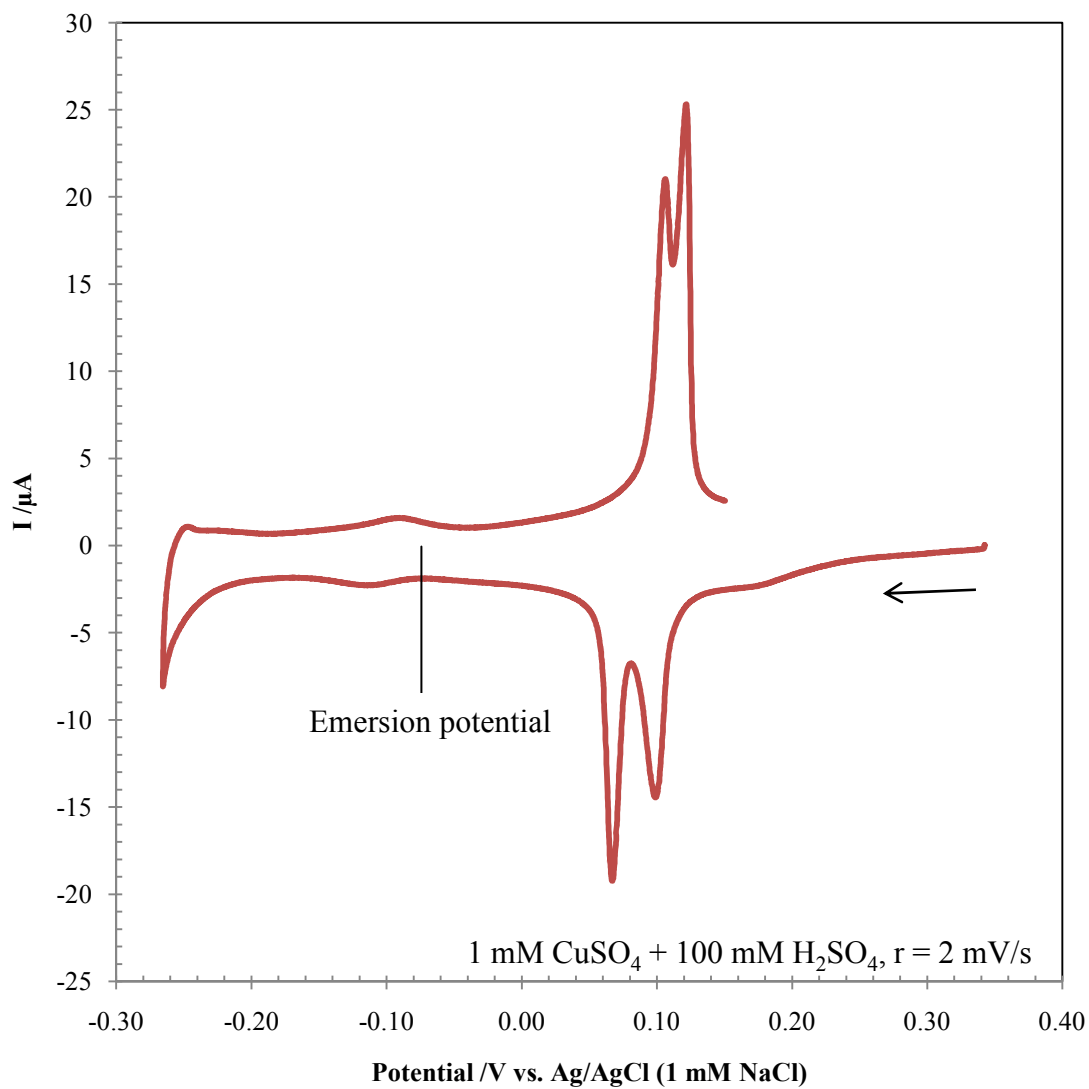
Fig. 13. CV of Pt(111) in CuSO₄ solution. Scan initiated from the OCP in the negative
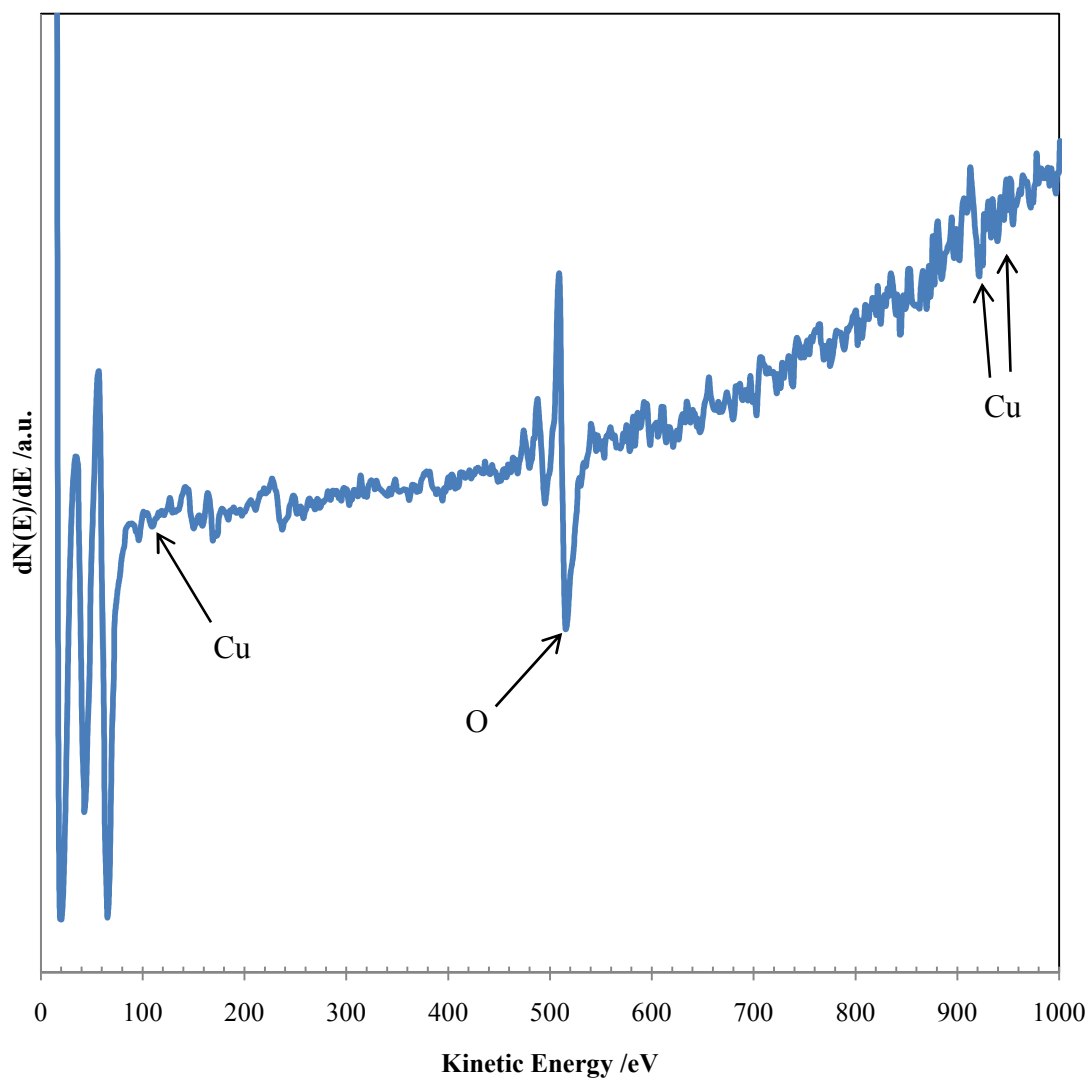
direction.

Fig. 14. AES spectrum of Cu-coated Pt(111).

Fig. 15 shows the LEED pattern for the Cu_{UPD}-covered Pt(111) electrode. The LEED pattern indicates Pt(111)-($\sqrt{3}\times\sqrt{3}$)R30°Cu adlayer structure. STM results also indicated the same honeycomb structure [197]. Ogasawara et al. [204] and Markovic et al. [205] also observed ($\sqrt{3}\times\sqrt{3}$)R30° LEED patterns for Cu_{UPD}/Pt(111) in H_2SO_4 and HF, respectively. In situ STM studies [197,206] also indicated ($\sqrt{3}\times\sqrt{3}$)R30° structure for the first Cu_{UPD} adlayer on Pt(111). Exactly same structures were reported for the first UPD of Cu on Au(111) in sulfuric acid ([206] and references therein). Based on these observations it is logical to infer that the widely spaced ($\sqrt{3}\times\sqrt{3}$)R30° structure is due to the presence of anions, such as Cl^-, SO_4^{2-} or HSO_4^- [204,206]. Bisulfate ions are known to form a ($\sqrt{3}\times\sqrt{3}$)R30° structure on Pt(111) prior to underpotential deposition of Cu. At the first UPD peak, the bisulfate ions are converted to sulfate ions as Cu is continuously adsorbed onto Pt(111) surface. At the second UPD peak, Cu adsorption proceeds via replacement with sulfate ions on Pt surfaces. Cu monolayer is completed at the end of the second UPD peak and the sulfate ions form a $\begin{pmatrix} 2 & 1 \\ 1 & 2 \end{pmatrix}$ structure on the (1×1) Cu layer [207]. It has been found that adsorption of bisulfate on Cu hinders further underpotential deposition. Excursion to more negative potentials changes the bisulfate to sulfate on Cu [204].

Unfortunately, the presence of sulfate or bisulfate on the Cu UPD cannot be fully ascertained by AES due to the overlapping of S peak with that for Pt. The AES spectrum of Cu_{UPD}/Pt(111), however, shows a peak at around 503 eV which is associated with oxygen. This oxygen might be due to the presence of sulfate or bisulfate adsorbed on Cu.
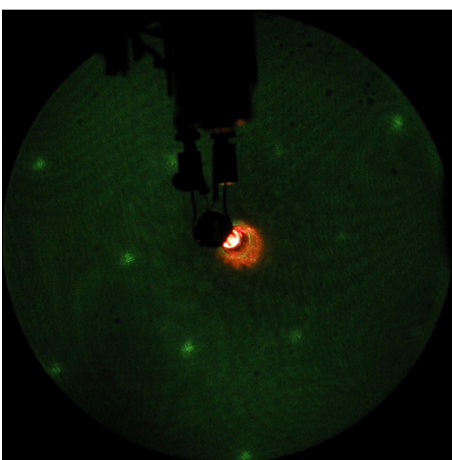
Fig. 15. LEED pattern of Cu$_{UPD}$ on Pt(111). Beam energy = 50 eV, Ip = 1 µA.

Following the completion of 1st SLR^3 cycle, a CV of Pd-modified Pt(111) electrode was recorded in pure electrolyte solution (Fig. 16). A pair of sharp peaks is observed at ca. -0.271 V. These peaks are associated with H$_{UPD}$ along with anion desorption/adsorption on the Pd monolayer deposited on Pt(111) [72,95]. No peak was observed in the Cu UPD region which indicates the absence of any residual Cu. This was further verified by AES and LEED. The AES spectrum of the Pd-modified electrode did not show the peaks associated with Cu rather 3 new peaks were observed which are the unique characteristics of Pd (Fig. 17). The LEED pattern also indicates a (1×1) structure which is consistent for pseudomorphic adlayer of Pd on Pt(111) Pt(111) (Fig. 18). These results imply that indeed there is complete exchange of Cu by Pd^{2+} cations and no residual Cu is present in the SLR^3-prepared Pd film.

The Pd coverage of the deposited films can be calculated by (a) measuring the deposition charge of Cu or by (b) measuring the charge of I$_{ads}$-catalyzed anodic dissolution of Pd using Faraday's law. The Pd coverage, Θ_{Pd}, can be defined as,

$$n \text{ ML when } \Theta_{Pd} = n \tag{15}$$

where $\Theta_{Pd} = \Gamma_{Pd} / \Gamma_{Pt}$ and Γ_{Pd} = packing density of Pd, Γ_{Pt} = packing density of Pt

The reactions involved are Cu deposition by UPD (eq. 13) and I$_{ads}$-catalyzed dissolution of Pd (eq. 16).

$$\text{Pt(111)-Pd -I}_{(ads)} \rightarrow \text{Pd}^{2+}{}_{(aq)} + \text{Pt(111)-I}_{(ads)} + 2e^- \text{ (Pd dissolution)} \tag{16}$$
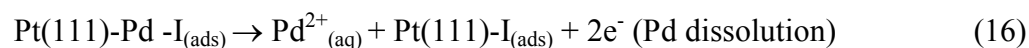
The calculated charge for 1 ML Cu is given by,

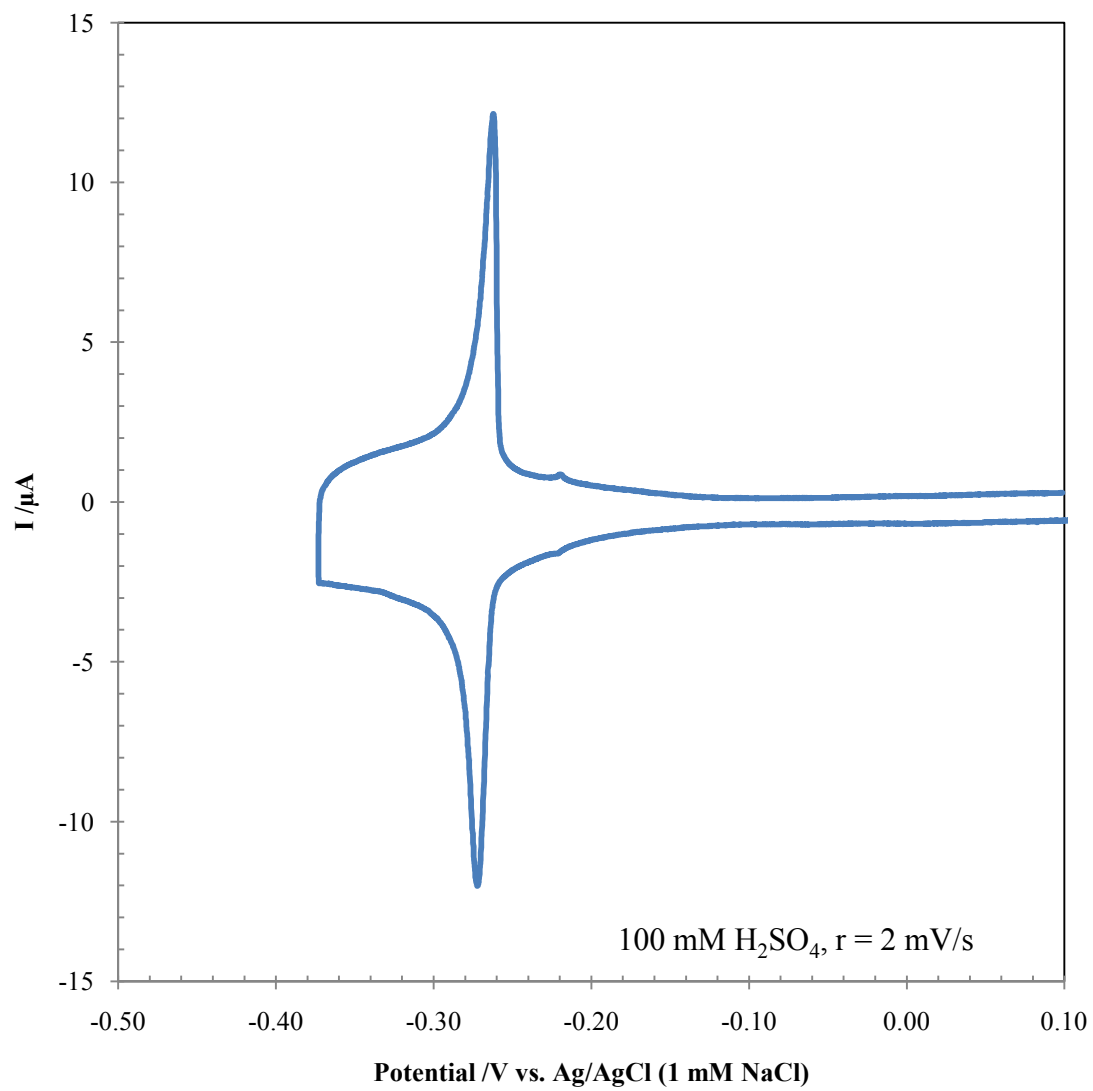$$Q_{1 \text{ ML Cu}} = nFA\Gamma_{Pt(111)} = 537.6 \text{ } \mu C \tag{17}$$

Fig. 16. CV of Pd/Pt(111) (after completion of 1st SLR^3 cycle) in pure electrolyte.
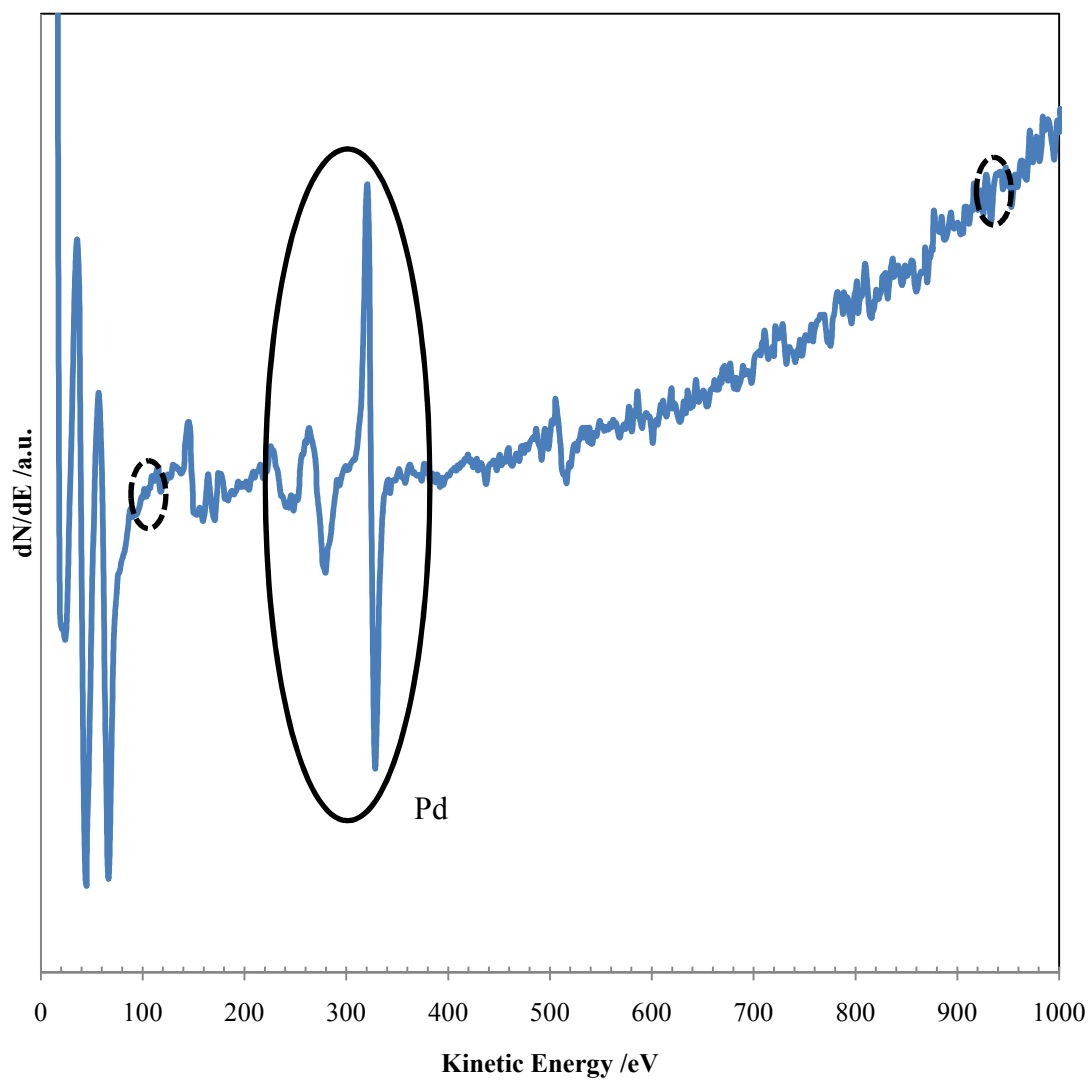
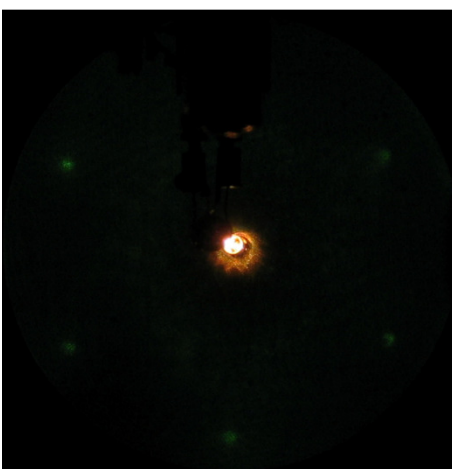**Fig. 17.** AES of Pd/Pt(111) after completion of the 1st SLR[3] cycle.

Fig. 18. LEED pattern of SLR^3-prepared Pd/Pt(111). Beam energy = 63 eV, Ip = 1μA.

Hence, the Cu deposition or I_{ads}-catalyzed Pd dissolution charge of 537.6 μC will be used to define 1 ML coverage. In other words,

$$Q_{n\ ML\ Pd} = n \times 537.6\ \mu C \qquad\qquad (18)$$

It has been shown that when a monolayer of iodine is adsorbed on Pd, it can quantitatively and selectively remove the Pd top layers [135-137,208-216]. This methodology has been successfully used to determine the coverage of Pd films deposited on Pt and Au substrates [106,171,217]. Iodine was adsorbed from 1 mM NaI in 100 mM sulfuric acid at OCP for 3 minutes.

Fig. 19 shows the AES spectrum for I-coated Pd/Pt(111) electrode. In addition to Pt and Pd peaks, two new peaks at around 511 and 520 eV indicate the presence of the iodine adlayer. The iodine AES peaks are small compared to Pd peaks due to smaller AES relative sensitivity factors for iodine as compared to those of Pd. The relative sensitivity factors for Pt, Cu, Pd, and I are 0.025, 0.225, 0.800, and 0.325, respectively [218] Fig. 20 displays the I_{ads}-catalyzed anodic stripping of SLR[3]-prepared 1 ML Pd film on Pt(111) in iodide free 100 mM sulfuric acid. Based on previous studies, the peaks at 0.58 and 0.84 V are assigned to Pd dissolution and iodine to iodate oxidation, respectively [212,215]. In all cases, the scan was started from OCP to positive potential during I_{ads}-catalyzed dissolution of Pd films. The Pd dissolution charge was determined by integrating the area of the Pd dissolution peak. When I-catalyzed stripping of Pd was complete, iodine was readsorbed on the electrode surface from fresh solution of 1 mM NaI and a second I_{ads}-catalyzed stripping was carried out. The second scan was used as the background to determine the charge due to Pd dissolution. Indeed, a linear
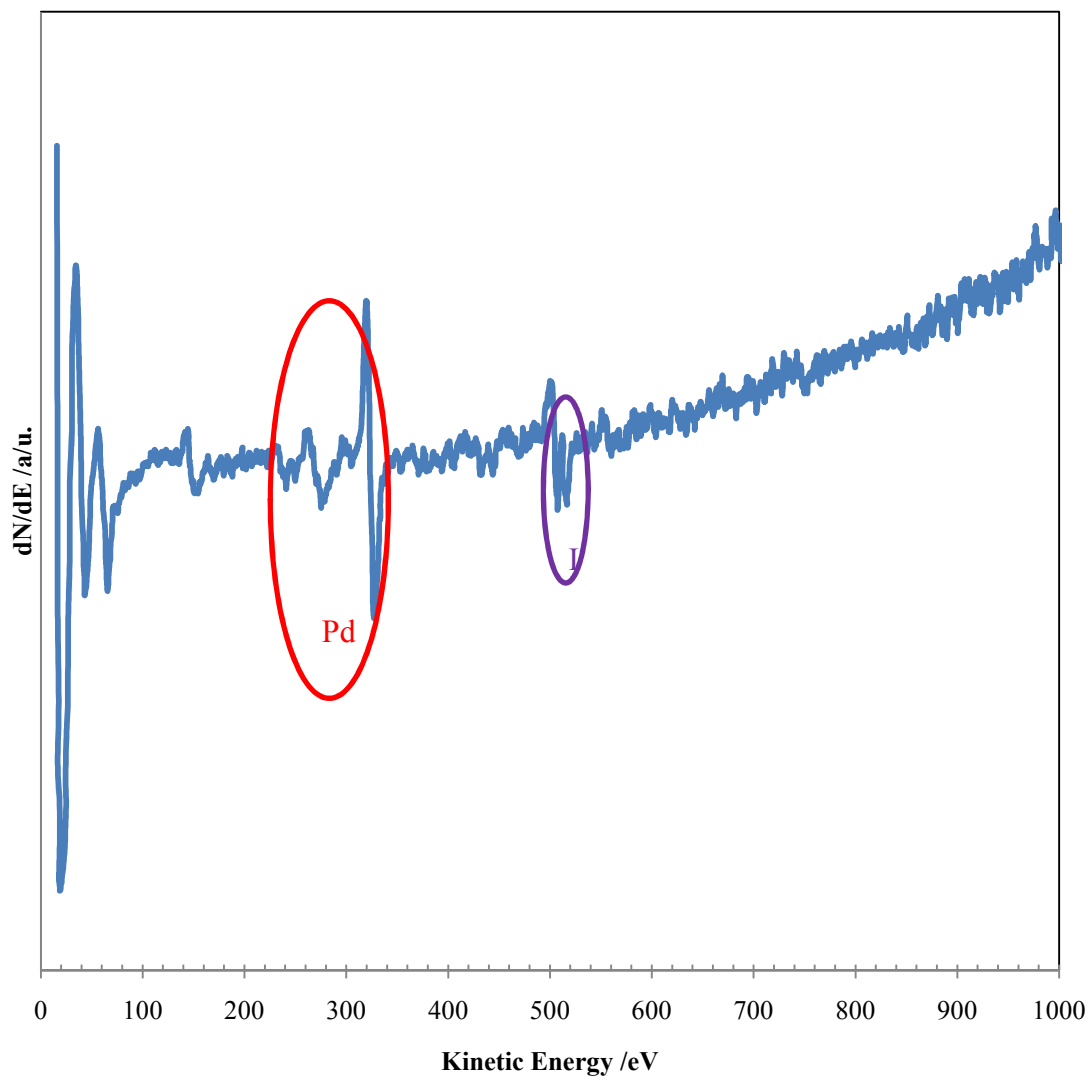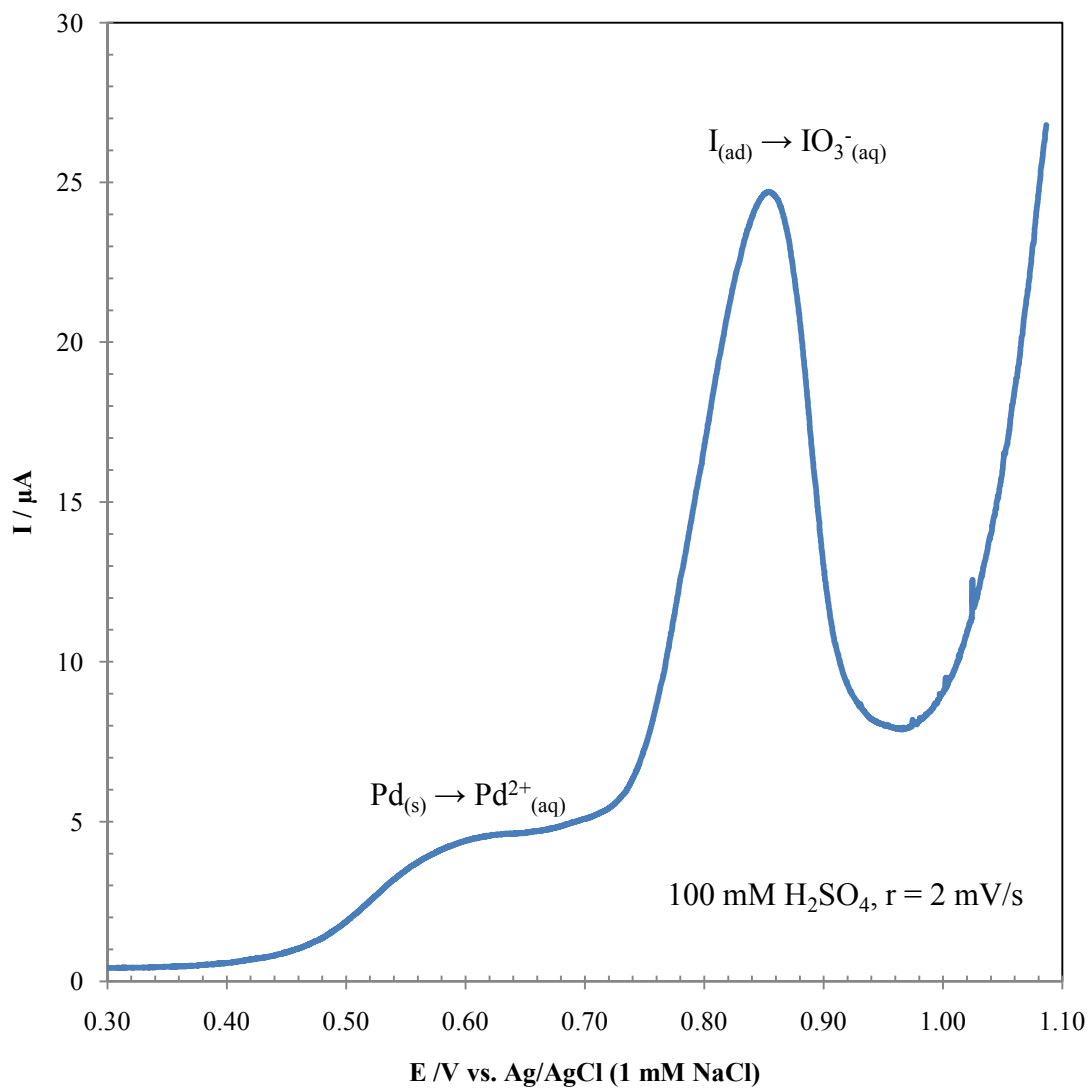
Fig. 19. AES of I/Pd/Pt(111) electrode.

Fig. 20. I_{ads}-catalyzed anodic stripping of Pd/Pt(111) after 1st SLR[3] cycle.

correlation was found between the Cu deposition charge and I_{ads}-catalyzed Pd dissolution charge (Fig. 21).

The AES spectrum and LEED pattern of I-coated Pt(111) electrode are shown in Fig. 22 and 23, respectively. The AES spectrum displays two peaks due to iodine adlayer on Pt surface. The LEED pattern is indicative of Pt(111)-(1×1)-($\sqrt{7}\times\sqrt{7}$)R19.1°-I adlattice structure. The same iodine adlayer structure was observed by Felter et al. [219] and Wasberg et al. [220].

In order to establish a standard procedure, it was deemed necessary to investigate the UPD of Cu on Pd film on Pt(111). Cu is expected to show a single UPD on Pd [200,203,221]. The CV of Pd modified Pt(111) electrode did not show any peak between 0.10 and -0.05 V which implies that the Pt(111) electrode surface is already fully covered and there is no bare Pt sites (Fig. 24). The peak around -0.07 V is due to Cu UPD on Pd film. Again, this finding is consistent with the observations reported in the literature [40,200]. Reappearance of peaks at 105, 920, and 940 eV in the AES spectrum indicates that Cu UPD indeed took place on SLR[3] prepared Pd film on Pt(111) (Fig. 25). The Cu UPD layer on ML Pd film showed (1×1) LEED pattern which is in agreement with literature findings (Fig. 26) [221].
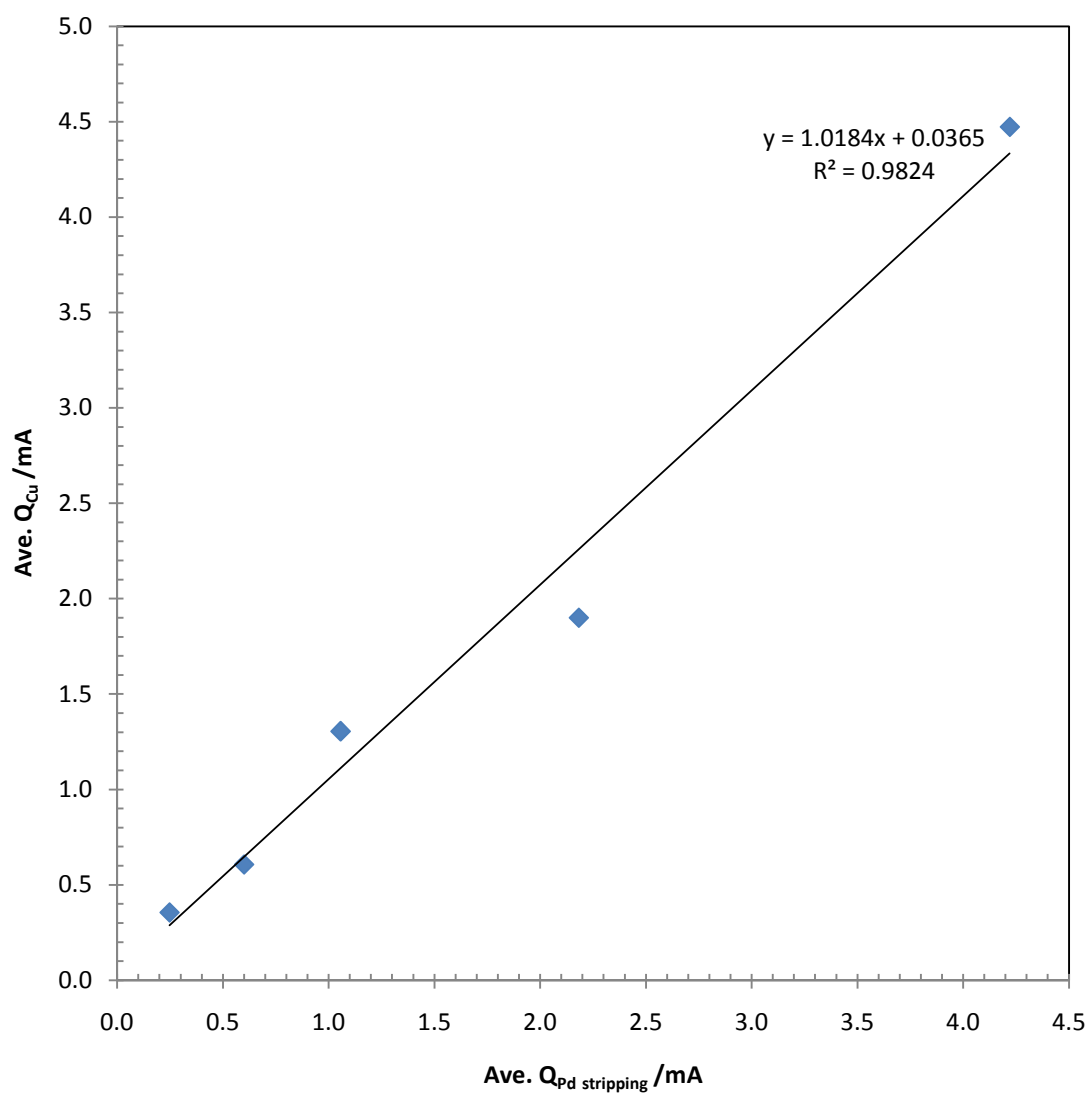
Fig. 21. Correlation of Cu deposition and I_{ads}-catalyzed Pd stripping charge.
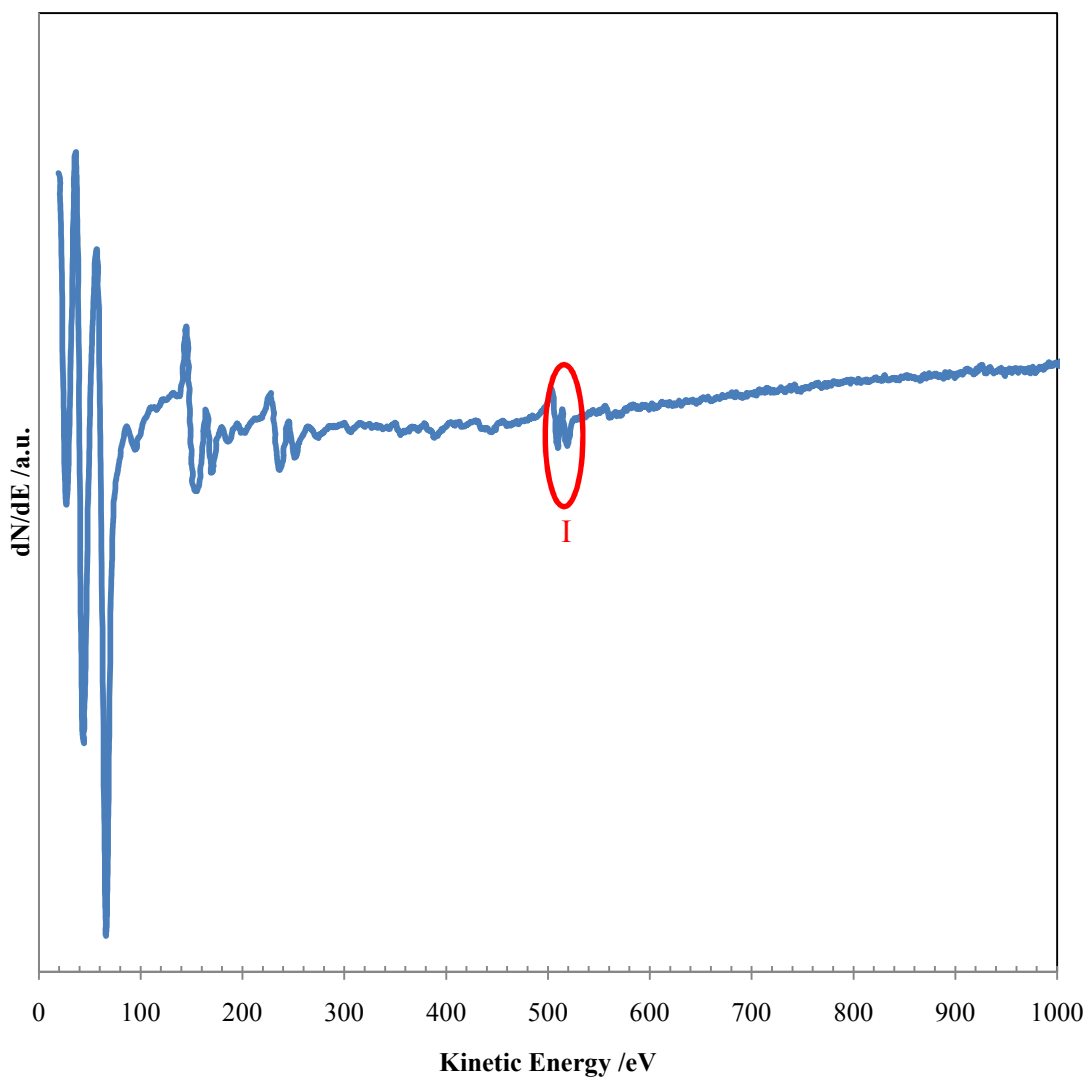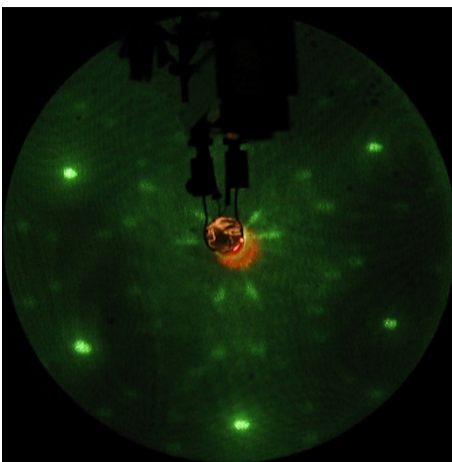
Fig. 22. AES spectrum of I/Pt(111) electrode.

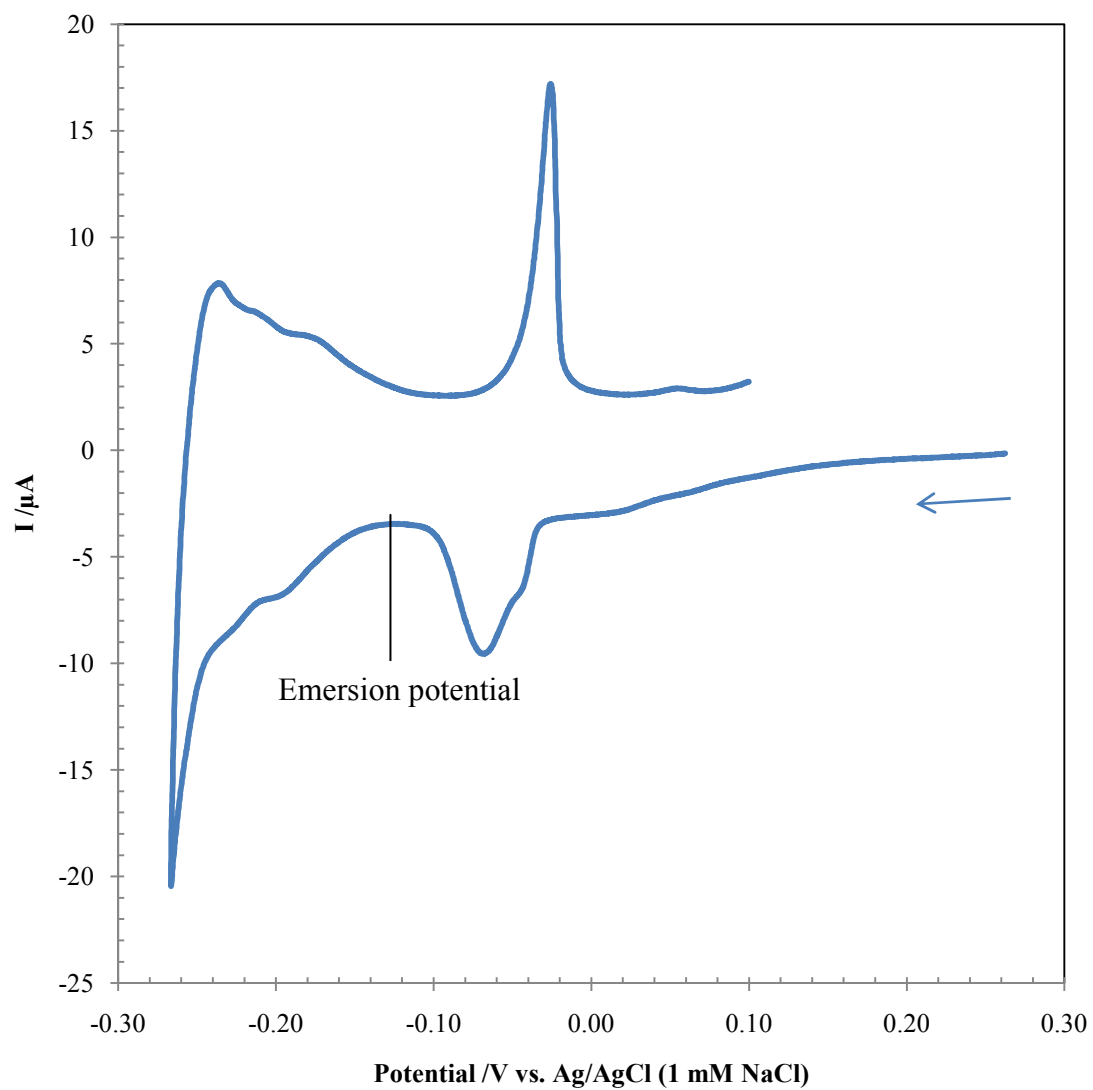**Fig. 23.** LEED pattern of I/Pt(111). Beam energy = 60 eV, I_P = 2 μA.

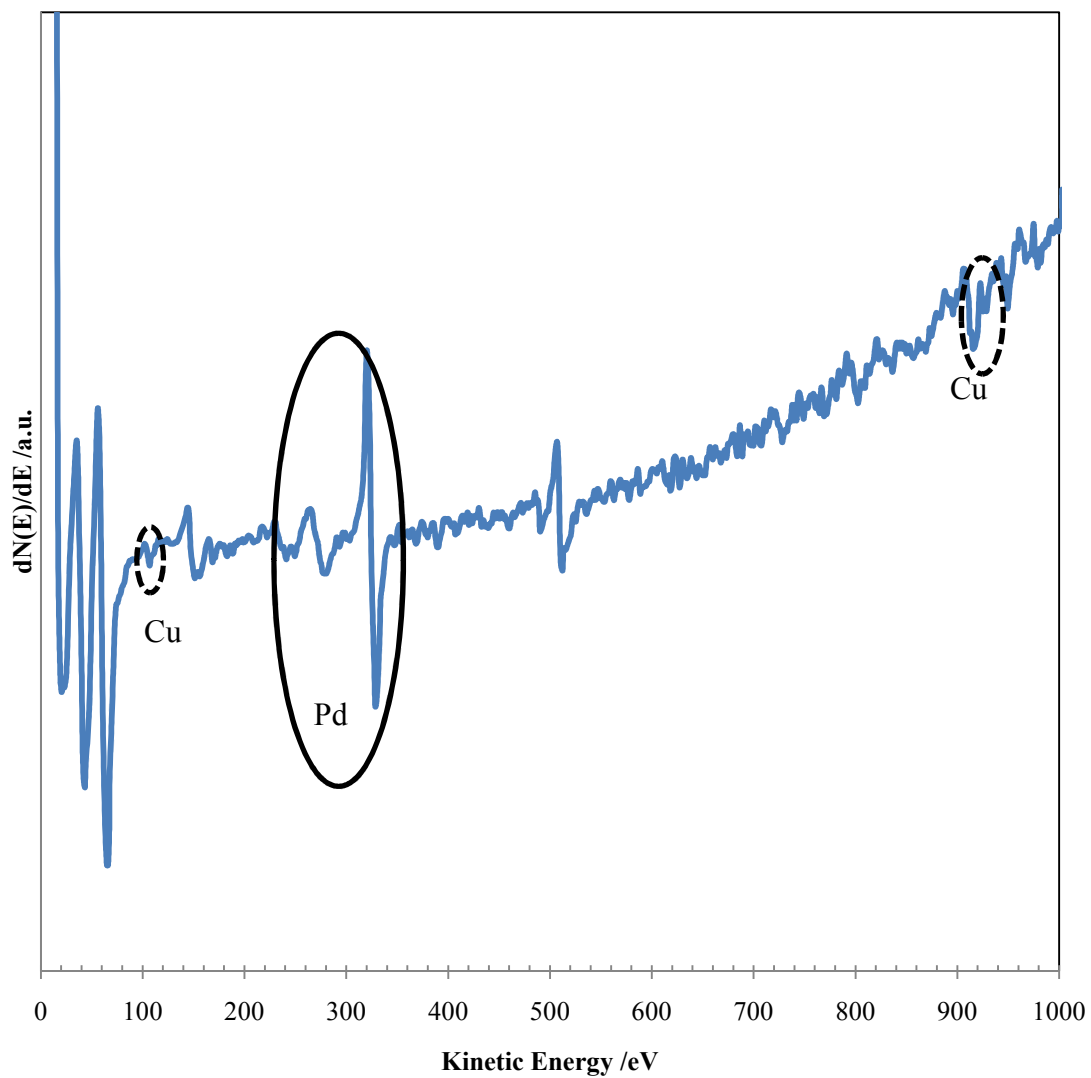**Fig. 24.** CV of Pd/Pt(111) in CuSO$_4$ in 100 mM H$_2$SO$_4$, r = 2 mV/s.
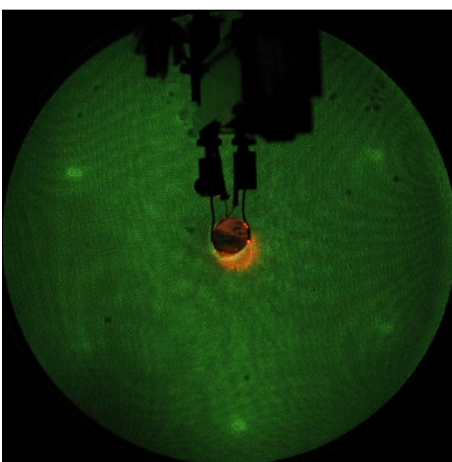
Fig. 25. AES spectrum of Cu/Pd/Pt(111) electrode.

Fig. 26. LEED pattern of Cu/Pd/Pt(111) electrode. Beam energy = 62 eV, I_P = 2 µA.

For the sake of simplicity and reproducibility, the Cu UPD was carried out by potential step, from OCP to predetermined values where the UPD takes place (typically -0.054 V for clean Pt surface and -0.100 V for Pd-covered Pt electrode), for 3 minutes and the coulometric charge was measured. The appropriate UPD potential was chosen based on the CV of Pt or Pd/Pt(111) in 1 mM $CuSO_4$ in 100 mM H_2SO_4 solution. Before each Cu UPD cycle, a blank coulogram was recorded in Cu^{2+} free 100 mM H_2SO_4 solution. All other procedures remained the same as described before.

In the current work, submonolayer to eight-monolayer Pd films were deposited on Pt(111) surfaces via SLR[3] using Cu as a sacrificial UPD layer. A linear correlation was observed between the cumulative Cu coverage and number of SLR[3] cycles performed (Fig. 27); each cycle produces ca. 0.8 ML Cu film. Hence, 0.8 ML Pd is expected to be obtained per cycle of galvanic displacement of Cu. One possible reason for this can be that some Cu was lost during the emersion and immersion steps between solutions. It has also been suggested that oxygen reduction and hydrogen evolution reactions are competitors for galvanic displacement of UPD adlayer with noble metal ions [222].

In the following sections, the electrochemical properties and interfacial structures of the Pd films deposited by two methods (galvanic displacement and controlled-potential deposition) will be compared by evaluating the differences and similarities in - cyclic voltammograms, AES spectra, LEED patterns, and linear sweep voltammograms for I_{ads}-catalyzed dissolution of Pd films. The results will be presented for a given Pd coverage at a time.
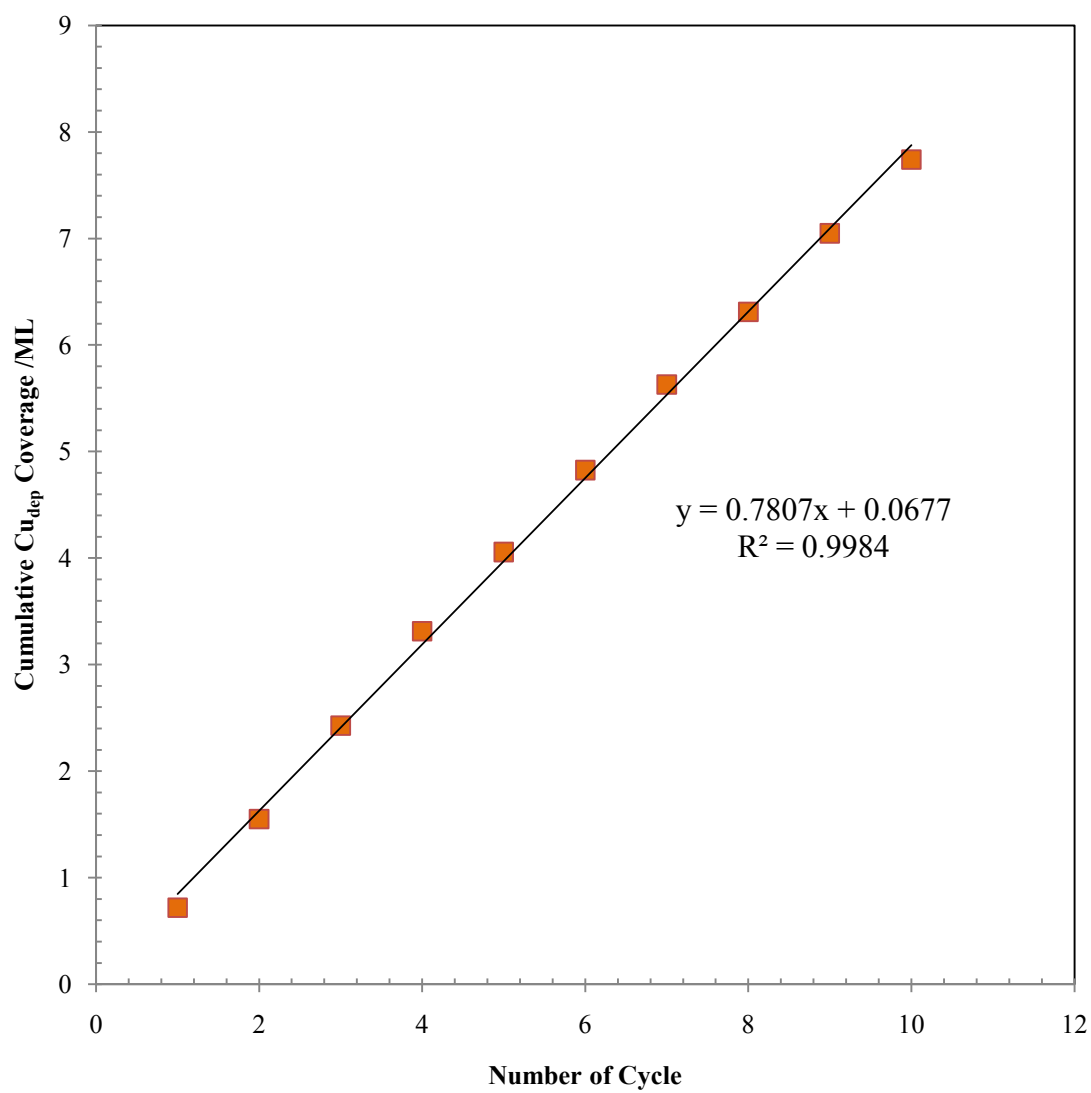
Fig. 27. Correlation of Pd coverage with number of SLR^3 cycles.

3 1 Θ_{Pd} = 0.5 ML

Fig. 28, 29, and 30 show the CVs, AES spectrum, and LEED patterns, respectively, for 0.5 ML Pd films. The cyclic voltammograms show two sharp peaks at -0.271 V. They are due to H adsorption/desorption on the Pd films on the terrace sites.

The SLR[3] films show only one peak. On the other hand, CPD film begins to show H_{UPD} peaks at -0.229 V. There are, however, controversies regarding the origin of the second peak. Ross and coworkers [72,78] argued that this peak is due to H adsorption/desorption combined with anion desorption/adsorption from the step sites while other authors, such as Clavilier [21], Lasia [97], and Kolb [95], assigned it to H_{UPD} from the terrace sites from subsequent layers of Pd films on Pt(111). It seems more plausible that the second peak is due to H_{UPD} from the step sites since it is not possible to grow subsequent terraces without formation of steps. If both the peaks were originated from H_{UPD} adsorption/desorption from the terrace sites the reason for their appearances at different potentials was not explained. Therefore, in the current study the second peak (at more positive potential) has been attributed to the hydrogen UPD from the step sites. Both of H_{UPD} peaks form terrace and step sites on Pd/Pt(111) in sulfuric acid have been reported to be dependent upon the scan rate. This might imply that the H_{UPD} process is kinetically controlled [97]. Moreover, the area under the H_{UPD} desorption peak (i.e., charge) in cyclic voltammograms for SLR[3] films is smaller compared to that for CPD films. It may be an indication of the formation of more uniform and smoother films via SLR[3]. Both films display large Pd peaks at 330 eV in the AES spectra (Fig. 29). The
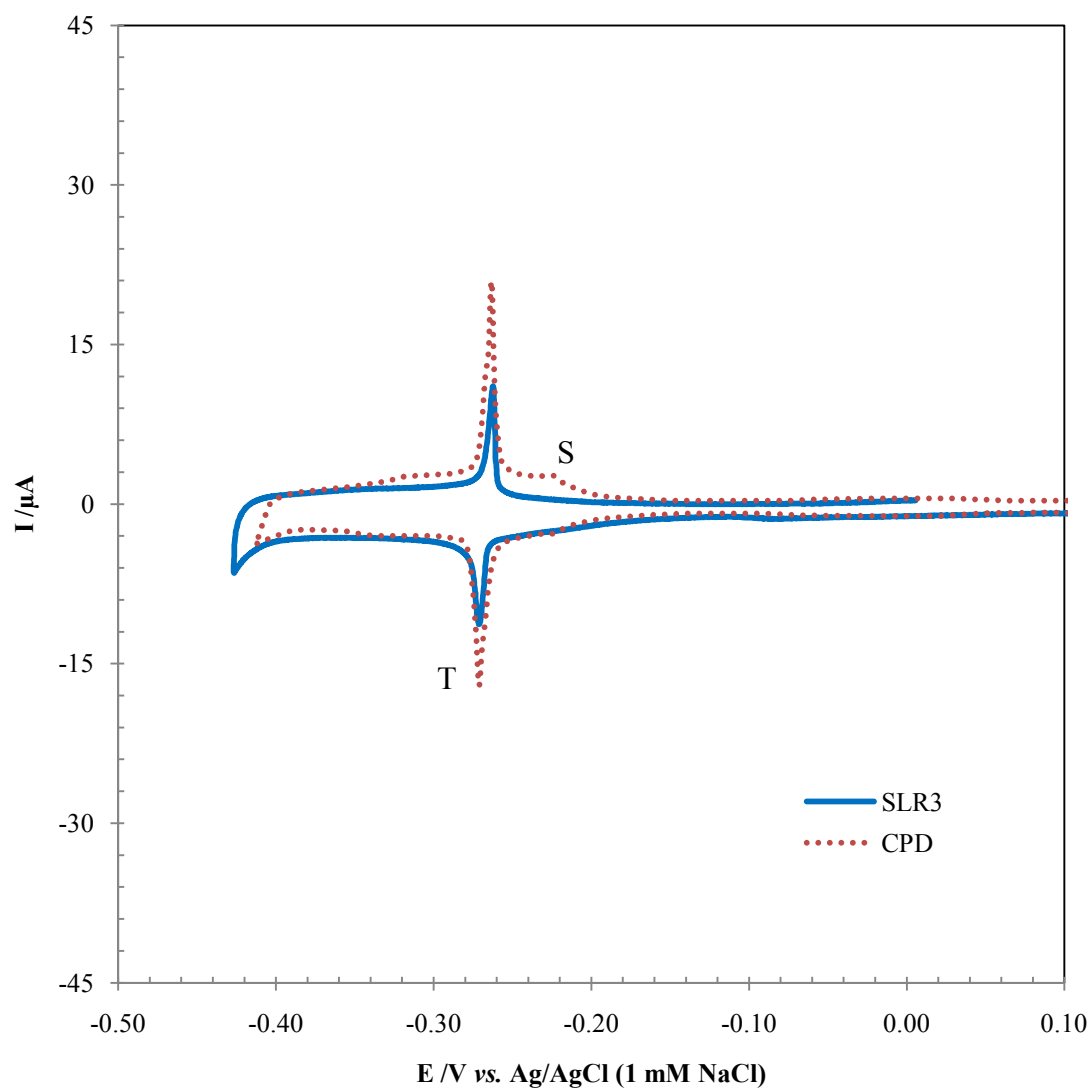
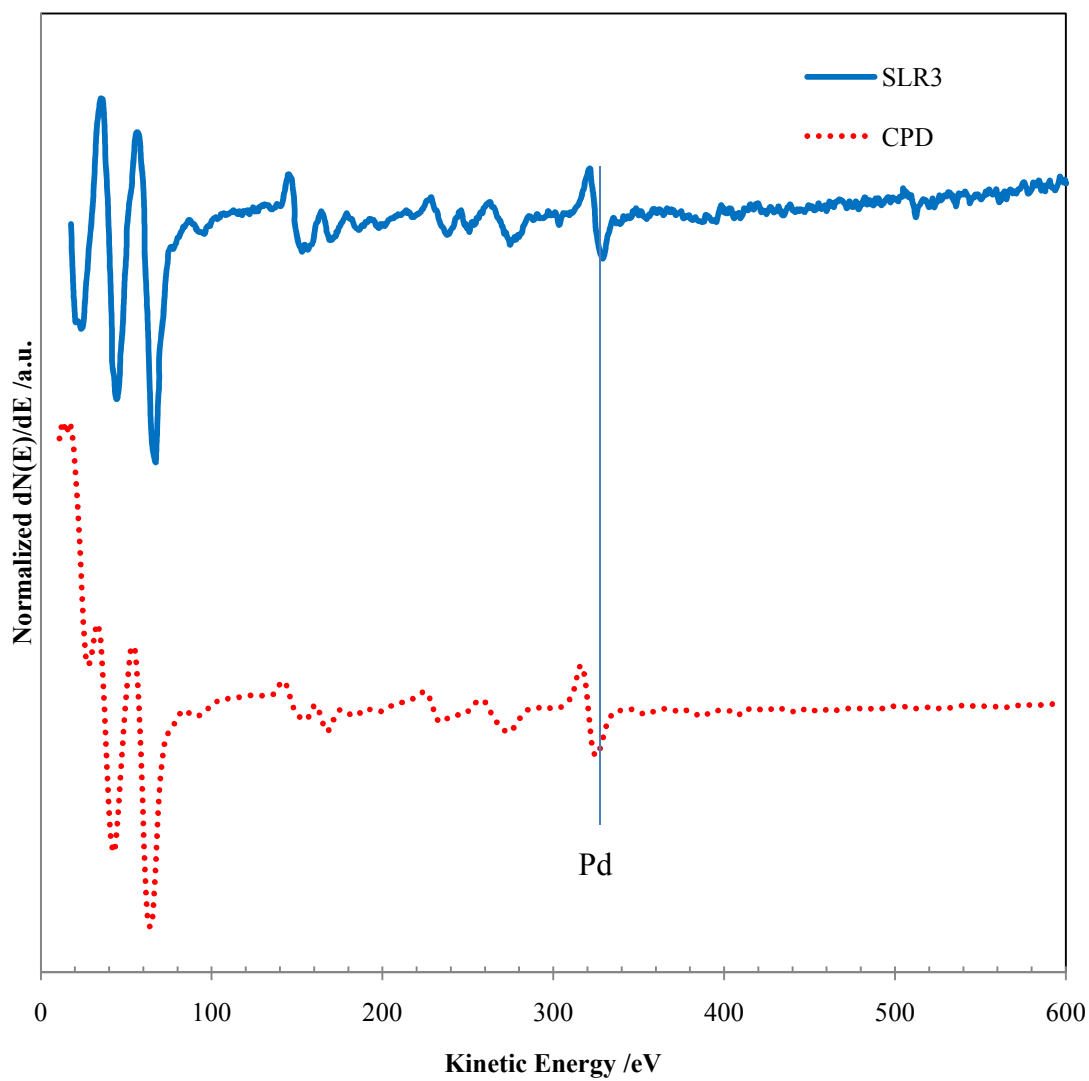**Fig. 28.** CV of 0.5 ML Pd film on Pt(111) in 100 mM sulfuric acid, r = 2 mV/s.
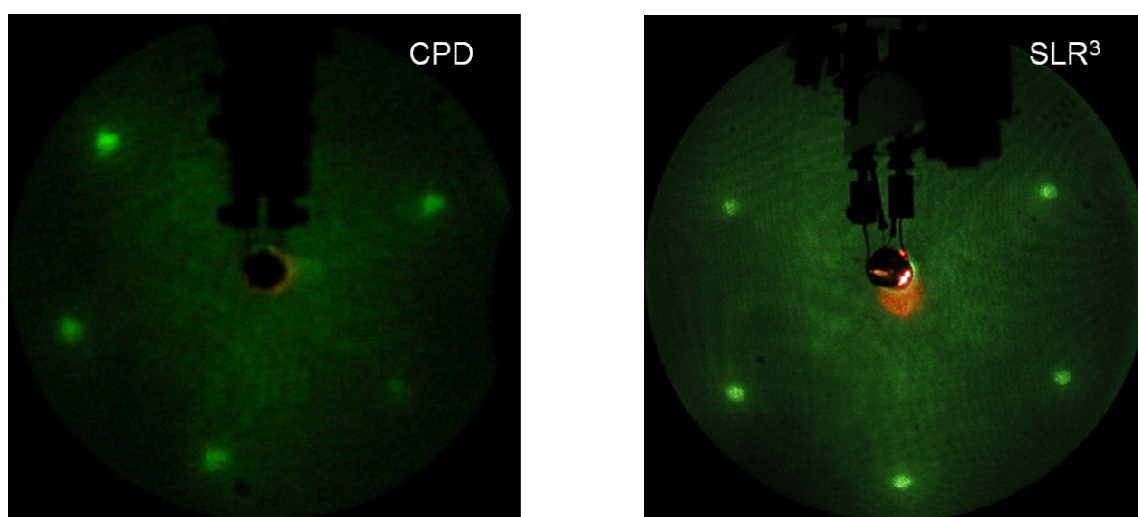
Fig. 29. AES spectra of 0.5 ML Pd films on Pt(111).

Fig. 30. LEED patterns for 0.5 ML Pd films on Pt(111). Beam energy 62 eV, Ip =2 µA.

characteristic Pt peaks (e.g., at 64, 94, and 237 eV) are still visible. These tend to suggest

that the Pt surface is not completely covered. The LEED patterns indicate (1×1) surface

structures for both films (Fig. 30). Based on AES and LEED data alone, however, it is

not possible to provide any definitive description regarding the surface structural

changes of the films prepared by these two methods. Further structural information could

have been derived by spot-intensity-vs.-beam-energy analysis. Such facility, however, is

currently unavailable in our laboratory. Nevertheless, an effort was made to evaluate the

intensities of the spots diffracted by the Pd films by analyzing the digital images of the

LEED patterns. The findings will be presented in a separate section.

3.2 $\Theta_{Pd} = 1$ ML

For monolayer Pd films on Pt(111), the H adsorption/desorption peaks at terrace

sites increased. They are sharper and larger for CPD films compared to SLR[3] films (Fig.

31). The H_{UPD} peaks at step sites are virtually non-existent for SLR[3] films (Fig. 31). The

AES spectra (Fig. 32) show similar features for both films. The AES peaks (e.g., at 94

and 237 eV) due to Pt are not as clear as those for 0.5 ML films. On the other hand, the

Pd peak at 330 eV increased compared to Pt peak (e.g., 237 eV). The absence of

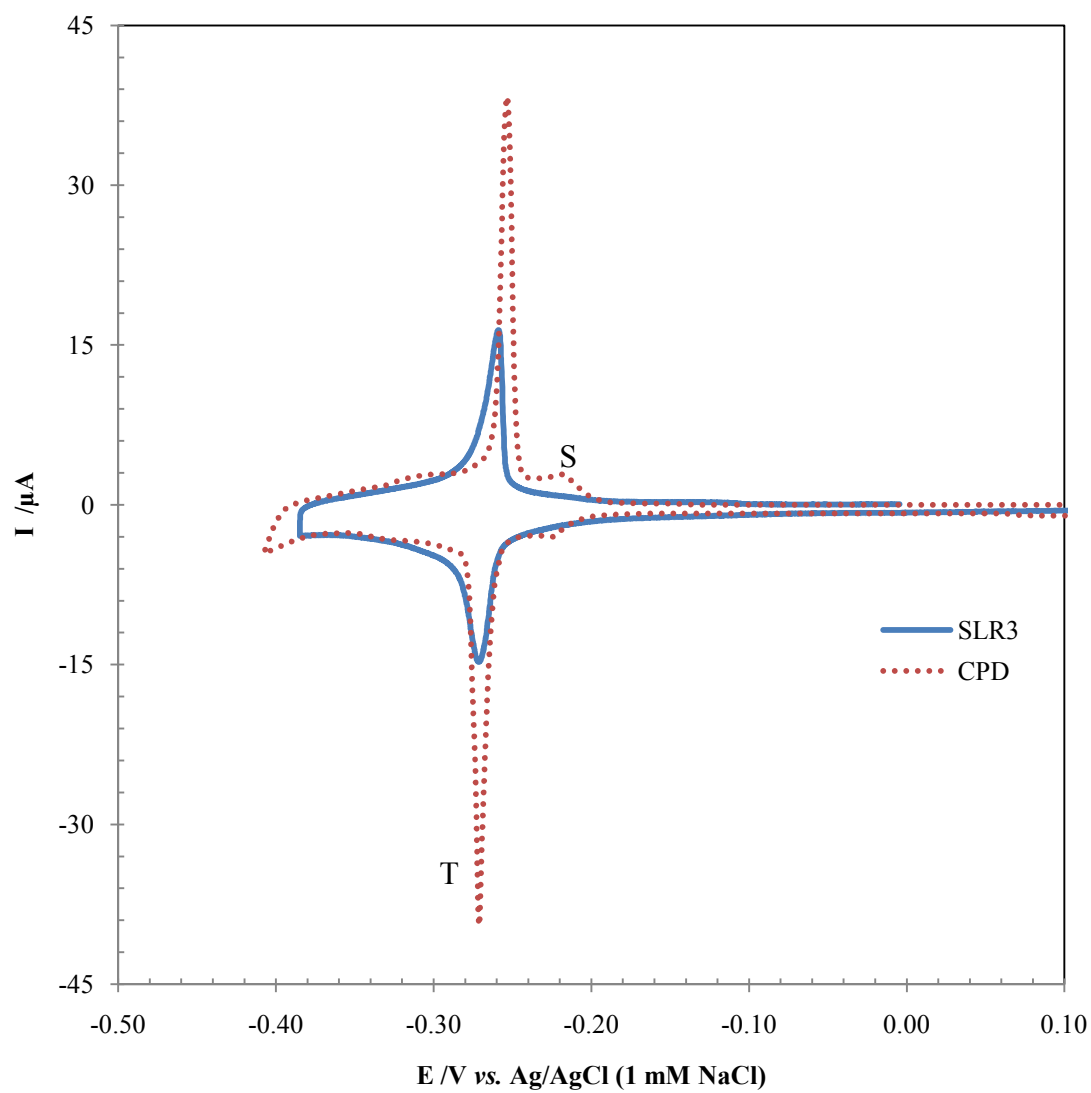characteristic Cu peak (at 105 eV) indicates complete exchange of Cu with Pd in SLR[3].

Fig. 31. CVs of 1 ML Pd films on Pt(111) in 100 mM sulfuric acid, r = 2 mV/s.
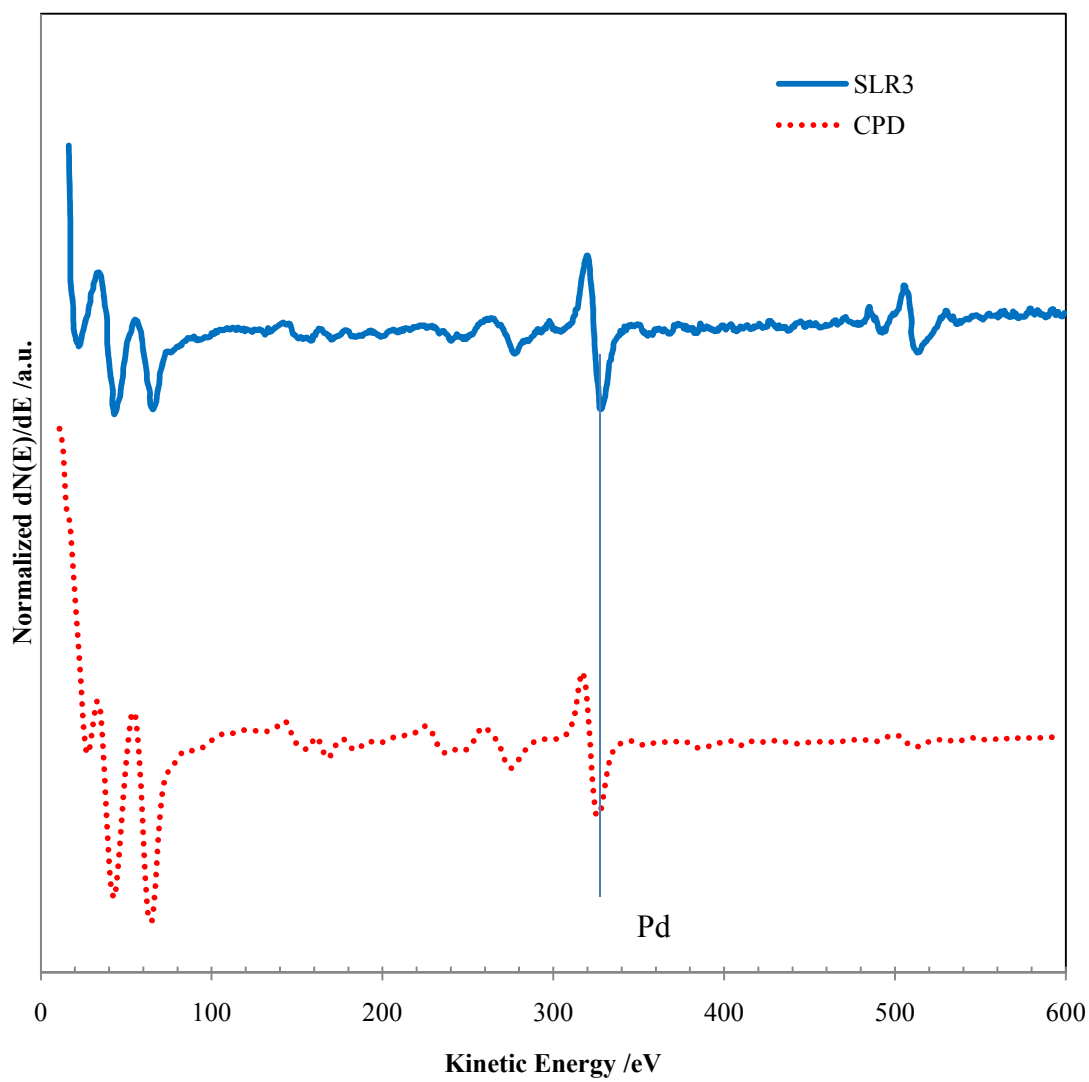
Fig. 32. AES spectra for 1 ML Pd films on Pt(111).

Both CPD and SLR^3 Pd films show (1×1) LEED patterns (Fig. 33). The spots are sharper

for the latter. The I_{ads}-catalyzed stripping of Pd films, however, looks somewhat different

for SLR^3 and CPD films (Fig. 34). The I_{ads}-catalyzed Pd dissolution peak at ca. 0.55 V

for SLR^3 film is not as well-defined as that for CPD film. The area under the Pd

dissolution peak (i.e., dissolution charge) is the same for both films though. For clarity,

the iodine to iodide oxidation peak for CPD films in the anodic stripping was not

displayed. In any case, this peak is expected to be same for both films and independent

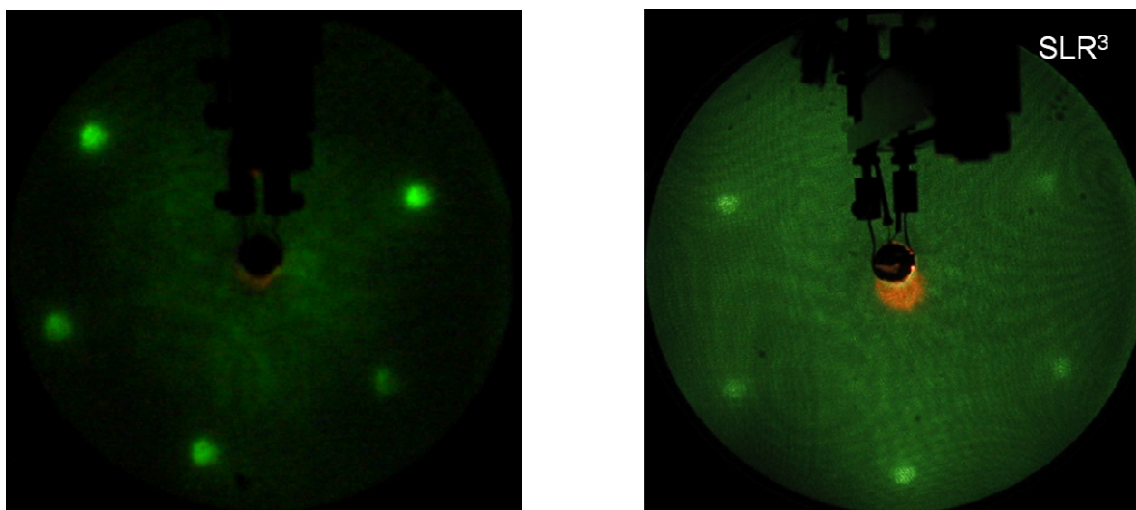of the Pd coverage since this is a surface-limited reaction.

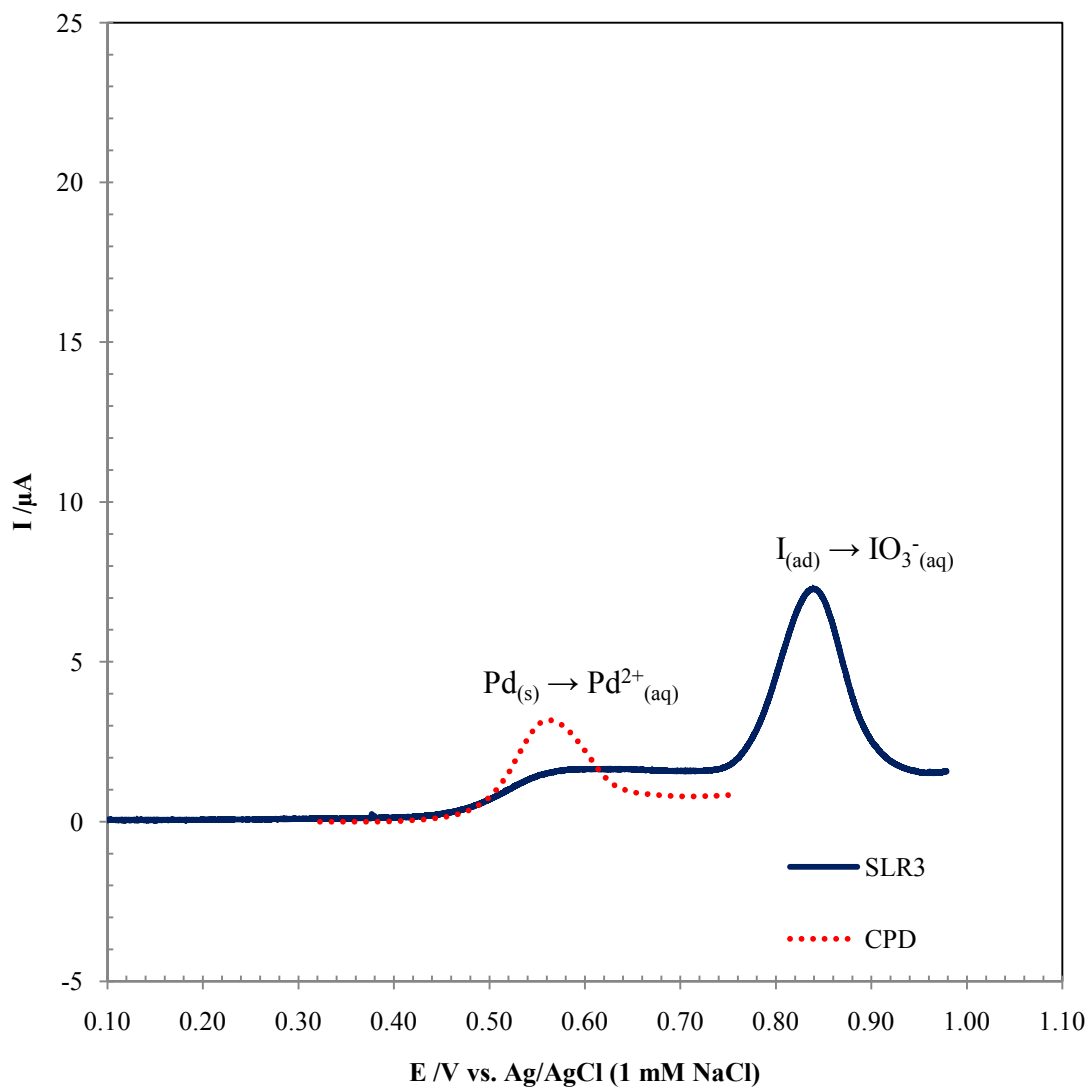**Fig. 33.** LEED patterns observed for 1 ML Pd film on Pt(111).

Fig. 34. I_{ads}-catalyzed stripping of 1 ML Pd film on Pt(111) in 100 mM sulfuric acid. (r = 0.5 mV/s).

3.3 $\Theta_{Pd} = 2$ ML

For 2 ML Pd films, the H_{UPD} peaks are sharper compared to those for the SLR[3] films. CPD films show a small peak at a little higher positive potential which have been assigned to H_{UPD} adsorption/desorption peaks at the step sites. SLR[3] film barely indicates the existence of this peak (Fig. 35). The AES spectra (Fig. 36) and LEED patterns (Fig. 37) for both films look similar. Again for SLR[3] films, there was no indication of Cu in the AES spectrum. The EC results tend to indicate that the films prepared via SLR[3] are more uniform and smoother.

3.4 $\Theta_{Pd} = 4$ ML

The CVs for 4 ML Pd films in the of H_{UPD} region are dramatically different (Fig. 38). For CPD films the H_{UPD} peak areas at step sites are higher than those at the terrace sites. This indicates that the films produced by SLR[3] are relatively smoother than those of made via CPD. The AES spectra (Fig. 39), LEED patterns (Fig. 40), and I_{ads}-catalyzed dissolution voltammetric waves (Fig. 41) for both Pd films are almost identical. The AES Pt features are masked by the Pd features. The peaks due to Cu are also absent in the AES spectrum for SLR[3] films (Fig. 39). LEED patterns indicate (1×1) structure for both films (Fig. 40). The I_{ads}-catalyzed stripping of Pd for SLR[3] films show a small peak at ca. 0.66 V. This feature, however, is not resolved for the CPD film (Fig. 41).
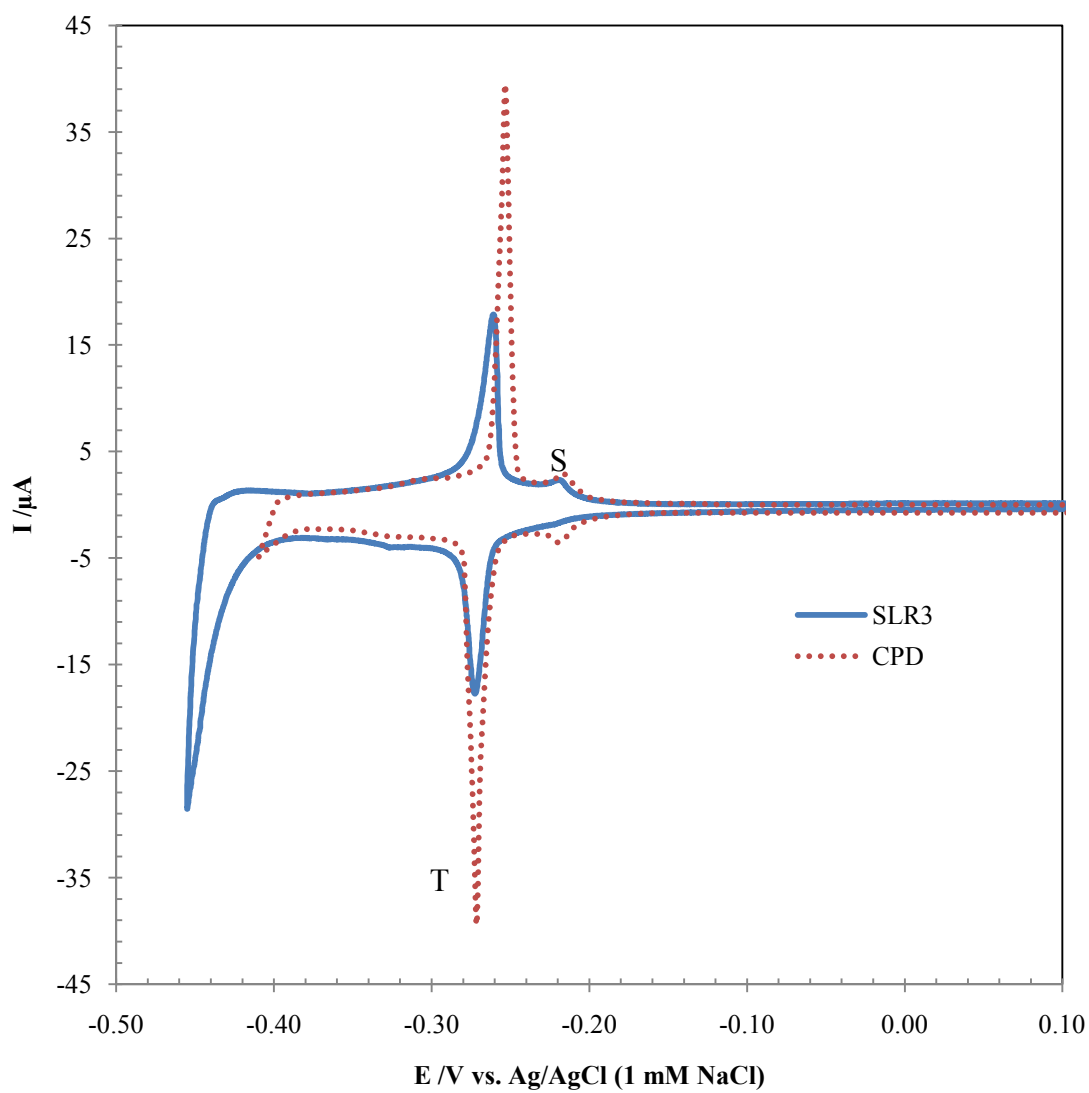
Fig. 35. CVs of 2 ML Pd films deposited on Pt(111) in 100 mM sulfuric acid, r = 2 mV/s.
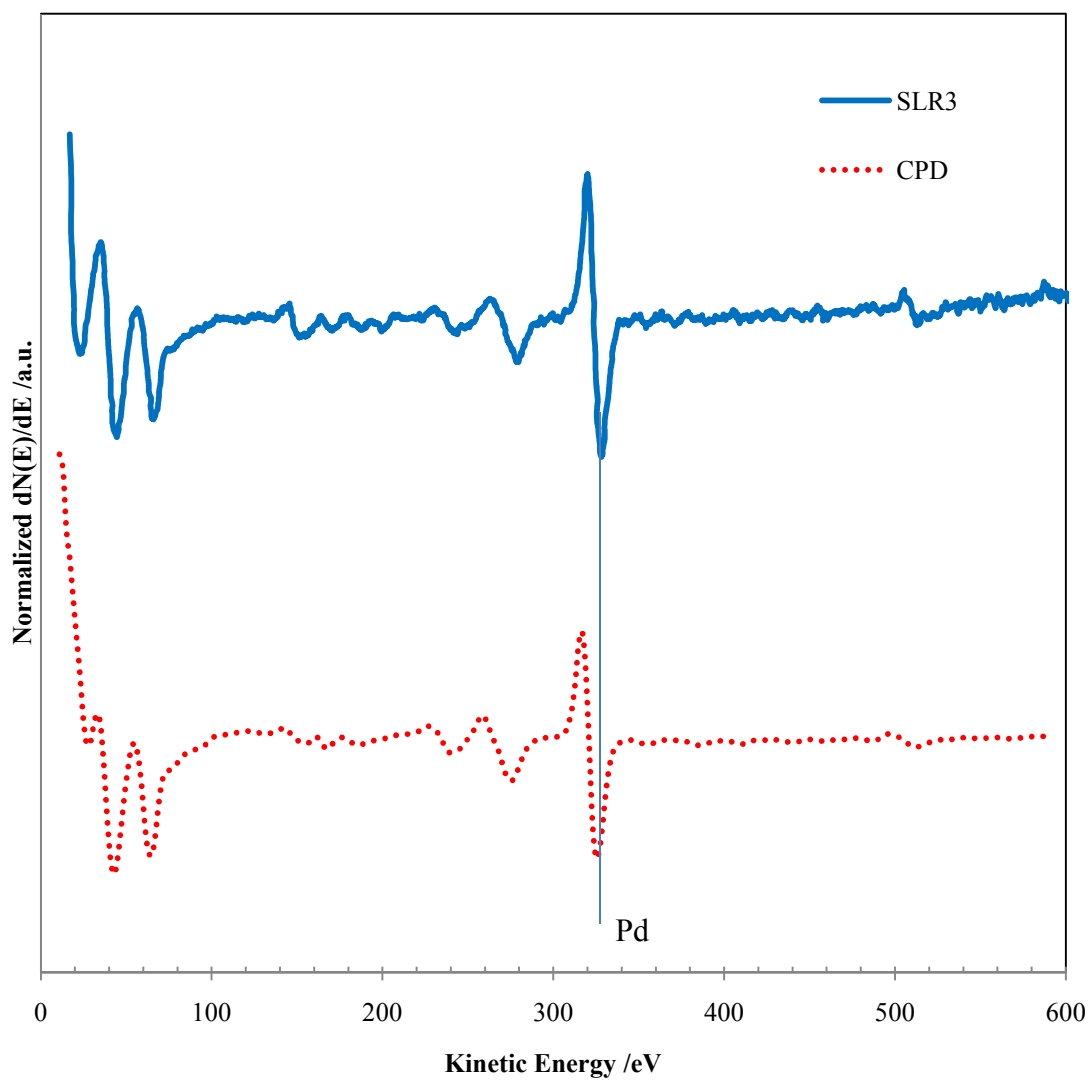
Fig. 36. AES spectra for 2 ML Pd films grown on Pt(111).

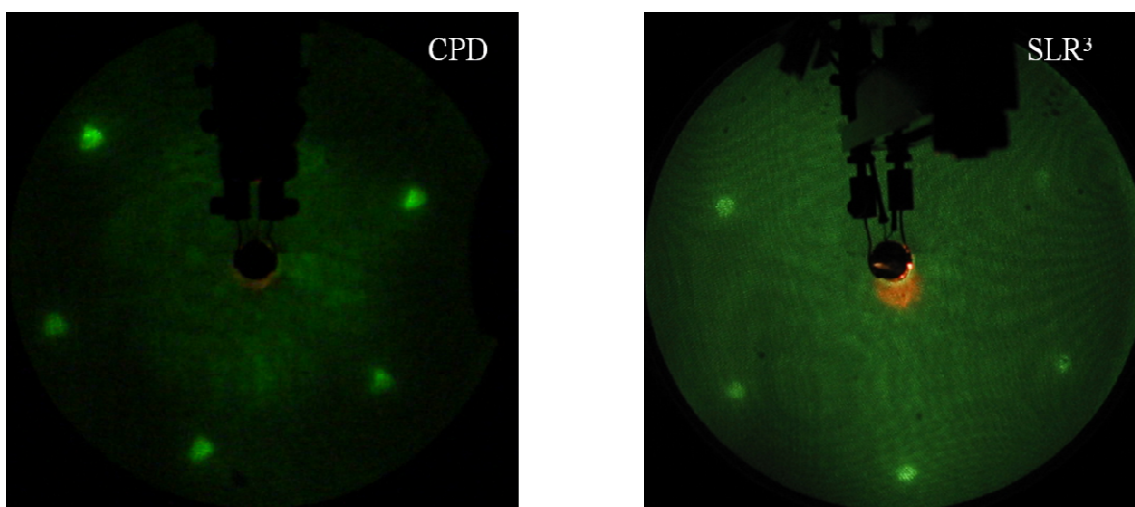**Fig. 37.** LEED patterns for 2 ML Pd films deposited on Pt(111), Beam energy = 62 eV, Ip = 2 μA.
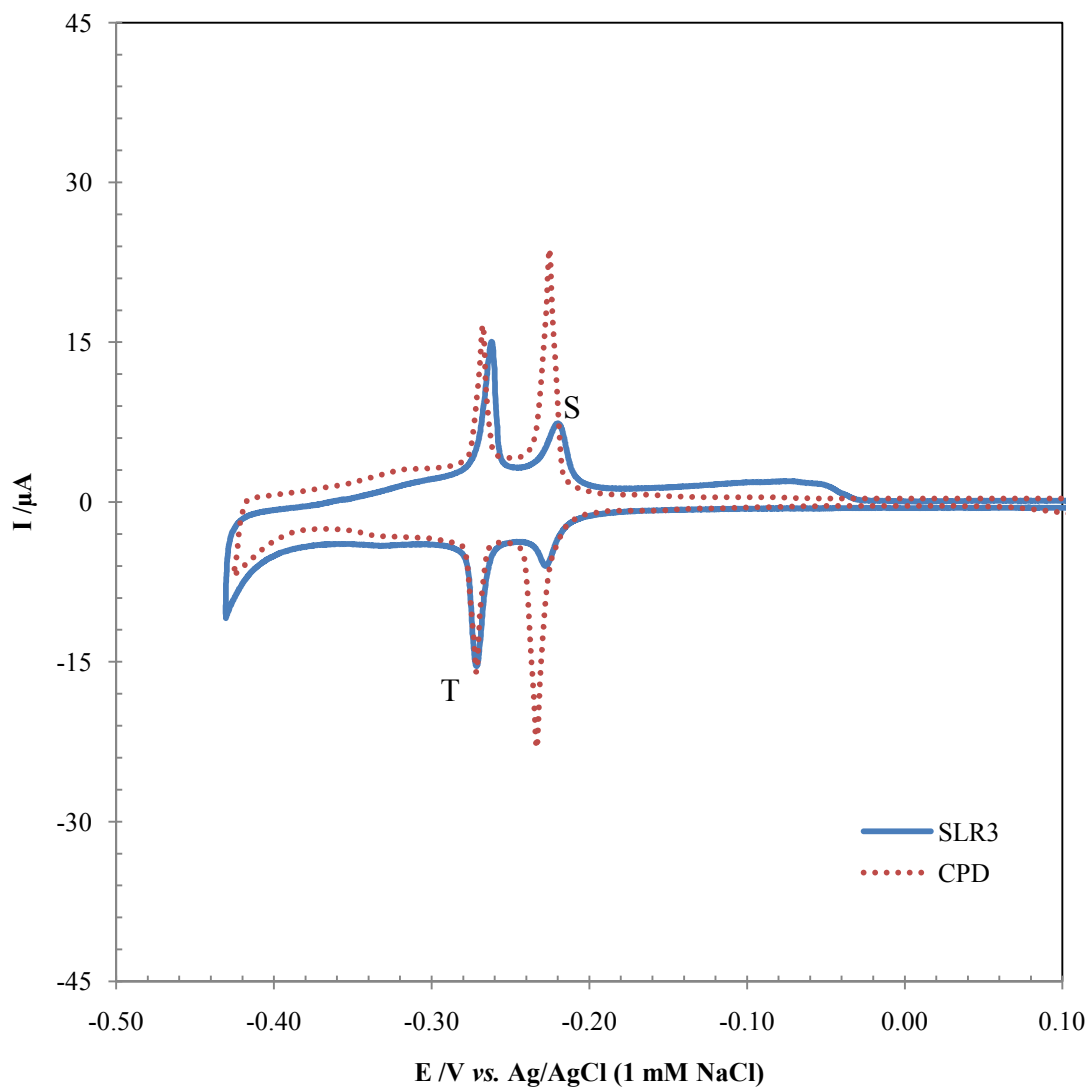
Fig. 38. CVs of 4 ML Pd films deposited on Pt(111) in 100 mM H_2SO_4.(r = 2 mV/s).
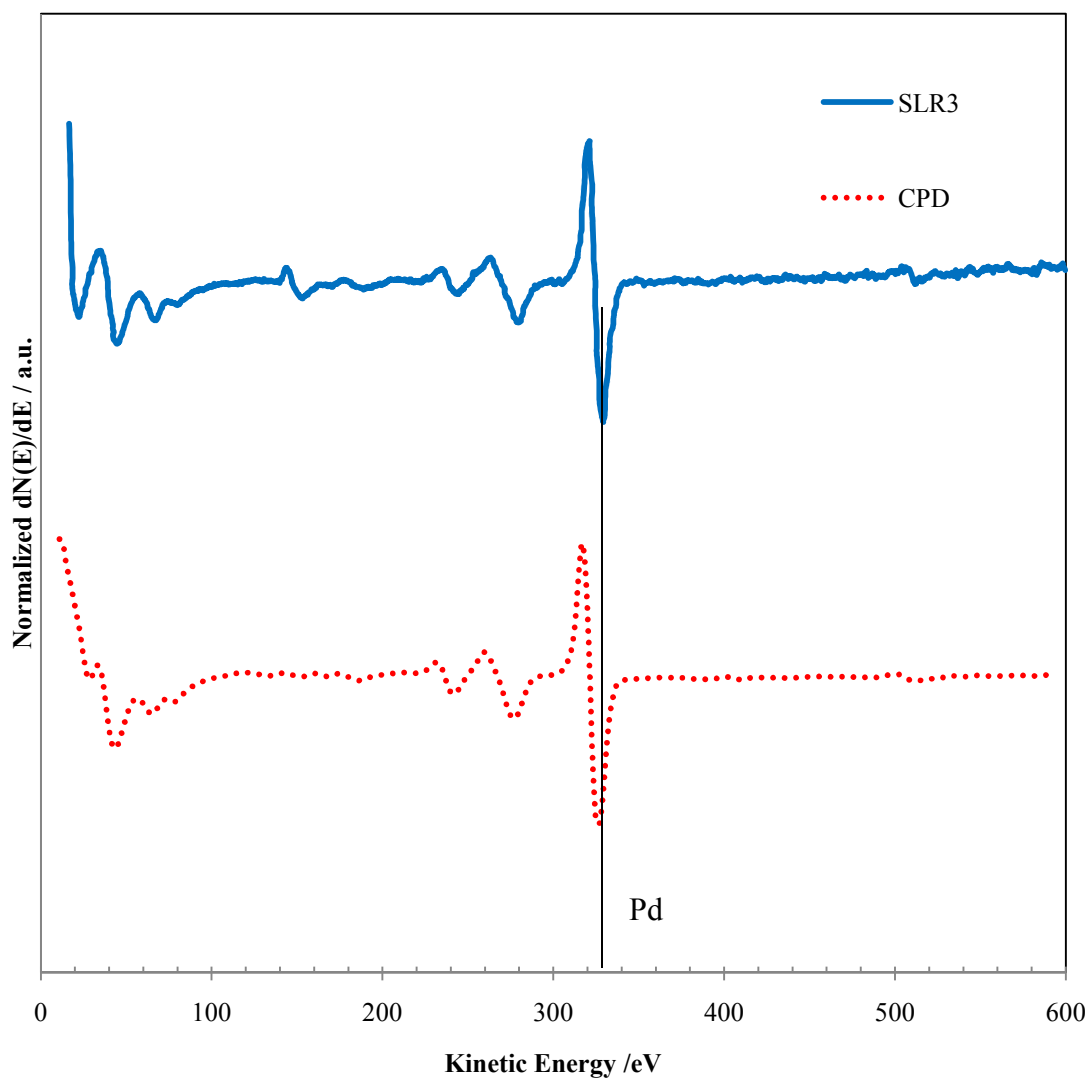
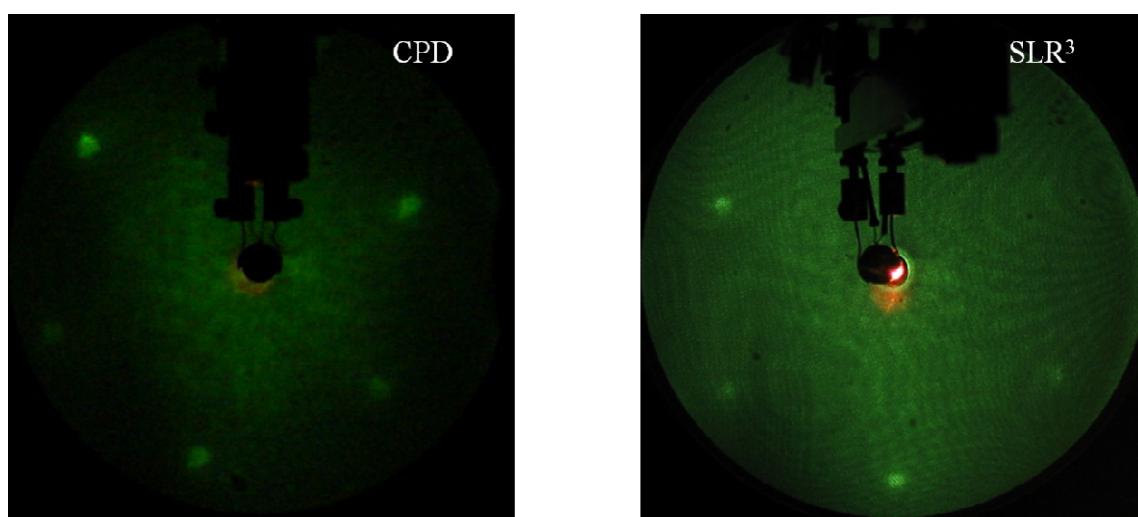**Fig. 39.** AES spectra for 4 ML Pd films deposited on Pt(111).

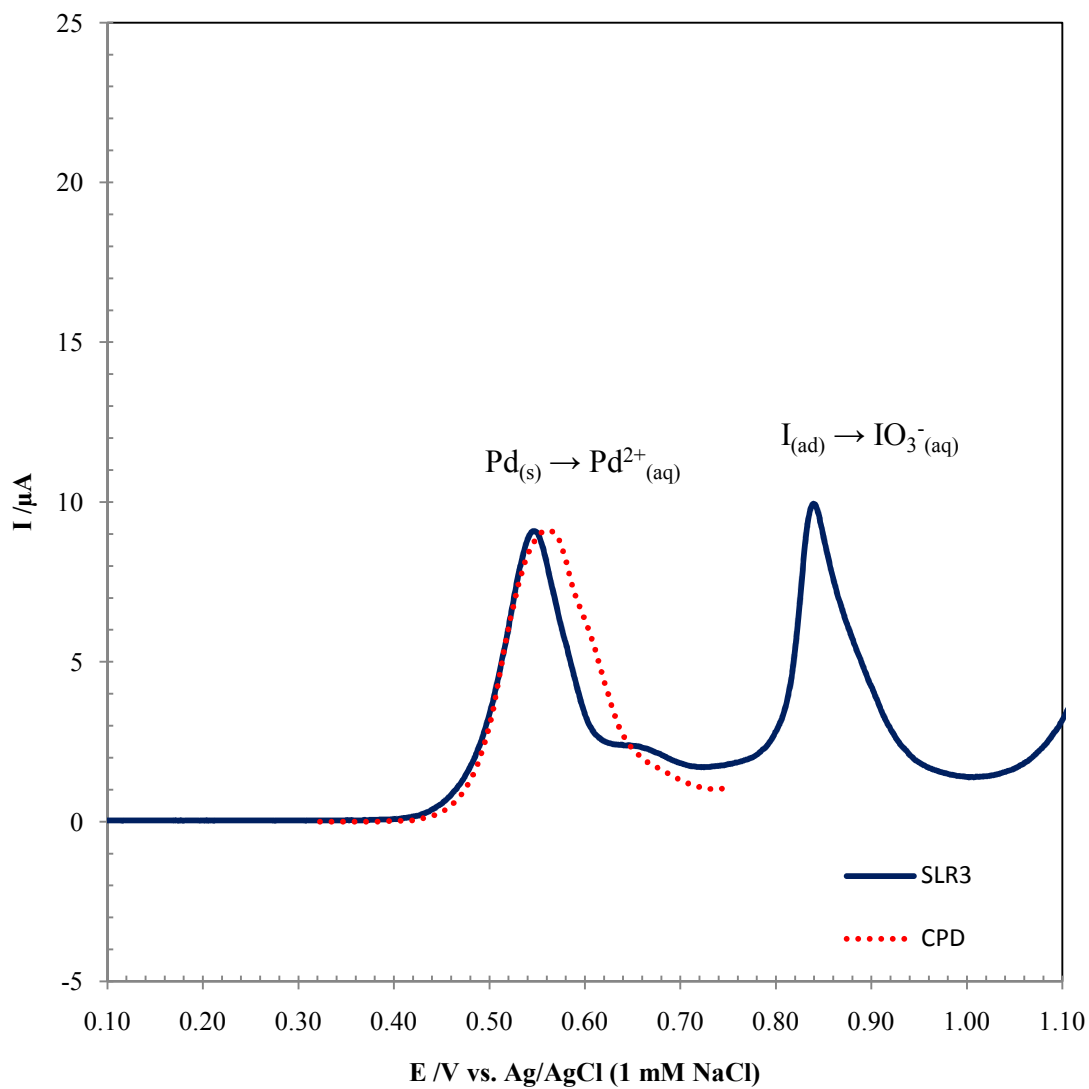**Fig. 40.** LEED patterns for 4 ML Pd films deposited on Pt(111).

Fig. 41. I_{ads}-catalyzed dissolution of 4 ML Pd films on Pt(111) in 100 mM H_2SO_4. (r = 0.5 mV/s).

3.5 Θ_{Pd} = 8 ML

For 8 ML thick-films, the H_{UPD} profiles are similar (Fig. 42) for both kinds of films. The presence of hydrogen adsorption/desorption peaks in CVs arising from the step sites indicate that the films are relatively rougher for both methods at this coverage. It is noteworthy that even at this high coverage, the AES spectrum for SLR[3] films did not show any signal associated with Cu (Fig. 43). Both films show (1×1) LEED patterns (Fig. 44). The I_{ads}-catalyzed dissolution of the films shows identical behavior (Fig. 45). Fig. 46 shows the I_{ads}-catalyzed anodic stripping of SLR[3] films at a higher scan rate (2 mV/s). This shows similar Pd dissolution features as observed for a scan rate of 0.5 mV/s. It was found that only one scan is enough to strip Pd films from Pt surface quantitatively. Fig. 47 shows the anodic stripping profile in iodide free 100 mM sulfuric acid where iodine was readsorbed following the anodic dissolution of 8 ML Pd films prepared by SLR[3]. The voltammogram is flat at potential regions where Pd to Pd^{2+} oxidation takes place and only the peak due to iodine to iodate oxidation observed. This indicates that the Pd films are completely removed by I_{ads}-catalyzed stripping. Fig. 48 shows the AES spectrum following 2 cycles of I_{ads}-catalyzed stripping of 8 ML SL[3] Pd films. The AES peaks associated with Pt also reemerged. It barely shows a hint of one of the three Pd AES peaks. Compared to the big Pd peaks in Fig. 43, the amount of Pd is insignificant given the higher AES relative sensitivity factor of Pd (S_{Pd} = 0.8). The surface structure of the electrode following the I_{ads}-catalyzed anodic dissolution of Pd
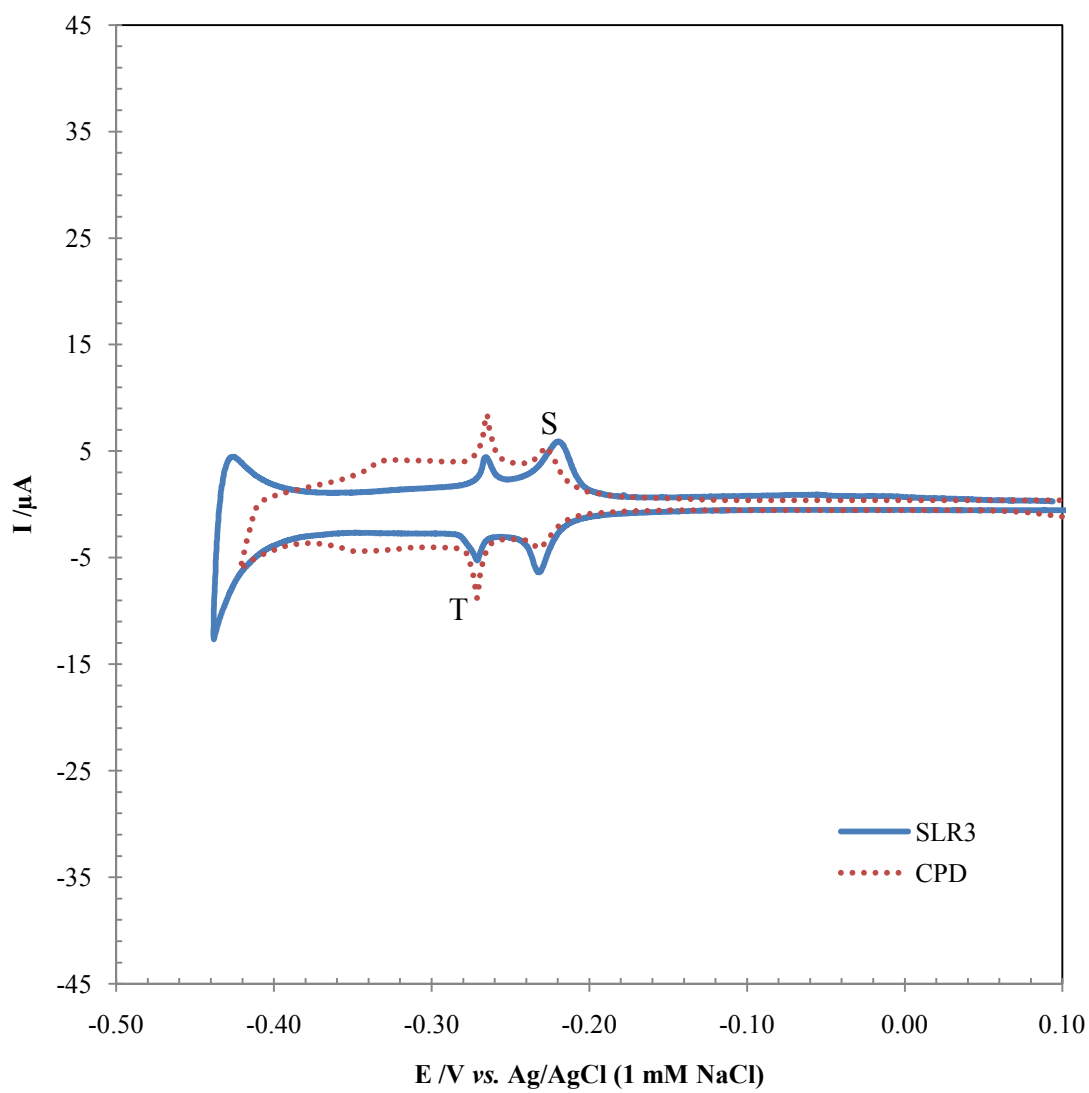
Fig. 42. CVs of 8 ML Pd films on Pt(111) in 100 mM H_2SO_4, r = 2 mV/s.
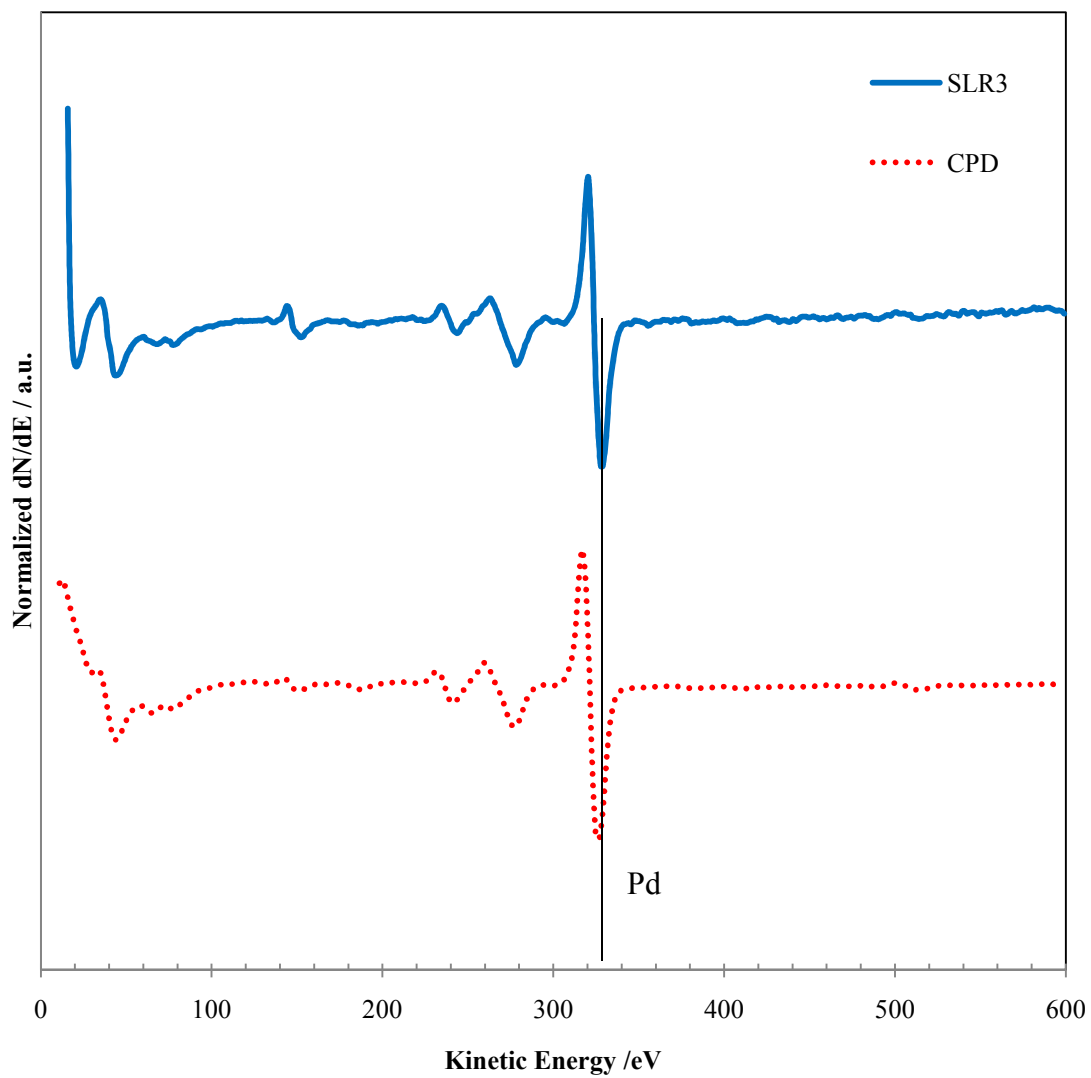
Fig. 43. AES spectra for 8 ML Pd films deposited on Pt(111).
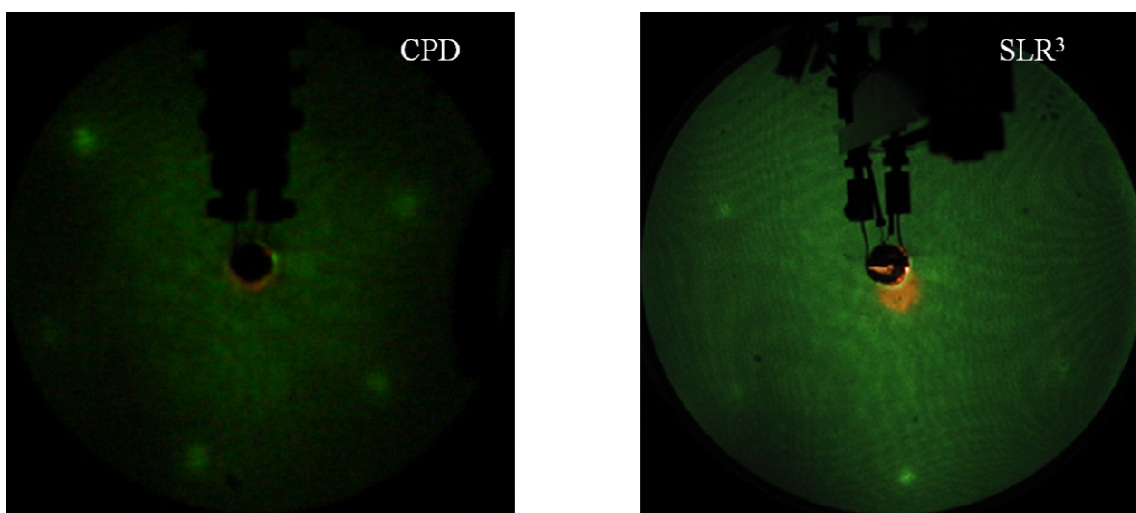
Fig. 44. LEED patterns for 8 ML Pd films deposited on Pt(111). Beam energy = 62 eV,

Ip = 2 μA.
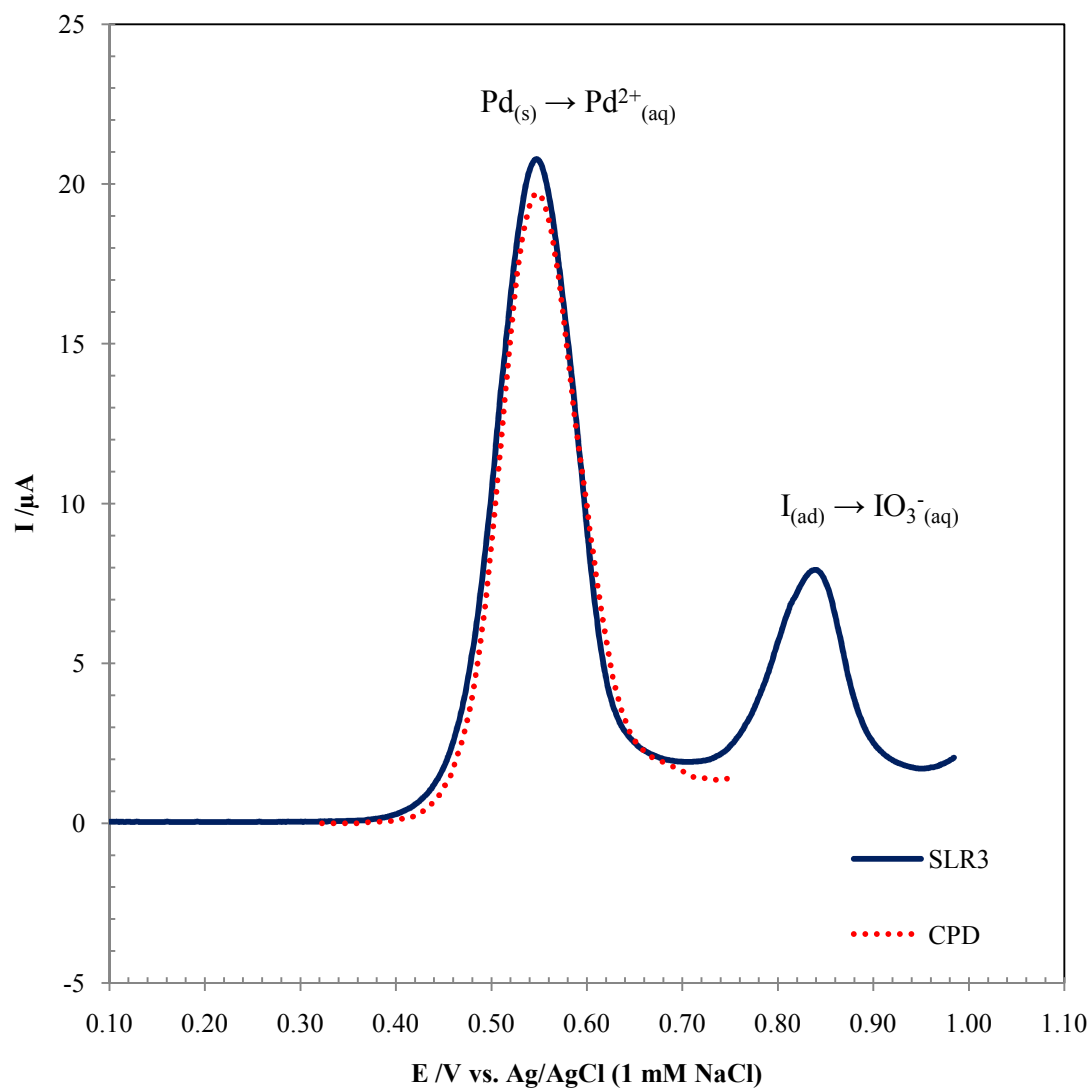
Fig. 45. I_{ads}-catalyzed anodic dissolution of 8 ML Pd films deposited on Pt(111) in 100 mM H_2SO_4. (r = 0.5 mV/s).
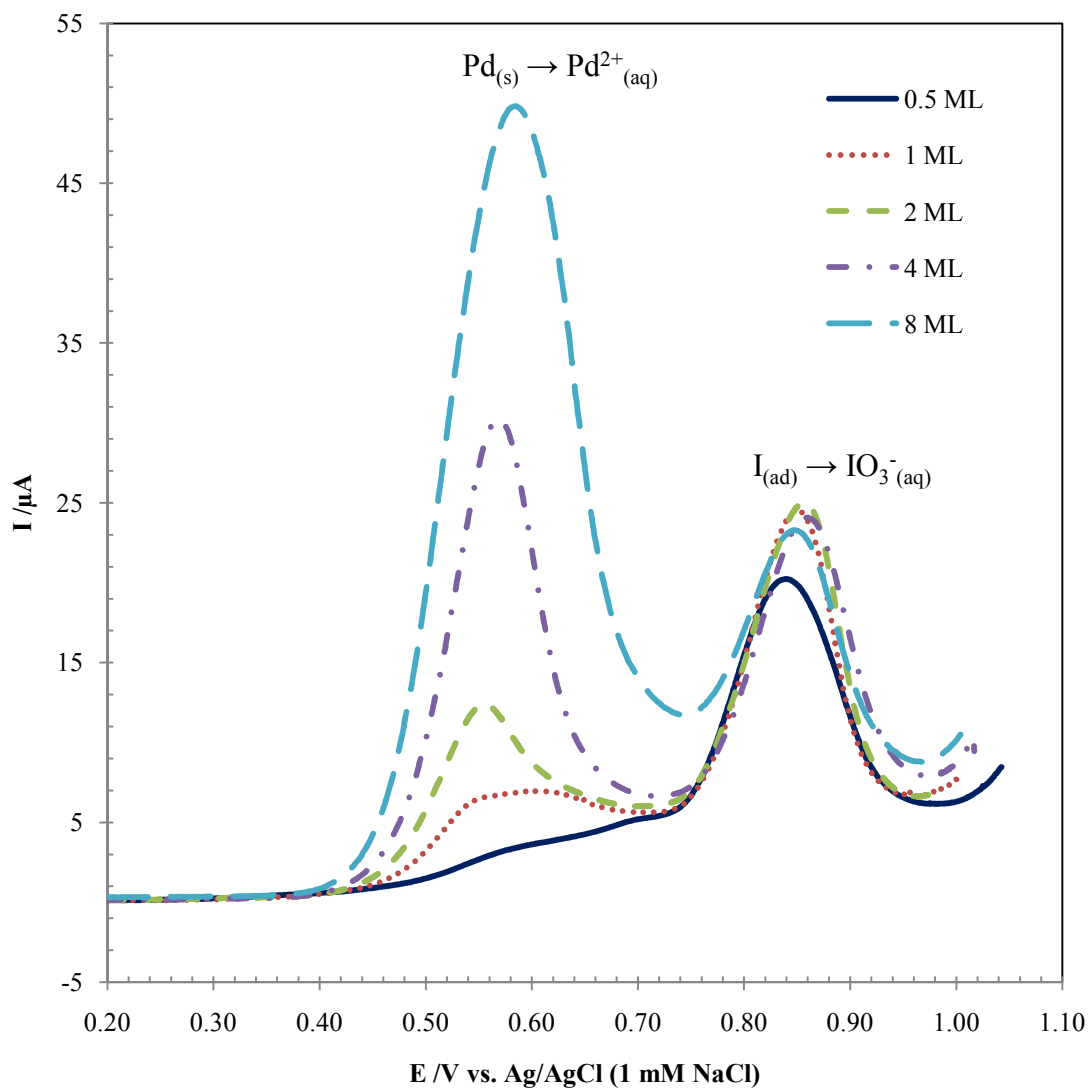
Fig. 46. I_{ads}-catalyzed anodic dissolution of SLR[3]-prepared Pd films deposited on Pt(111) in 100 mM H_2SO_4, r = 2 mV/s.
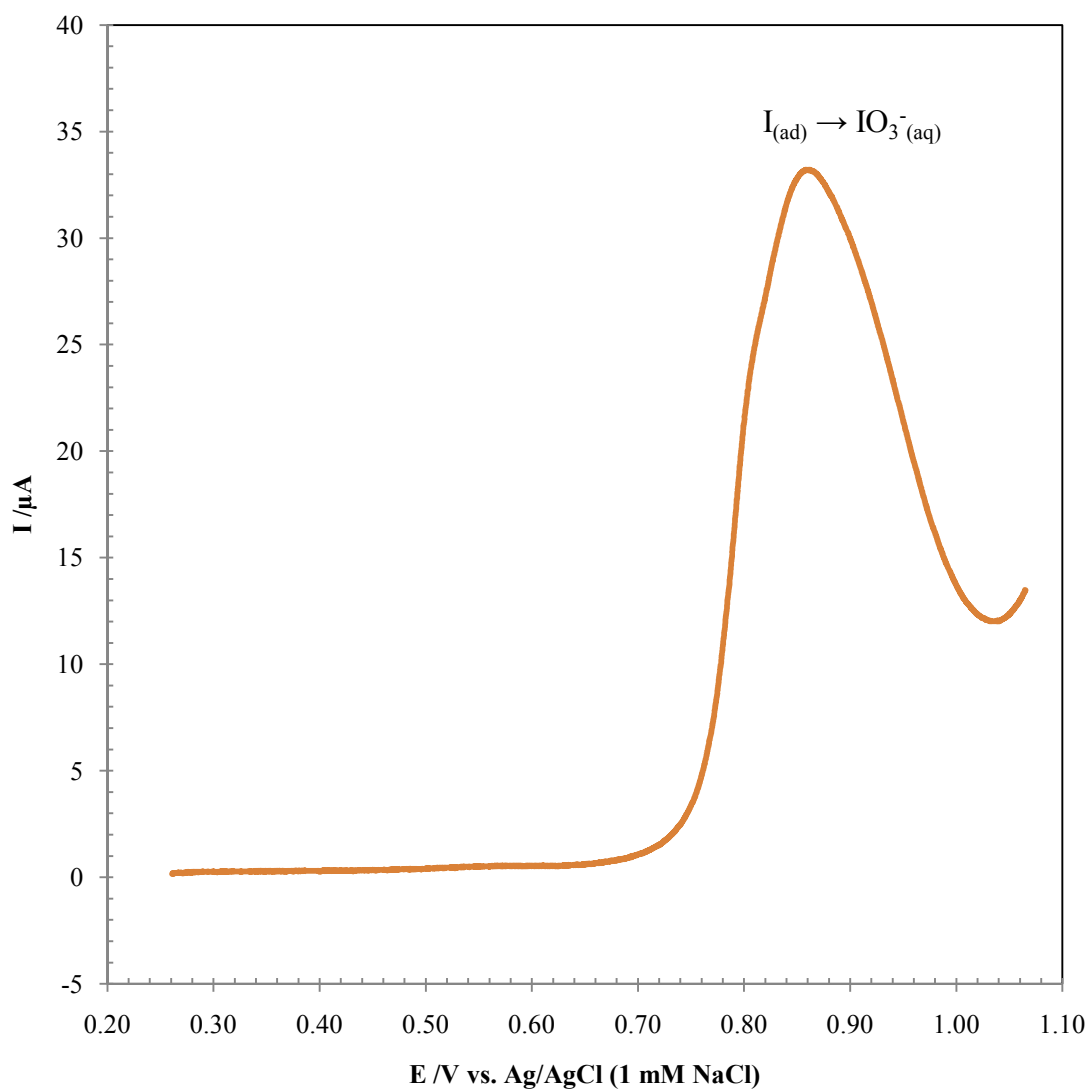
Fig. 47. 2nd scan of I_{ads}-stripping of SLR^3-prepared 8 ML Pd on Pt(111) (following readsorption of iodine) in 100 mM H_2SO_4 (r = 2 mV/s).
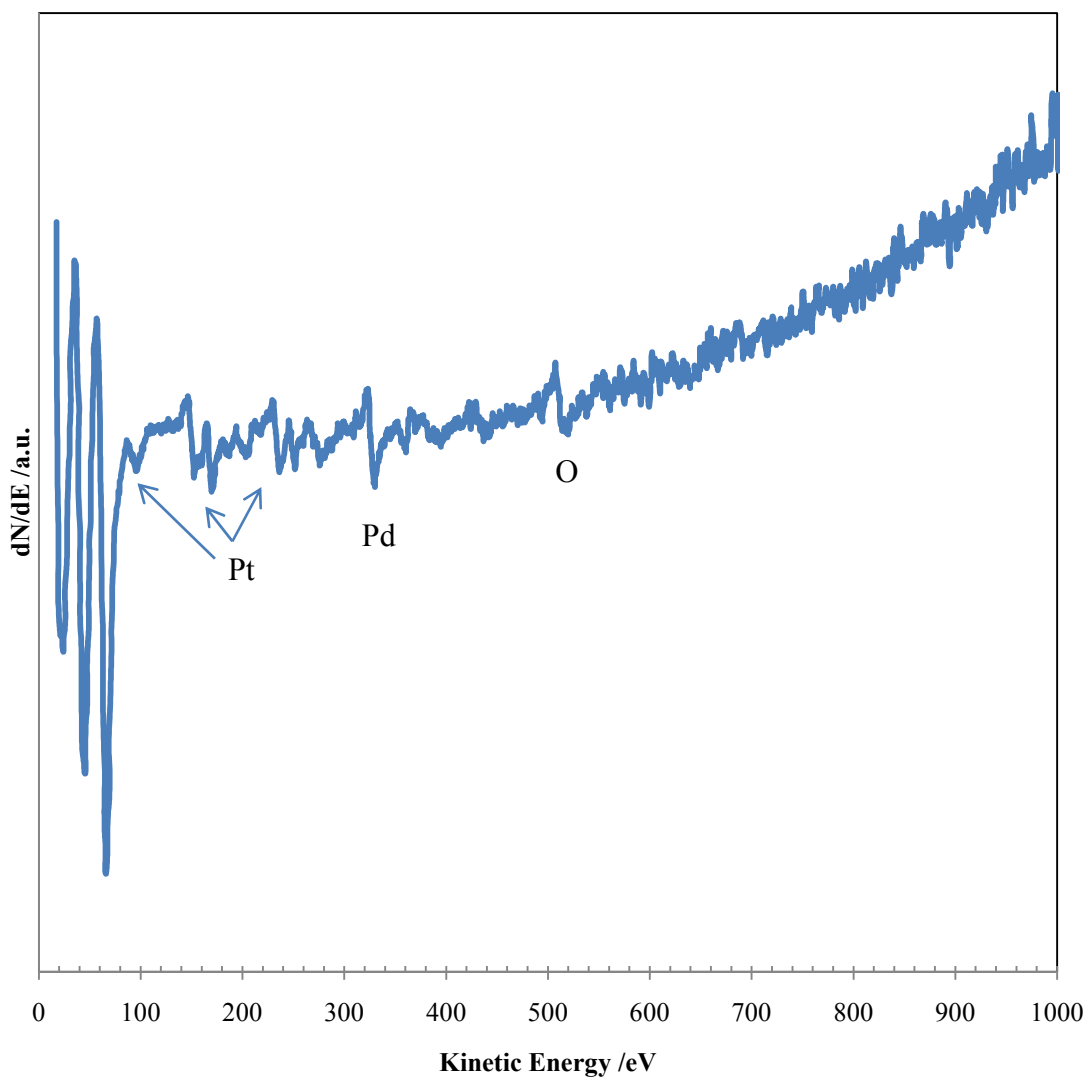
Fig. 48. AES spectrum following 2 cycles of I$_{ads}$-catalyzed stripping of SLR^3-prepared 8 ML Pd/Pt(111).

films is dependent on the emersion potential and history. Typically, the surface is disordered following the stripping of Pd films as Pt surface is also oxidized at these potentials. If the electrode is emersed and rinsed at OCP, the surface order is restored as can be seen in Fig. 49. This (1×1) LEED pattern was obtained when the electrode was emersed and allowed to equilibrate at OCP following I-catalyzed removal of ca. 3.2 ML (after 4 cycles of SLR[3]) Pd films.

3.6 Trends

Analysis of the data collected for both SLR[3] and CPD films demonstrates a few trends. According to electron spectroscopic observations, both films showed similar properties and indicated the formation of ordered ultrathin films. The digital images of the LEED patterns were analyzed by Origin Pro 8.5 software. Fig. 50 represents the 3D colormap surface of the digital image of the LEED pattern for a clean Pt(111) electrode. The brightest spot was selected for detailed analysis. The same spot was utilized for all LEED images to evaluate the pixel intensity profiles. A typical line trace analysis of the LEED spot is displayed in Fig. 51. The blue trace at the top of Fig. 51 shows the pixel intensity profile along the horizontal line passing through the selected spot while the red trace on the right side represents that along the vertical line. The horizontal line profile was used to compare the LEED images for various Pd films.

Fig. 49. LEED pattern of Pt(111) following the I_{ads}-catalyzed stripping of SLR^3-prepared ca. 3.2 ML Pd. After the stripping, the electrode was rinsed with blank at OCP. (Beam energy = 62 eV, I_P = 2 µA).
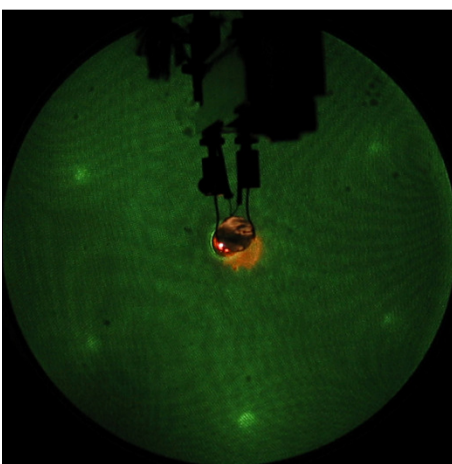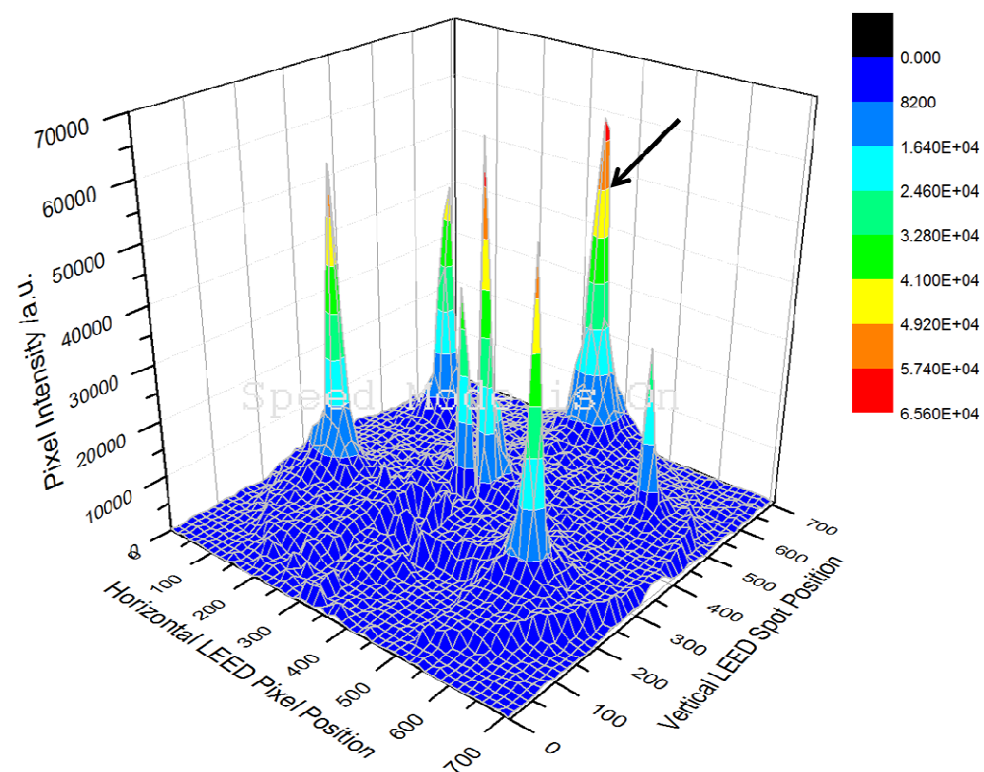
Fig. 50. 3D colormap surface of the image of the LEED pattern for clean Pt(111) electrode. The arrow indicates the spot chosen for pixel intensity analysis.
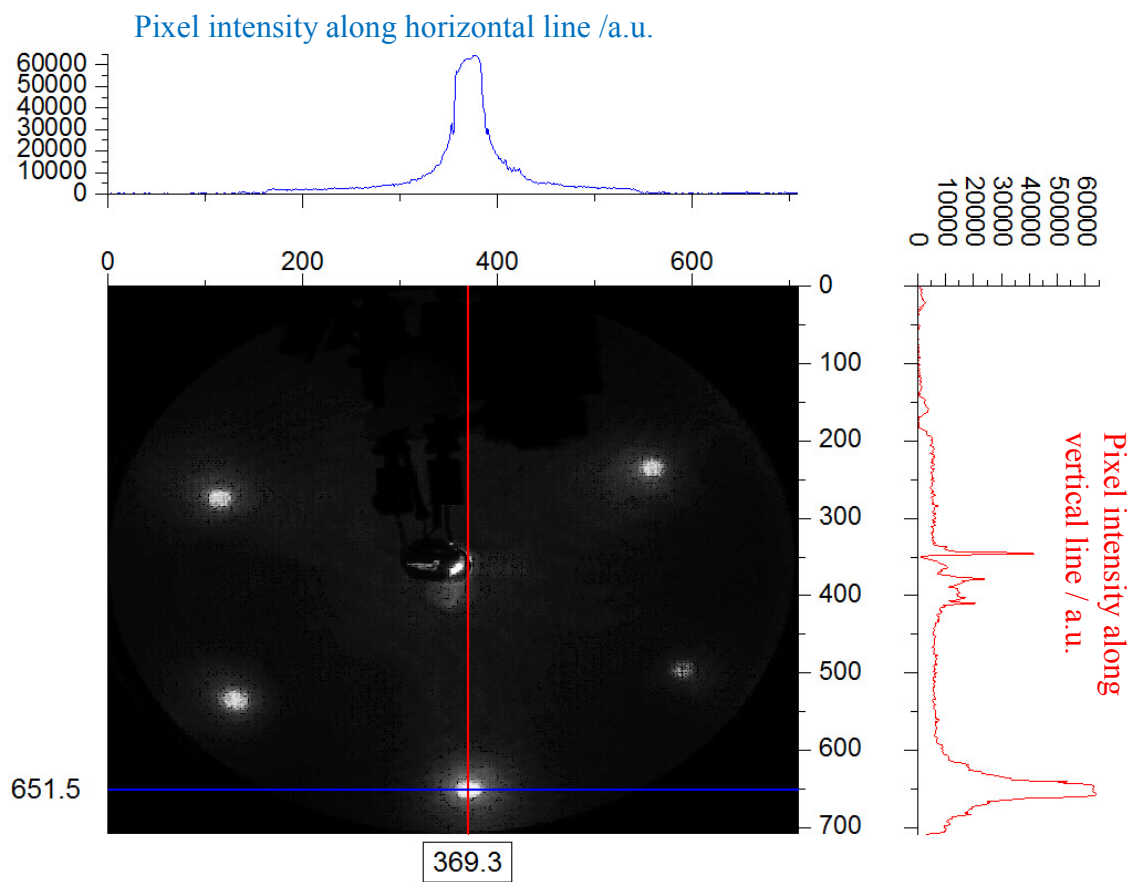
Fig. 51. Line trace analysis of LEED spot.

Fig. 52 displays the normalized pixel intensities from the analysis of LEED spots at various Pd coverages. The intensities were normalized with respect to intensities from clean Pt(111) LEED patterns for SLR[3] and CPD Pd film studies. Fig. 53 refers to the full-width at half maximum of the line trace analysis of the LEED spot. The variation in spot diameters with Pd film thickness is given in Fig. 54. For both films, the LEED spots get a little dimmer with increasing coverage but they were still sharp indicating long range surface order of the resulting films. It should be underscored, however, that the LEED spot analysis performed here is for qualitative evaluations only. Electrochemical methods, on the other hand, reveal some details and minor differences. First of all, both films maintain ultrathin properties even at 8 ML coverage and show unique voltammetric signatures in the hydrogen UPD region. Such behavior is non-existent for bulk Pd surfaces.

Figs. 55 and 56 show the variation of H_{UPD} desorption charge with Pd coverage for CPD and SLR[3] films, respectively. The H_{UPD} desorption charge was measured by integrating the area under the desorption peak in the cyclic voltammograms (in 100 mM H_2SO_4 at 2 mV/s) as illustrated by Hoyer et al. [95]. Initially, both films show an increase of H_{UPD} desorption charge from terrace sites with increase in Pd coverage. Then at a coverage of ca. 4 ML, the H_{UPD} desorption charge decreases with further increase in Pd coverage whereas the H_{UPD} charge from steps sites or terrace sites on multilayer Pd films starts to increase at a coverage of 4 ML. The total H_{UPD} desorption charge also starts to decline after 2 ML.

Fig. 52. Comparison of pixel intensities from the LEED spot analysis for Pd films at various coverages.

Fig. 53. FWHM of LEED spot line trace analysis profiles for Pd films.

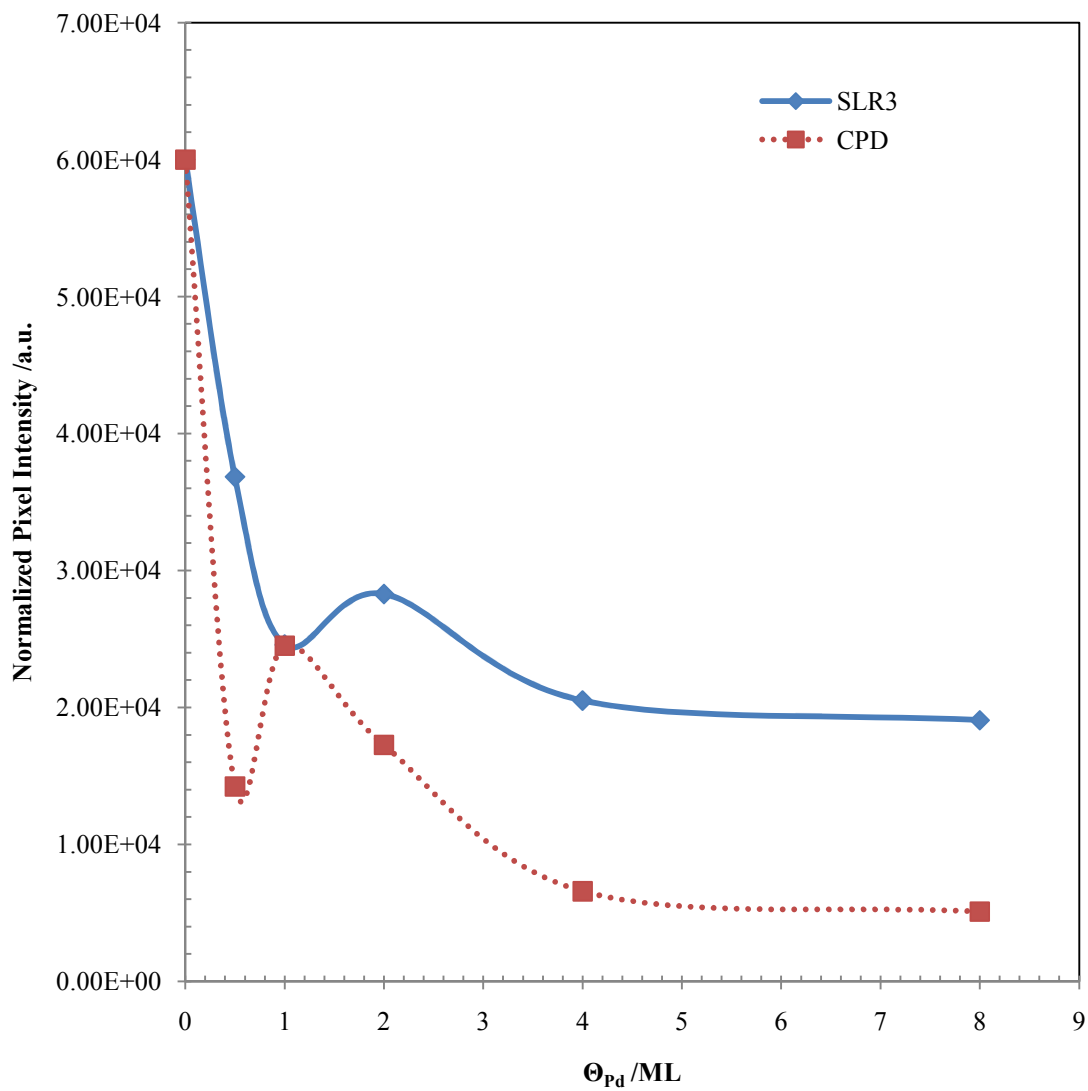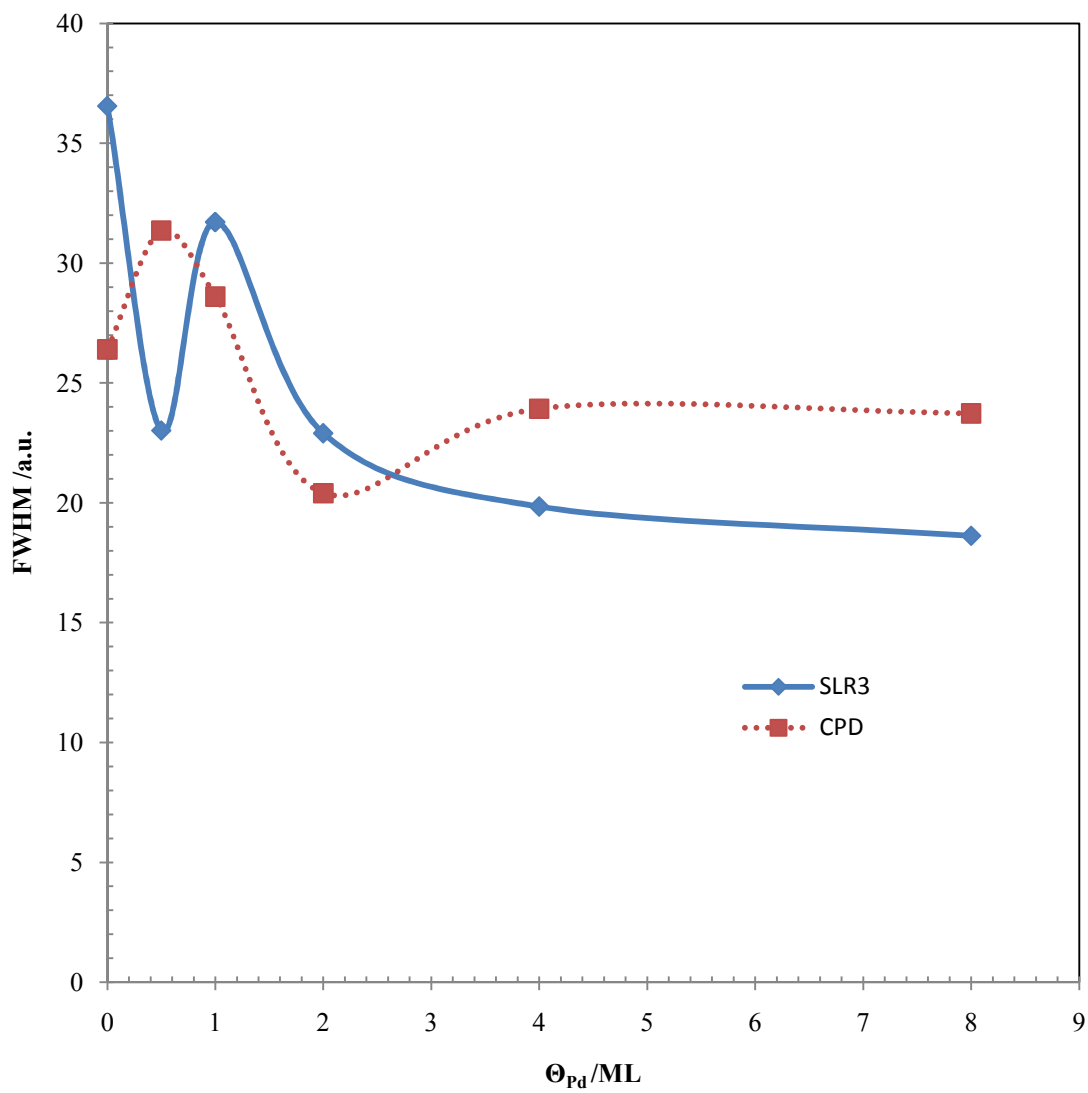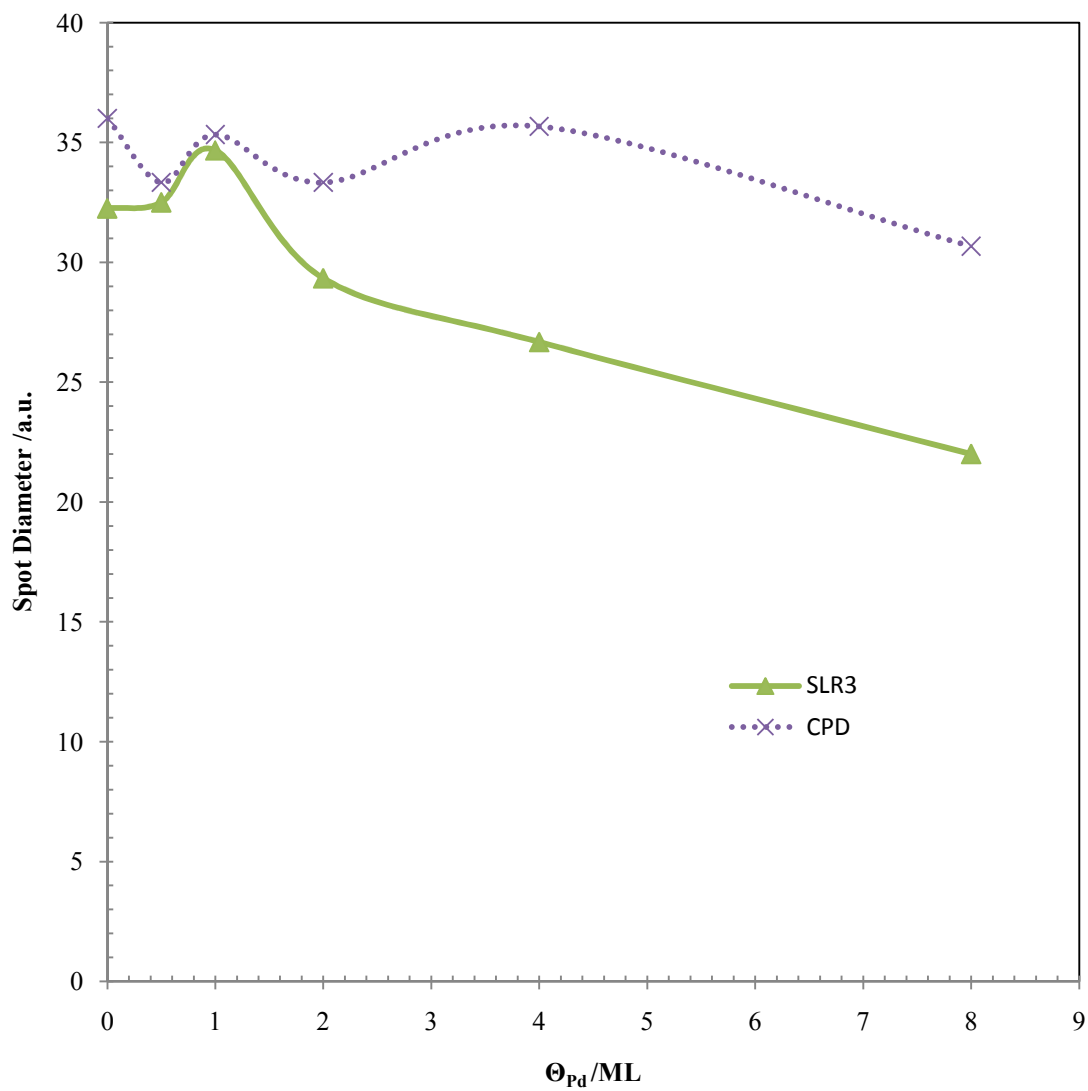**Fig. 54.** Variation of LEED spot diameter with Pd coverage.
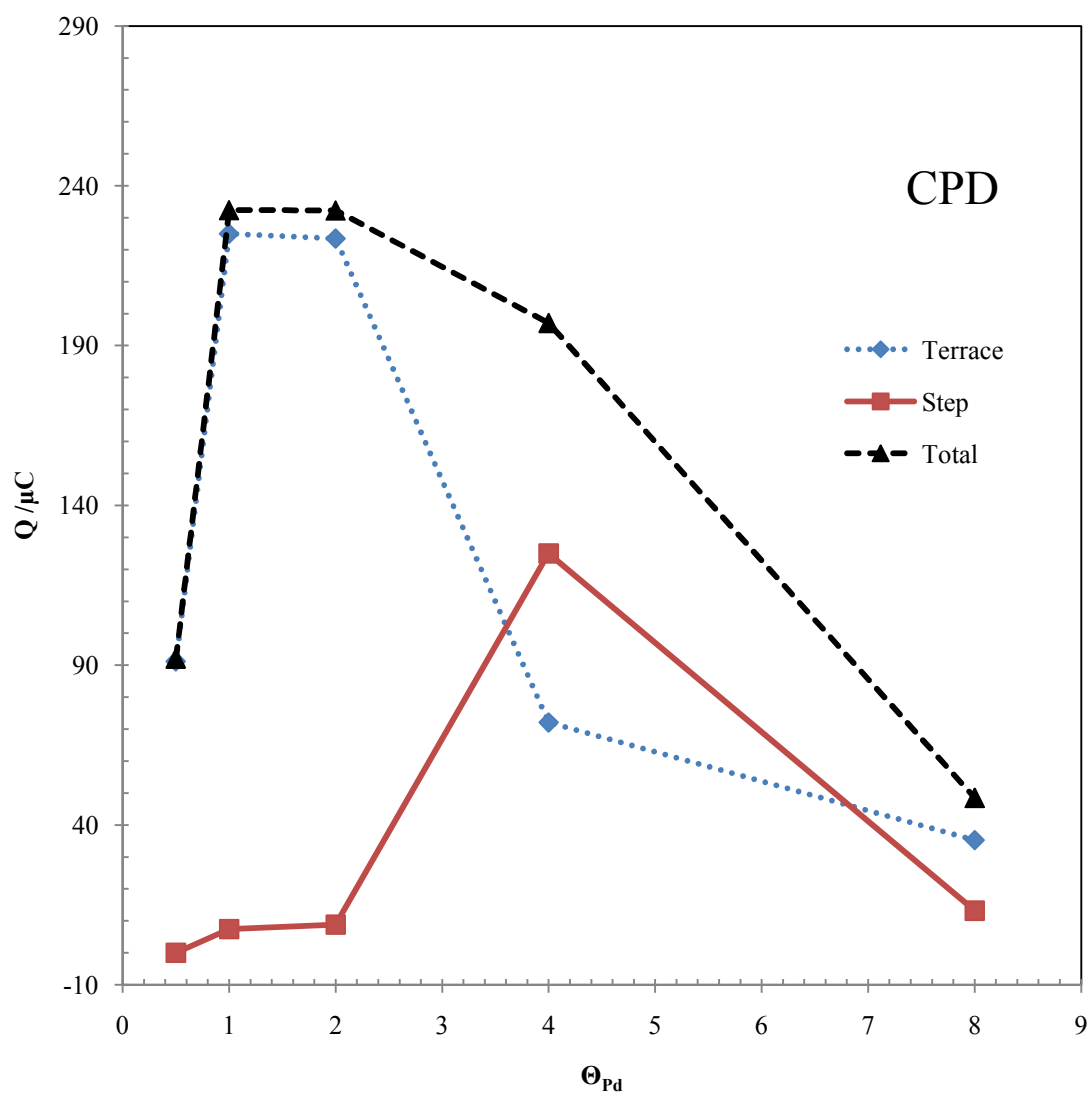
Fig. 55. Effect of Pd coverage on H_{UPD} desorption charge for CPD films.
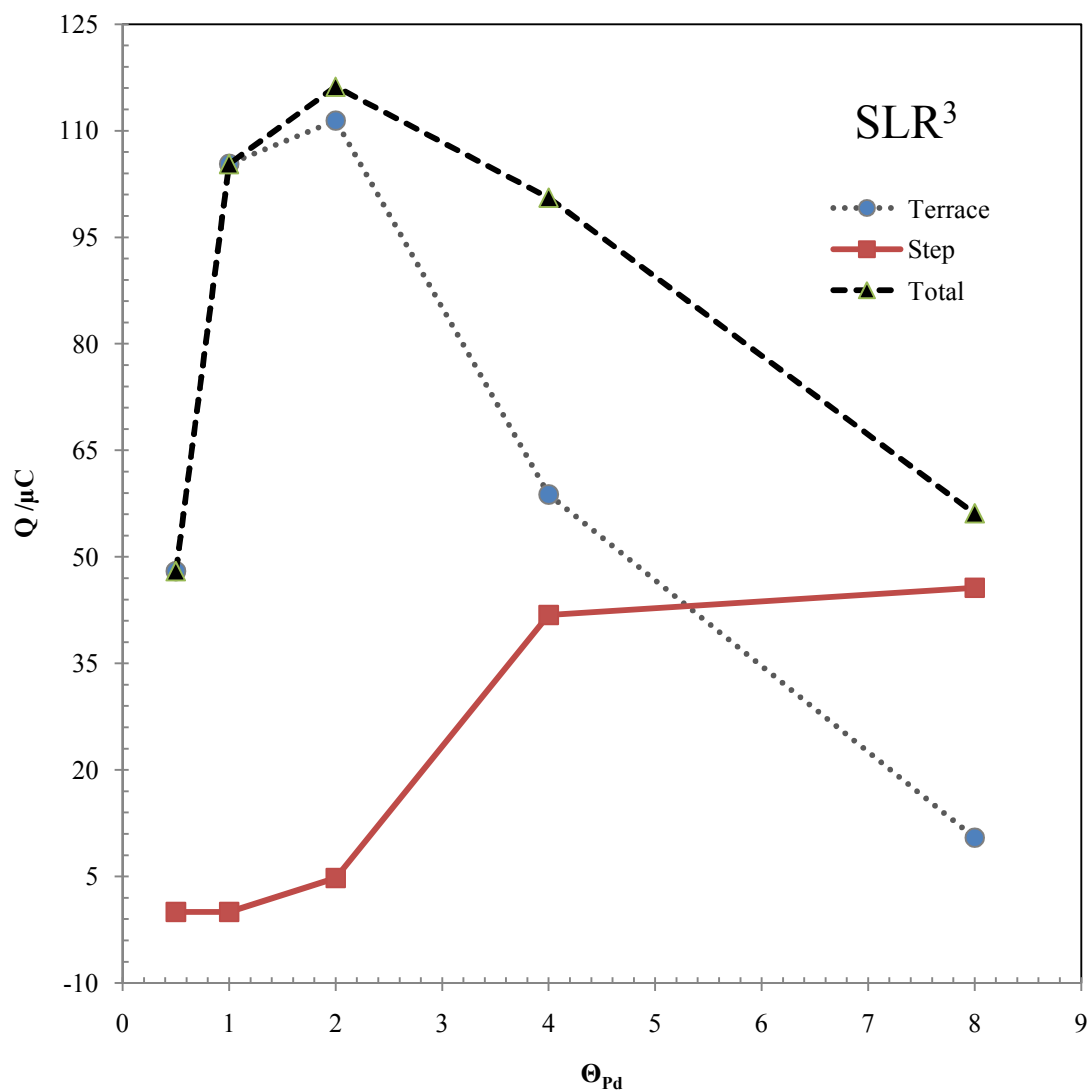
Fig. 56. Effect of Pd coverage on H_{UPD} desorption charge for SLR^3 Pd films.

Fig. 57 displays the % terrace H_{UPD} desorption charge for both films. For coverages up to 2 ML, terrace sites account for more than 90% of the total charge for CPD films. The SLR[3] films on the other hand show H_{UPD} desorption charge exclusively from terrace sites. This indicates that SLR[3] films are slightly more uniform and smoother. Earlier, the increase in contribution to H_{UPD} charge from step sites were interpreted as indication of rougher film growth specially at higher coverages [171].

Fig. 58 demonstrates the variation of full-width at half maximum (FWHM) of the HUPD desorption peaks with increasing Pd film coverage. The FWHM goes through a maximum at 1 ML, then decreases up to 4 ML, and then slowly increases up to 8 ML for terrace sites for both films. The increase in FWHM between 4 to 8 ML is more pronounced for steps sites in both films. Ideally, the decrease in FWHM of H_{UPD} peak would imply the formation of smoother and uniform films [64]. In the present case, however, this rationale might not be applicable since two competing processes (hydrogen adsorption and absorption) take place concurrently as the Pd film thickness increases.

Attard and Bannister [90] have observed only the HUPD originating from terrace sites on spontaneously deposited Pd films on Pt(111). In a separate study [64], they also investigated the electrochemical properties of the Pd films on Pt(111) prepared under UHV. In agreement with their earlier findings, only H_{UPD} from terrace sites are observed for Pd coverages below one monolayer. For thicker films, a second H_{UPD} peak (at more positive potential) was obtained. At Pd coverage of 4 ML, the H_{UPD} peak due to terrace sites disappears and the onset of bulk diffusion of hydrogen is implied by the irreversible
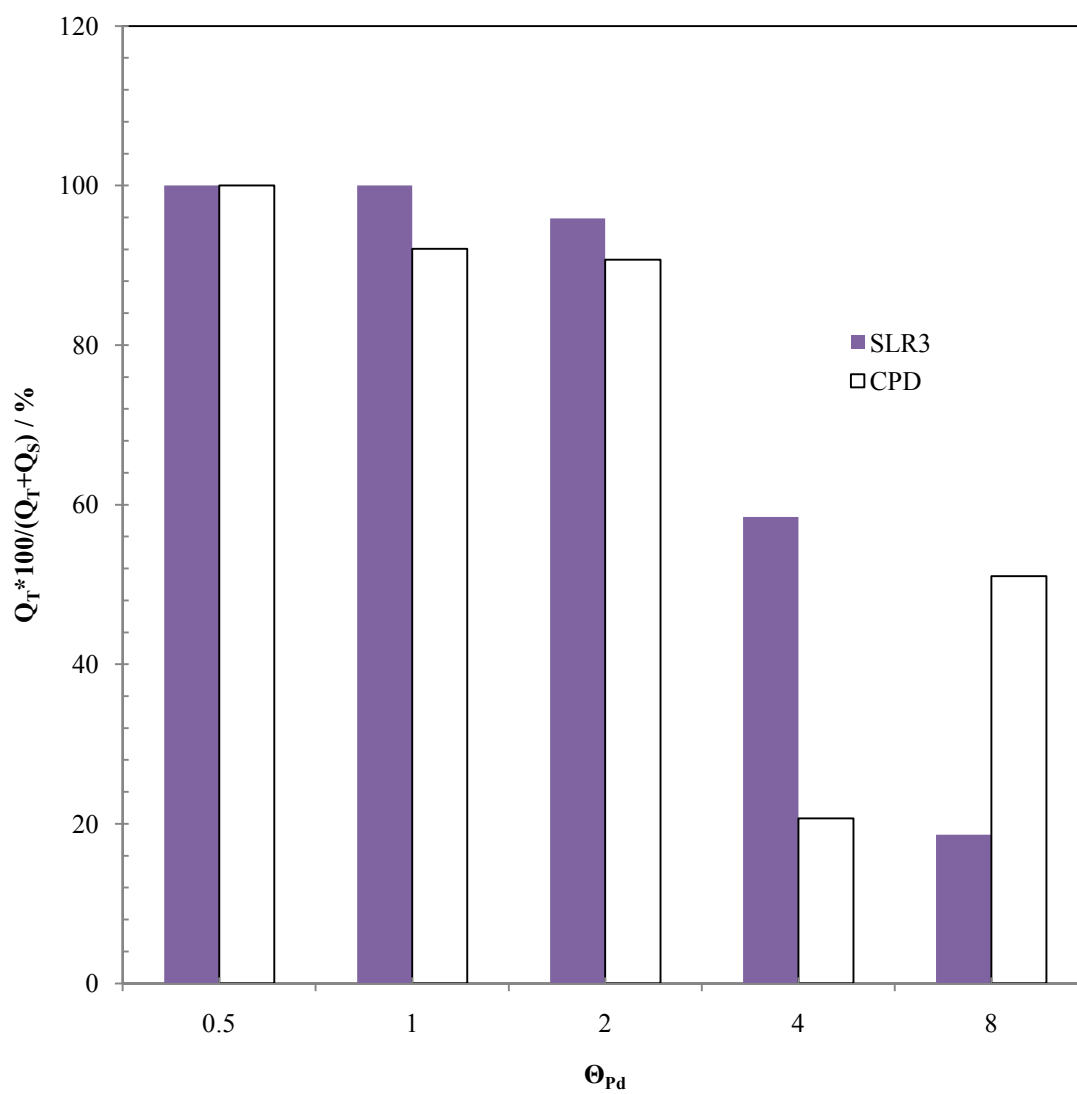
Fig. 57. Comparison of %Q_T with Pd coverage.
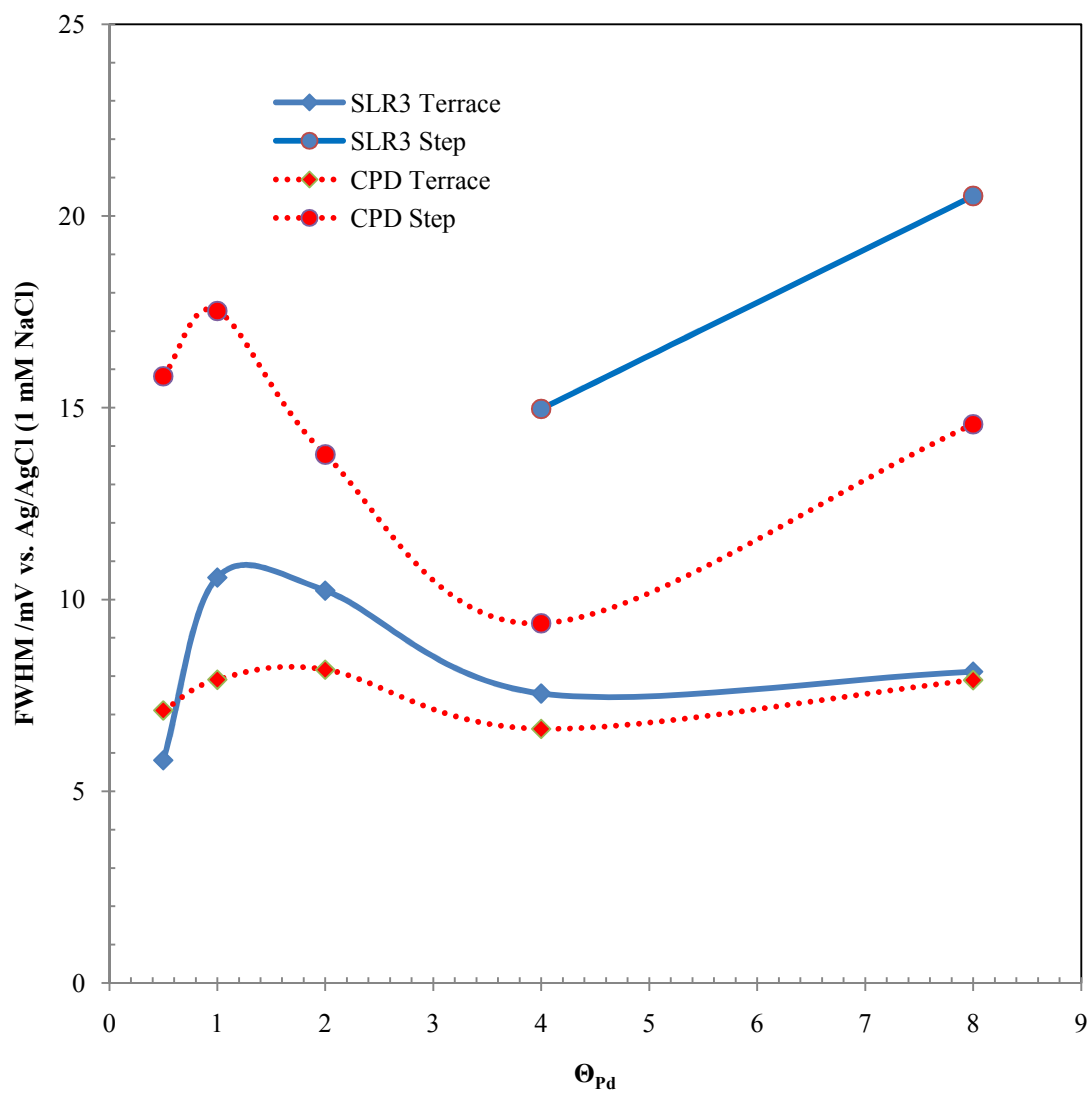
Fig. 58. FWHM of H_{UPD} desorption peaks at various Pd coverages.

peak starting at 0 V (vs. Pd/H), which is closely associated with bulk Pd. Clavilier [65] also observed the second H_{UPD} peak for Pd films synthesized by forced deposition exceeding the coverage of 1 ML. Ross and coworkers have also reported similar observations for electrodeposited Pd films on Pt(111). At $\Theta_{Pd} > 2$ ML, the step H_{UPD} peak is the dominant feature in the cyclic voltammogram, which led them to suggest much greater number of step sites compared to terrace sites [78]. The decrease of terrace hydrogen adsorption/desorption peak, however, might have been caused by hydrogen absorption.

According to Kolb and colleagues [95], the H_{UPD} peak potentials for electrodeposited Pd films on Pt(111) is independent of deposition solution while their shape and charges are. For 3 ML Pd films, the terrace peak is much smaller in chloride containing solution compared to H_{UPD} peak from step sites whereas it is absent when the coverage increases to 5 ML. In sulfate anion containing solution, the step peak is almost as large as the terrace peak. Upon increase of Pd coverage further, the step becomes predominant. It takes, however, 10 ML of Pd for complete disappearance of terrace H_{UPD} peak in sulfate ion containing solution. One important point of this study is that both H_{UPD} peaks decrease in size and become sharper with increasing Pd coverage irrespective of the anions present. We have also observed similar trend for both SLR[3] and CPD Pd films. Our findings are also in agreement with those reported by Duncan et al. [97].

In addition, *in situ* STM images reported by Kolb and coworkers [95] indicate that smoother Pd films are deposited from $[PdCl_4]^{2-}$ containing solution as compared to

those for sulfate containing solution. In the presence of chloride ions, up to 2 ML smooth Pd films grows except for a few holes. After completion of 2 ML, the third layer starts to grow in the same way. The fourth layer, however, begins to grow before completion of the third layer. Thus as the Pd film thickness increases, the number of defects is slightly increases which results in a relatively flat surface having a fractal-like shape. On the other hand, in chloride free sulfate containing solution Pd forms small 3D clusters which are one to four layers high instead of monoatomic high islands. The clusters preferentially nucleate at the defect sites (e.g., steps).

A recent IRAS and TDS on SiO_2 supported Pt nanoparticles study [223] investigated the development of terrace and step sites with the increase of particle size. The IRAS spectra show characteristic peaks high-wave number and low-wave number peaks due to CO at terrace- and step-like sites, respectively. Similarly, TDS spectra also show CO desorption peaks at 350 and 450 K from terrace- and step-like sites, respectively. It was found that as the particle size increased the number of steps sites also increased initially as indicated by gradual emergence of CO desorption peak at 450 K in the TDS spectra. When the particle diameter reached 3.3 nm a second CO desorption peak evolved at 350 K which is associated with CO desorption from the step sites. Further increase in the particle size does not increase the number of step sites appreciably while the number of terrace sites continue to grow. These experimental results were found to be consistent with the simple hard sphere model of a truncated cubooctahedron.

Following similar arguments, it is unlikely that pseudomorphic Pd films would grow rougher films at higher coverages (between 4 to 8 ML) particularly for films prepared via SLR^3. The reduction of the first H_{UPD} peaks from terrace like sites rather may be indicative transition from thin-film to bulk like property. The possible absence of hydrogen absorption (especially at lower coverages) may be due to the pinning of the first Pd adlayer to the Pt lattice, where hydrogen absorption is nonexistent. This pinned layer of Pd prevents expansion of the topmost layers to accommodate hydrogen due to high strain energy [72]. The smaller values of H_{UPD} desorption charge for SLR^3 films compared to CPD films might be due to differences in surface morphology or due to differences in sulfate or bisulfate adsorption/desorption.

A slight difference was observed between SLR^3 and CPD methods prepared Pd films in the I_{ads}-catalyzed dissolution of Pd, particularly at $\Theta_{Pd} \leq 1$. The Pd dissolution peak for SLR^3 films at such low coverages is not well-defined. More investigation is necessary to delineate the origins of these differences for these films.

Lastly, the effect of Pd coverage on Cu UPD was investigated (Fig. 59). After each irreversible deposition of Pd via SLR^3, a cyclic voltammogram was recorded in 1 mM $CuSO_4$ in 100 mM sulfuric acid. The scan was initiated at OCP towards the negative direction and was stopped at the initial potential to avoid any undue perturbation to the adlayer. It was found that initially the Cu UPD adsorption/desorption peaks were increasing with thickness for up to 4th SLR3 cycle. After the 4th cycle, the Cu UPD peaks decreased with increasing coverage. It was observed that the Cu UPD peaks shifted to more positive values with each new SLR^3 cycle. Moreover, a few additional peaks
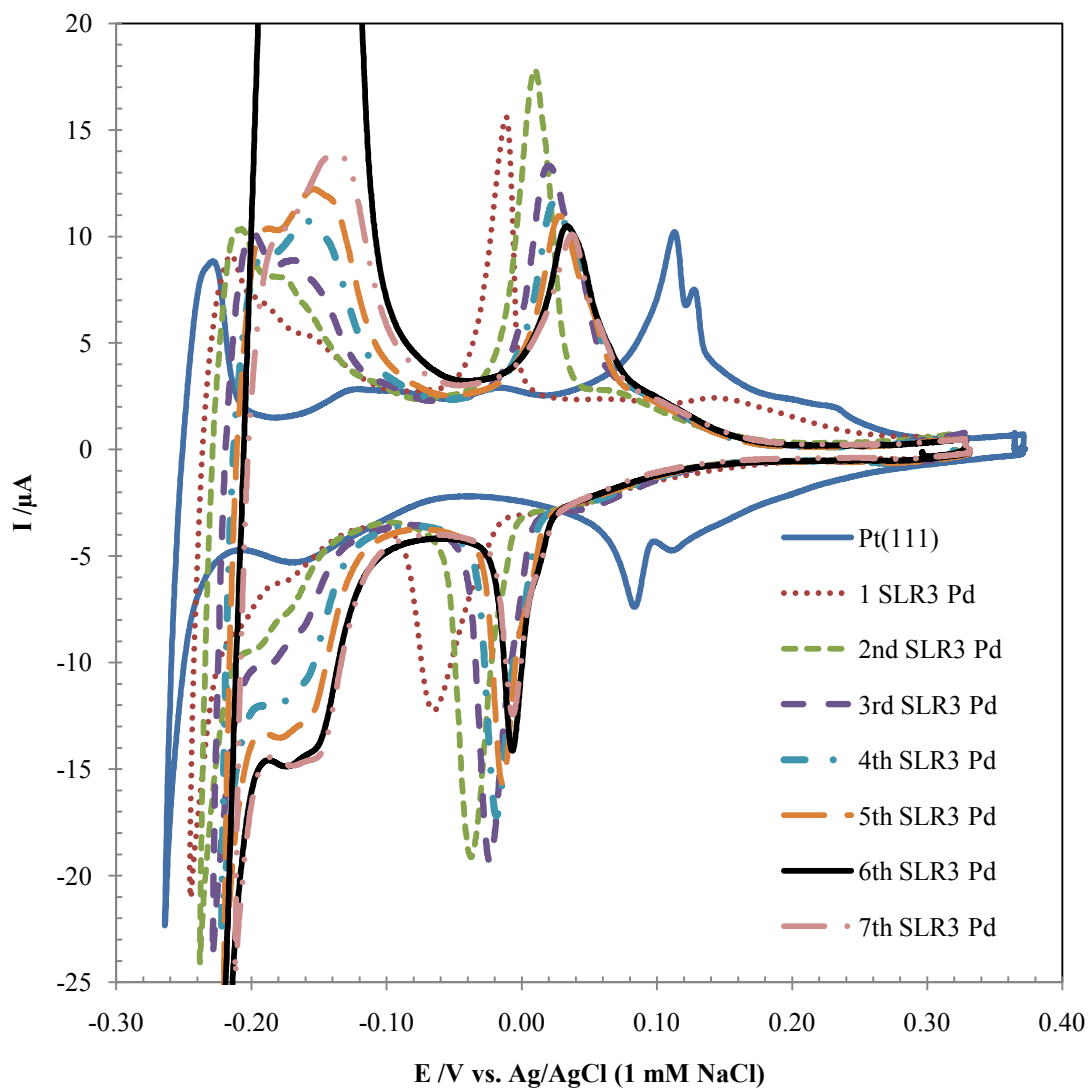
Fig. 59. CVs of SLR^3 prepared Pd in 1 mM CuSO$_4$ in 100 mM H$_2$SO$_4$ after each

deposition cycle, r = 2 mV/s.

started to form at the negative end of the main Cu UPD peak. It should be noted that only one Cu UPD peak is observed for bulk Pd(111) electrodes [200]. To rule out any possibility that scanning the electrode in between SLR[3] cycles might have disturbed the surface, the experiment was repeated. This time, CVs were recorded after the completion of 6th (ca. 4.8 ML Pd) and 7th (ca. 5.6 ML Pd) SLR[3] cycles (Fig. 60) and the same trend was observed. The Cu UPD peaks get smaller and shift towards more positive potentials. An additional CV is included in Fig. 54 for controlled-potential deposited 5.2 ML Pd films in same $CuSO_4$ solution. The shape, size, and position of Cu_{UPD} peaks for this film are comparable to those for SLR[3] films. This finding is significant that this might be a thin film property. The second implication is that Cu UPD adsorption/desorption cycles may not alter the irreversibly adsorbed Pd films on Pt. In fact, this has been confirmed by Itaya for Pt(111) surfaces [197]. Scouring of the literature as to the origin of the extra peaks, it was found that similar Cu UPD peaks were observed on Pd nanoparticles supported on glassy carbon electrodes [45]. The origin of these peaks have been found to be due to the adsorption of anions on the Cu adlayer [201].

In summation, for film coverages of $0.5 \leq \Theta_{Pd} \leq 2$, a relatively smooth Pd surface is formed which is indicative of layer-by-layer growth.

At $4 \leq \Theta_{Pd} \leq 8$, the film growth follows Stranski-Krastanov or 3D growth mode, where the first layer completely covers the substrate and the subsequent layers grow in islands. This is in agreement with the STM observations made by Hoyer and coworkers [95]. Fig. 61 displays an illustration of the formation of step sites along the edges of the Pd clusters that are expected in Stranski-Krastanov growth mode.
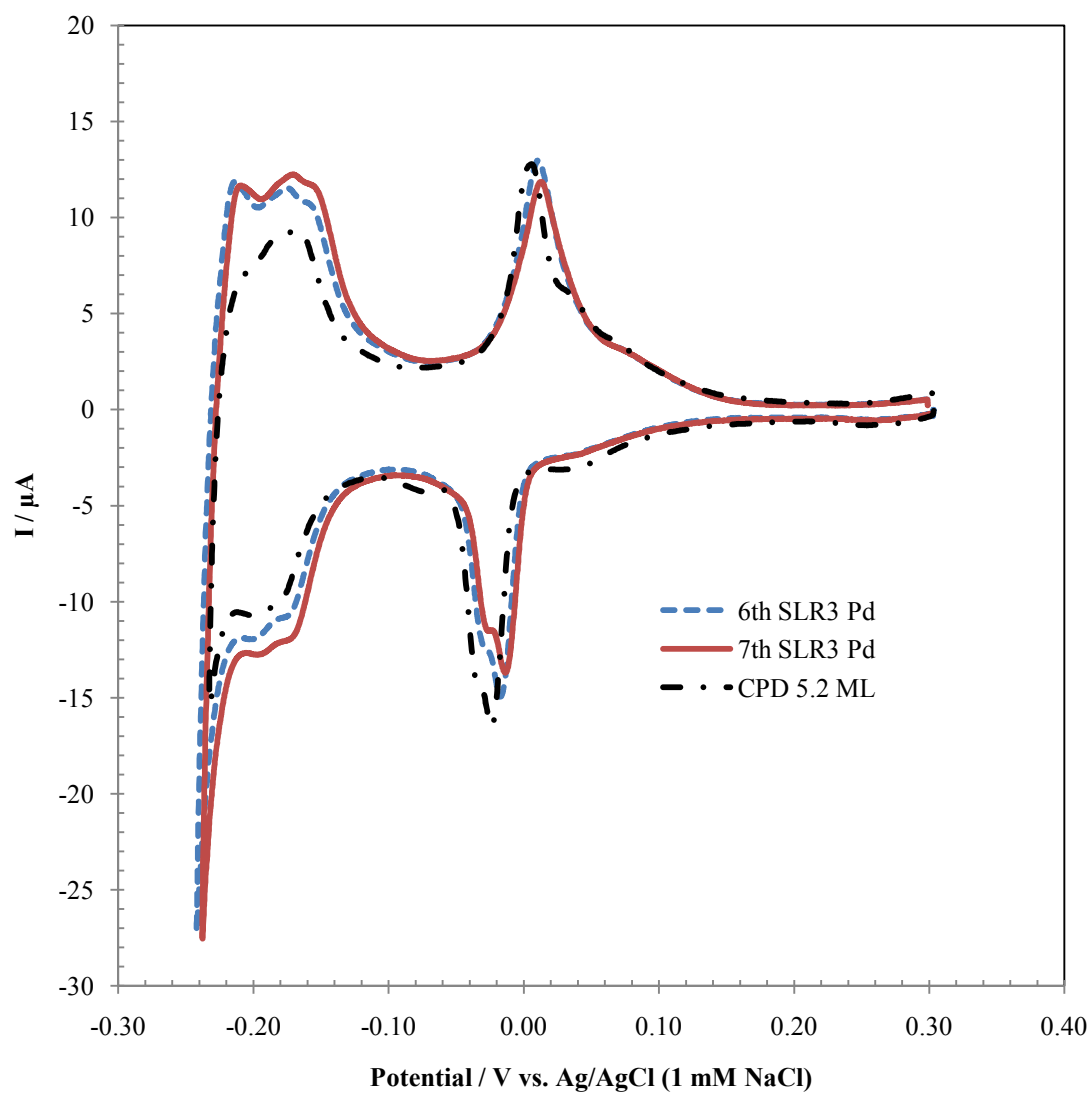
Fig. 60. CVs of SLR^3-prepared Pd films in 1 mM CuSO$_4$ in 100 mM H$_2$SO$_4$ after the completion of 6th and 7th cycle of deposition of Pd.(r = 2 mV/s).
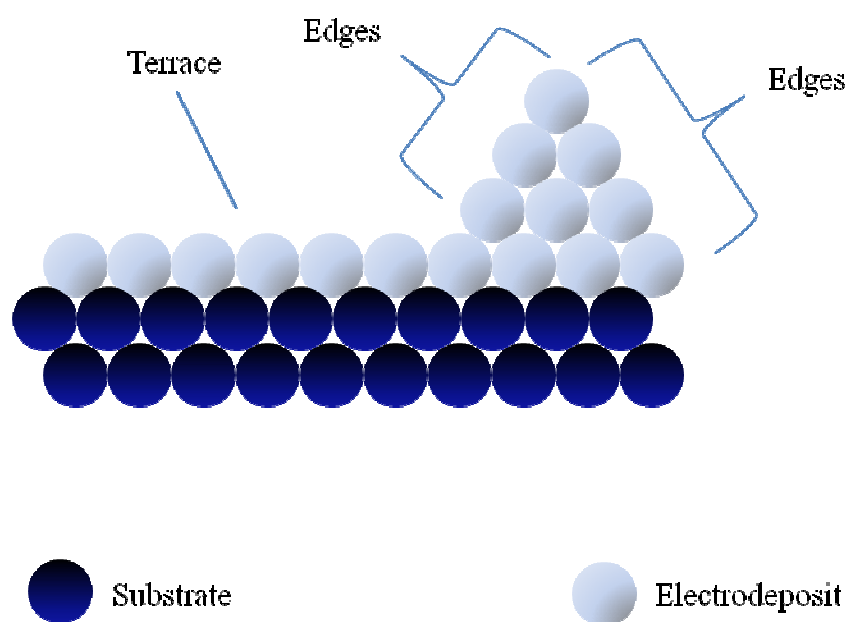
Fig. 61. An illustration of the formation of step sites along the edges of the Pd cluster.

CONCLUSIONS

Based on the observations made in this study, the following conclusions can be drawn:

1. SLR^3 appears capable to prepare atomically smooth ultrathin films on Pt(111) without any additional thermal or electrochemical annealing. For $0.5 \leq \Theta_{Pd} \leq 8$ ML coverages, both CPD and SLR^3 produce epitaxial films on Pt(111).

2. There is nearly 1:1 correlation between the cumulative charge of underpotentially deposited Cu (i.e., Pd deposition charge) and that for I_{ads}-catalyzed Pd stripping of SLR^3-prepared films on Pt(111) surfaces. However, each SLR^3 cycle produces *ca.* 0.8 ML of Cu (i.e., Pd) on Pt(111).

3. As in the case of CPD Pd films, SLR^3-prepared Pd films show H$_{UPD}$ peaks on terrace- and step-sites that are indicators of the thin film property. Even at 8 ML true bulk properties are not observed.

4. CPD films show H$_{UPD}$ peaks that are due to step-sites at $\theta_{Pd} = 0.5$ to 8. For SLR^3-prepared Pd films, the H$_{UPD}$ peaks from step sites, start to appear when $\theta_{Pd} \geq 2$ which may indicate formation of slightly smoother films prepared by SLR^3 compared to CPD films.

5. Both SLR^3 and CPD Pd films may be following the Stranski-Krastanov growth mode at higher coverages.

REFERENCES

[1] J. C. Goloboy, W. G. Klemperer, Angew. Chem. Int. Ed. Engl. 48 (2009) 3562-3564.

[2] Y. Hayashibe, PRECIOUS METALS, in: W. Paul, T. Alan, and P. Colin, (Eds.), Encyclopedia of Analytical Science, Elsevier, Oxford, 2005, pp. 277-287.

[3] J. Petró, É. Polyánszky, Z. Csürös, J. Catal. 35 (1974) 289-296.

[4] A. J. Arvia, R. C. Salvarezza, W. E. Triaca, J .New Mater. Electrochem. Syst. 7 (2004) 133-143.

[5] A. J. Appleby, Chemistry, Electrochemistry, and Electrochemical Applications | Platinum Group Metals, in: J. Garche, (Ed.), Encyclopedia of Electrochemical Power Sources, Elsevier, Amsterdam, 2009, pp. 853-875.

[6] S. B. Lyon, Corrosion of Noble Metals, in: J. A. R. Tony, (Ed.), Shreir's Corrosion, Elsevier, Oxford, 2010, pp. 2205-2223.

[7] A. Jhalani, L. D. Schmidt, Catal. Lett. 104 (2005) 103-110.

[8] J. Bodis, L. Lefferts, T. E. Mueller, R. Pestman, J. A. Lercher, Catal. Lett. 104 (2005) 23-28.

[9] A. C. Basagiannis, P. Panagiotopoulou, X. E. Verykios, Top. Catal. 51 (2008) 2-12.

[10] G. A. Somorjai, H. Frei, J. Y. Park, J. Am. Chem. Soc. 131 (2009) 16589-16605.

[11] S. D. Elliott, Langmuir 26 (2010) 9179-9182.

[12] S. Strbac, A. Wieckowski, Noble Metal Nanoislands Decoration of Au(111) and Pt(111) Single Crystal Surfaces, in: S. S. Djokic, (Ed.), Electrodeposition, vol. 48, Springer, New York, 2010, pp. 71-116.

[13]   A. J. Bard, L. R. Faulkner, Electrochemical Methods: Fundamentals and Applications, second ed., John Wiley & Sons, Inc., New York, 2001.

[14]   C. W. Jowett, B. J. Hopkins, Surf. Sci. 22 (1970) 392-410.

[15]   B. G. Baker, B. B. Johnson, G. L. C. Maire, Surf. Sci. 24 (1971) 572-586.

[16]   A. Kiejna, K. F. Wojciechowski, Prog. Surf. Sci. 11 (1981) 293-338.

[17]   G. A. Gaudin, M. J. G. Lee, Surf. Sci. 201 (1988) 540-558.

[18]   G. H. M. Gubbels, R. Metselaar, Surf. Sci. 226 (1990) 407-411.

[19]   T. J. Schmidt, V. Stamenkovic, M. Arenz, N. M. Markovic, P. N. Ross, Electrochim. Acta 47 (2002) 3765-3776.

[20]   N. M. Markovic, R. R. Adzic, B. D. Cahan, E. B. Yeager, J. Electroanal. Chem. 377 (1994) 249-259.

[21]   M. J. Llorca, J. M. Feliu, A. Aldaz, J. Clavilier, J. Electroanal. Chem. 351 (1993) 299-319.

[22]   E. Herrero, B. Alvarez, J. M. Feliu, S. Blais, Z. Radovic-Hrapovic, G. Jerkiewicz, J. Electroanal. Chem. 567 (2004) 139-149.

[23]   M. D. Maciá, J. M. Campiña, E. Herrero, J. M. Feliu, J. Electroanal. Chem. 564 (2004) 141-150.

[24]   J. S. Spendelow, A. Wieckowski, Phys. Chem. Chem. Phys. 6 (2004) 5094-5118.

[25]   M. P. Soriaga, Prog. Surf. Sci. 39 (1992) 325-443.

[26]   A. T. Hubbard, R. G. Compton, Structure of the Solid-Liquid Interface, Comprehensive Chemical Kinetics, vol. 28, Elsevier, New York, 1989, pp. 1-67.

[27]   S. Ye, T. Kondo, N. Hoshi, J. Inukai, S. Yoshimoto, M. Osawa, K. Itaya, Electrochemistry (Tokyo, Japan) 77 (2009) 2-20.

[28]   R. A. Campbell, J. A. Rodriguez, D. W. Goodman, Phys. Rev. B 46 (1992) 7077-7087.

[29]   P. A. P. Nascente, M. F. Carazzolle, A. de Siervo, S. S. Maluf, R. Landers, G. G. Kleiman, J. Mol. Catal. A: Chem. 281 (2008) 3-8.

[30]   B. R. Cooper, J. Vac. Sci. Technol. 10 (1973) 713-716.

[31]   M. Andersen, O. Lytken, J. Engbæk, G. Nielsen, N. Schumacher, M. Johansson, I. Chorkendorff, Catal. Today 100 (2005) 191-197.

[32]   F. Maroun, F. Ozanam, O. M. Magnussen, R. J. Behm, Science 293 (2001) 1811-1814.

[33]   M. Watanabe, S. Motoo, J. Electroanal. Chem. 60 (1975) 275-283.

[34]   W. F. Lin, M. S. Zei, M. Eiswirth, G. Ertl, T. Iwasita, W. Vielstich, J. Phys. Chem. B 103 (1999) 6968-6977.

[35]   G. A. Somorjai, Surf. Sci. 242 (1991) 481-488.

[36]   B. Alvarez, V. Climent, A. Rodes, J. M. Feliu, Phys. Chem. Chem. Phys. 3 (2001) 3269-3276.

[37]   M. Okada, S. Ogura, W. A. Diño, M. Wilde, K. Fukutani, T. Kasai, Appl. Catal. A: General 291 (2005) 55-61.

[38]   M. Okada, S. Ogura, W. A. Diño, M. Wilde, K. Fukutani, T. Kasai, Appl. Surf. Sci. 246 (2005) 68-71.

[39]   B. Hammer, J. K. Norskov, Nature (London) 376 (1995) 238-240.

[40]   A. Al-Akl, G. A. Attard, J Phys Chem B 101 (1997) 4597-4606.

[41]   F. Abild-Pedersen, J. Greeley, J. Nørskov, Catal. Lett. 105 (2005) 9-13.

[42]   B. Hammer, J. K. Norskov, Advances in Catalysis 45 (2000) 71-129.

[43]   A. Ruban, B. Hammer, P. Stoltze, H. L. Skriver, J. K. Nørskov, J. Mol. Catal. A: Chem. 115 (1997) 421-429.

[44]   K. Sasaki, Y. Mo, J. X. Wang, M. Balasubramanian, F. Uribe, J. McBreen, R. R. Adzic, Electrochim. Acta 48 (2003) 3841-3849.

[45]   J. Zhang, Y. Mo, M. B. Vukmirovic, R. Klie, K. Sasaki, R. R. Adzic, J. Phys. Chem. B 108 (2004) 10955-10964.

[46]   M. H. Shao, T. Huang, P. Liu, J. Zhang, K. Sasaki, M. B. Vukmirovic, R. R. Adzic, Langmuir 22 (2006) 10409-10415.

[47]   L. Piccolo, A. Piednoir, J.-C. Bertolini, Surf. Sci. 600 (2006) 4211-4215.

[48]   J. S. Spendelow, P. K. Babu, A. Wieckowski, Curr. Opin. Solid State Mater. Sci. 9 (2005) 37-48.

[49]   K. A. Friedrich, K. P. Geyzers, A. J. Dickinson, U. Stimming, J. Electroanal. Chem. 524-525 (2002) 261-272.

[50]   W. Chrzanowski, A. Wieckowski, Langmuir 14 (1998) 1967-1970.

[51]   O. A. Hazzazi, G. A. Attard, P. B. Wells, F. J. Vidal-Iglesias, M. Casadesus, J. Electroanal. Chem. 625 (2009) 123-130.

[52]   N. Fujiwara, K. A. Friedrich, U. Stimming, J. Electroanal. Chem. 472 (1999) 120-125.

[53]   G. K. H. Wiberg, K. J. J. Mayrhofer, M. Arenz, Fuel Cells 10 (2010) 575-581.

[54]   C. Paoletti, A. Cemmi, L. Giorgi, R. Giorgi, L. Pilloni, E. Serra, M. Pasquali, J. Power Sources 183 (2008) 84-91.

[55]   B. S. Mun, C. Lee, V. Stamenkovic, N. M. Markovic, J. P. N. Ross, Journal of Chemical Physics 122 (2005) 184712-184714.

[56]   J. A. Rodriguez, Surf. Sci. Rep. 24 (1996) 223-287.

[57]   G. R. Rao, Current Science 75 (1998) 901-910.

[58]   W. K. Kuhn, R. A. Campbell, D. W. Goodman, Chemical Physics of Solid Surfaces 6 (1993) 157-183.

[59]   A. M. El-Aziz, R. Hoyer, L. A. Kibler, D. M. Kolb, Electrochim. Acta 51 (2006) 2518-2522.

[60]   A. M. El-Aziz, L. A. Kibler, D. M. Kolb, Electrochem. Commun. 4 (2002) 535-539.

[61]   L. A. Kibler, A. M. El-Aziz, D. M. Kolb, J. Mol. Catal. A Chem. 199 (2003) 57-63.

[62]   R. Hoyer, L. A. Kibler, D. M. Kolb, Surf. Sci. 562 (2004) 275-283.

[63]   L. A. Kibler, M. Kleinert, R. Randler, D. M. Kolb, Surf. Sci. 443 (1999) 19-30.

[64]   G. A. Attard, R. Price, A. Alakl, Electrochim. Acta 39 (1994) 1525-1530.

[65]   J. Clavilier, M. J. Llorca, J. M. Feliu, A. Aldaz, J. Electroanal. Chem. 310 (1991) 429-435.

[66]   A. L. N. Pinheiro, M. S. Zei, M. F. Luo, G. Ertl, Surf. Sci. 600 (2006) 641-650.

[67]   A. Piednoir, M. A. Languille, L. Piccolo, A. Valcarcel, F. J. Cadete Santos. Aires, J. C. Bertolini, Catal. Lett. 114 (2007) 110-114.

[68]   L. A. Kibler, M. Kleinert, V. Lazarescu, D. M. Kolb, Surf. Sci. 498 (2002) 175-185.

[69]   L. A. Kibler, M. Kleinert, D. M. Kolb, Surf. Sci. 461 (2000) 155-167.

[70]   B. Alvarez, V. Climent, J. M. Feliu, A. Aldaz, Electrochem. Commun. 2 (2000) 427-430.

[71]   M. P. Soriaga, Y.-G. Kim, J. E. Soto, Interfacial Chemistry of Palladium Electrodes, in: A. Wieckowski, (Ed.), Interfacial Electrochemistry: Theory, Experiment, and Applications, Marcel Dekker, New York, 1999, pp. 249-267.

[72]   V. Climent, N. M. Markovic, P. N. Ross, J. Phys. Chem. B 104 (2000) 3116-3120.

[73]   C. Lebouin, Y. S. Olivier, E. Sibert, P. Millet, M. Maret, R. Faure, J. Electroanal. Chem. 626 (2009) 59-65.

[74]   J. Inukai, M. Ito, J. Electroanal. Chem. 358 (1993) 307-315.

[75]   M. Han, P. Mrozek, A. Wieckowski, Phys. Rev. B 48 (1993) 8329-8335.

[76]   M. I. Rojas, M. G. Del Popolo, E. P. M. Leiva, Langmuir 16 (2000) 9539-9546.

[77]   T. J. Schmidt, N. M. Markovic, V. Stamenkovic, P. N. Ross, G. A. Attard, D. J. Watson, Langmuir 18 (2002) 6969-6975.

[78]   M. J. Ball, C. A. Lucas, N. M. Markovic, V. Stamenkovic, P. N. Ross, Surf. Sci. 518 (2002) 201-209.

[79]   M. Arenz, V. Stamenkovic, T. J. Schmidt, K. Wandelt, P. N. Ross, N. M. Markovic, Surf. Sci. 523 (2003) 199-209.

[80]   B. Alvarez, A. Rodes, J. M. Perez, J. M. Feliu, J. Phys. Chem. B 107 (2003) 2018-2028.

[81]   M. J. Ball, C. A. Lucas, N. M. Markovic, V. Stamenkovic, P. N. Ross, Surf. Sci. 540 (2003) 295-302.

[82]   Z. Dohnalek, J. Kim, B. D. Kay, Surf. Sci. 600 (2006) 3461-3471.

[83]   K. H. Kim, J. K. Yu, H. S. Lee, J. H. Choi, S. Y. Noh, S. K. Yoon, C. S. Lee, T. S. Hwang, Y. W. Rhee, Korean J. Chem. Eng. 24 (2007) 518-521.

[84]   J. T. Zhang, M. H. Huang, H. Y. Ma, F. Tian, W. Pan, S. H. Chen, Electrochem. Commun. 9 (2007) 1298-1304.

[85]   K. Umezawa, E. Narihiro, Y. Ohta, Y. Ohira, M. Yoshimura, Nucl. Instrum. Methods Phys. Res., Sect. B 266 (2008) 1903-1907.

[86]   P. P. Wells, E. M. Crabb, C. R. King, R. Wiltshire, B. Billsborrow, D. Thompsett, A. E. Russell, Phys. Chem. Chem. Phys. 11 (2009) 5773-5781.

[87]   I. Pasti, S. Mentus, J. Alloys Compd. 497 (2010) 38-45.

[88]   J. Souza-Garcia, E. A. Ticianelli, V. Climent, J. M. Feliu, Electrochim. Acta 54 (2009) 2094-2101.

[89]   D. A. J. Rand, R. Wood, J. Electroanal. Chem. Inter. Electrochem. 44 (1973) 83-89.

[90]   G. A. Attard, A. Bannister, J. Electroanal. Chem. Interfacial Electrochem. 300 (1991) 467-485.

[91]   B. Alvarez, A. Berna, A. Rodes, J. M. Feliu, Surf. Sci. 573 (2004) 32-46.

[92]   R. Gómez, A. Rodes, J. M. Pérez, J. M. Feliu, A. Aldaz, Surf. Sci. 327 (1995) 202-215.

[93]   J. M. Feliu, B. Alvarez, V. Climent, A. Rodes, Thin Films: Prep., Charact., Appl., [Proc. Symp. Am. Chem. Soc.] (2002) 37-52.

[94]   N. M. Markovic, C. A. Lucas, V. Climent, V. Stamenkovic, P. N. Ross, Surf. Sci. 465 (2000) 103-114.

[95]   R. Hoyer, L. A. Kibler, D. M. Kolb, Electrochim. Acta 49 (2003) 63-72.

[96]   Y. S. Park, J. Baricuatro, M. Hossain, M. P. Soriaga, ECS Trans. 3 (2007) 65-103.

[97]   H. Duncan, A. Lasia, J. Electroanal. Chem. 621 (2008) 62-68.

[98]   M. H. Martin, A. Lasia, Electrochim. Acta 53 (2008) 6317-6322.

[99]   L. L. Jewell, B. H. Davis, Appl. Catal. A: General 310 (2006) 1-15.

[100]   H. Duncan, A. Lasia, Electrochim. Acta 53 (2008) 6845-6850.

[101]   H. Duncan, A. Lasia, Electrochim. Acta 52 (2007) 6195-6205.

[102]   M. Baldauf, D. M. Kolb, Electrochim. Acta 38 (1993) 2145-2153.

[103]   M. Baldauf, D. M. Kolb, J. Phys. Chem. 100 (1996) 11375-11381.

[104]   A. N. Frumkin, O. A. Petrii, Electrochim. Acta 20 (1975) 347-359.

[105]   V. Climent, N. García-Araez, E. Herrero, J. Feliu, Russ. J. Electrochem. 42 (2006) 1145-1160.

[106]   E. A. Lafferty, Ph.D. Dissertation, Texas A&M University, College Station, 1999.

[107] M. Arenz, V. Stamenkovic, T. J. Schmidt, K. Wandelt, P. N. Ross, N. M. Markovic, Surf. Sci. 506 (2002) 287-296.

[108] M. Arenz, V. Stamenkovic, T. J. Schmidt, K. Wandelt, P. N. Ross, N. M. Markovic, Surf. Sci. 523 (2003) 199-209.

[109] H. Naohara, S. Ye, K. Uosaki, J.Phys. Chem. B 102 (1998) 4366-4373.

[110] W. Kern, K. K. Schuegraf, Deposition Technologies and Applications: Introduction and Overview, in: K. Seshan, (Ed.), Handbook of Thin-Film Deposition Processes and Techniques - Principles, Methods, Equipment and Applications, William Andrew Publishing/Noyes, Norwich, 2002, pp. 11-43.

[111] G. A. Somorjai, Y. Li, Introduction to Surface Chemistry and Catalysis, Second ed., Wiley, Hoboken, 2010.

[112] R. Vasilic, N. Dimitrov, Electrochem. Solid State Lett. 8 (2005) C173-C176.

[113] Y.-G. Kim, J. Y. Kim, D. Vairavapandian, J. L. Stickney, J. Phys. Chem. B 110 (2006) 17998-18006.

[114] E. Herrero, L. J. Buller, H. D. Abruña, Chem. Rev. 101 (2001) 1897-1930.

[115] E. Lamy-Pitara, J. Barbier, Applied Catalysis A: General 149 (1997) 49-87.

[116] H. Gerischer, D. M. Kolb, M. Pazasnyski, Surf. Sci. 43 (1974) 662-666.

[117] D. M. Kolb, H. Gerischer, Surf. Sci. 51 (1975) 323-327.

[118] D. M. Kolb, M. Przasnyski, H. Gerischer, J. Electroanal. Chem. Interfacial Electrochem. 54 (1974) 25-38.

[119] E. Leiva, Electrochim. Acta 41 (1996) 2185-2206.

[120] G. Kokkinidis, J. Electroanal. Chem. Interfacial Electrochem. 201 (1986) 217-236.

[121] A. Aramata, Underpotential Deposition on Single-Crystal Metals, in: J. O. M. Bockris, (Ed.), Mod. Aspects Electrochem., vol. 31, Plenum Press, New York, 1997.

[122] J.-W. Lee, S.-I. Pyun, Journal of the Korean Electrochemical Society 4 (2001) 176-181.

[123] J. Clavilier, D. Armand, J. Electroanal. Chem. 199 (1986) 187-200.

[124] S. Trasatti, Z. Phys. Chem. (Frankfurt am Main) 98 (1975) 75-94.

[125] C. Sánchez, E. Leiva, J. Electroanal. Chem. 458 (1998) 183-189.

[126] M. F. Mrozek, Y. Xie, M. J. Weaver, Anal. Chem. 73 (2001) 5953-5960.

[127] E. Bauer, J. H. van der Merwe, Phys. Rev. B 33 (1986) 3657.

[128] K. Sieradzki, S. R. Brankovic, N. Dimitrov, Science 284 (1999) 138-141.

[129] S. R. Brankovic, N. Dimitrov, K. Sieradzki, Electrochem. Solid State Lett. 2 (1999) 443-445.

[130] L. T. Viyannalage, Ph.D. Dissertation, State University of New York, Binghamton, 2008.

[131] S. Hwang, I. Oh, J. Kwak, J. Am. Chem. Soc. 123 (2001) 7176-7177.

[132] S. R. Brankovic, J. X. Wang, R. R. Adzic, Surf. Sci. 474 (2001) L173-L179.

[133] K. Sasaki, J. X. Wang, H. Naohara, N. Marinkovic, K. More, H. Inada, R. R. Adzic, Electrochim. Acta 55 (2010) 2645-2652.

[134] Y. Du, K. Lv, B. Su, N. Zhang, C. Wang, J. Appl. Electrochem. 39 (2009) 2409-2414.

[135] J. B. Abreu, R. J. Barriga, W. Temesghen, J. A. Schimpf, M. P. Soriaga, J. Electroanal. Chem. 381 (1995) 239-241.

[136] J. A. Schimpf, A. Carrasquillo, Jr., M. P. Soriaga, Electrochim. Acta 40 (1995) 1203-1205.

[137] M. P. Soriaga, J. A. Schimpf, A. Carrasquillo, Jr., J. B. Abreu, W. Temesghen, R. J. Barriga, J. J. Jeng, K. Sashikata, K. Itaya, Surf. Sci. 335 (1995) 273-280.

[138] Y.-G. Kim, J. Y. Kim, C. Thambidurai, J. L. Stickney, Langmuir 23 (2007) 2539-2545.

[139] Y. Bi, G. Lu, Chem. Commun. (Cambridge, United Kingdom) (2008) 6402-6404.

[140] N. Dimitrov, R. Vasilic, N. Vasiljevic, Electrochem. Solid State Lett. 10 (2007) D79-D83.

[141] M. Huang, Y. Jin, H. Jiang, X. Sun, H. Chen, B. Liu, E. Wang, S. Dong, J. Phys. Chem. B 109 (2005) 15264-15271.

[142] Y. Jin, Y. Shen, S. Dong, J. Phys. Chem. B 108 (2004) 8142-8147.

[143] J. Y. Kim, Y. G. Kim, J. L. Stickney, ECS Trans. 2 (2007) 329-335.

[144] J. Y. Kim, Y.-G. Kim, J. L. Stickney, ECS Trans. 1 (2006) 41-48.

[145] J. Y. Kim, Y.-G. Kim, J. L. Stickney, J. Electrochem. Soc. 154 (2007) D260-D266.

[146] J. Y. Kim, Y.-G. Kim, J. L. Stickney, J. Electroanal. Chem. 621 (2008) 205-213.

[147] W. Li, H. Ma, J. Zhang, X. Liu, X. Feng, J. Phys. Chem. C 113 (2009) 1738-1745.

[148] P. Liu, X. Ge, R. Wang, H. Ma, Y. Ding, Langmuir 25 (2009) 561-567.

[149] Y.-K. Park, S.-H. Yoo, S. Park, Langmuir 24 (2008) 4370-4375.

[150] C. Thambidurai, N. Jayaraju, Y. G. Kim, J. L. Stickney, ECS Trans. 11 (2007) 103-112.

[151] C. Thambidurai, Y.-G. Kim, J. L. Stickney, Electrochim. Acta 53 (2008) 6157-6164.

[152] D. Vairavapandian, J. L. Stickney, ECS Trans. 3 (2007) 329-336.

[153] V. Venkatasamy, N. Jayaraju, S. M. Cox, C. Thambidurai, J. L. Stickney, J. Electrochem. Soc. 154 (2007) H720-H725.

[154] L. T. Viyannalage, R. Vasilic, N. Dimitrov, ECS Trans. 2 (2007) 307-314.

[155] L. T. Viyannalage, R. Vasilic, N. Dimitrov, J. Phys. Chem. C 111 (2007) 4036-4041.

[156] J. Zhai, M. Huang, S. Dong, Electroanalysis 19 (2007) 506-509.

[157] C.-C. Qiu, J.-T. Zhang, H.-Y. Ma, Solid State Sciences 12 (2010) 822-828.

[158] M. Van Brussel, G. Kokkinidis, I. Vandendael, C. Buess-Herman, Electrochem. Commun. 4 (2002) 808-813.

[159] R. E. Rettew, J. W. Guthrie, F. M. Alamgir, J. Electrochem. Soc. 156 (2009) D513-D516.

[160] M. B. Vukmirovic, J. Zhang, K. Sasaki, A. U. Nilekar, F. Uribe, M. Mavrikakis, R. R. Adzic, Electrochim. Acta 52 (2007) 2257-2263.

[161] M. B. Vukmirovic, J. Zhang, K. Sasaki, Y. Xu, A. U. Nilekar, M. Mavrikakis, F. Uribe, R. R. Adzic, Proc. - Electrochem. Soc. 2005-11 (2006) 188-199.

[162] D. K. Gebregziabiher, Y.-G. Kim, C. Thambidurai, V. Ivanova, P.-H. Haumesser, J. L. Stickney, Journal of Crystal Growth 312 (2010) 1271-1276.

[163] R. E. Rettew, J. W. Guthrie, C. Jaye, D. Fischer, F. Alamgir, ECS Trans. 19 (2009) 97-106.

[164] J. X. Wang, H. Inada, L. Wu, Y. Zhu, Y. Choi, P. Liu, W.-P. Zhou, R. R. Adzic, J. Am. Chem. Soc. 131 (2009) 17298-17302.

[165] T. Ghosh, M. B. Vukmirovic, F. J. DiSalvo, R. R. Adzic, J. Am. Chem. Soc. 132 (2009) 906-907.

[166] W.-P. Zhou, K. Sasaki, D. Su, Y. Zhu, J. X. Wang, R. R. Adzic, J. Phys. Chem. C 114 (2010) 8950-8957.

[167] K. Gong, D. Su, R. R. Adzic, J. Am. Chem. Soc. 132 (2010) 14364-14366.

[168] F. H. B. Lima, J. Zhang, M. H. Shao, K. Sasaki, M. B. Vukmirovic, E. A. Ticianelli, R. R. Adzic, J. Solid State Electrochem. 12 (2008) 399-407.

[169] Y.-S. Park, J. H. Baricuatro, M. A. Hossain, M. P. Soriaga, ECS Trans. 19 (2009) 25-42.

[170] J. H. Baricuatro, M. A. Hossain, Y.-S. Park, M. P. Soriaga, Electrocatalysis 1 (2010) 28-33.

[171] Y. S. Park, Ph.D. Dissertation, Texas A&M University, College Station, 2005.

[172]   A. T. Hubbard, J. L. Stickney, M. P. Soriaga, V. K. F. Chia, S. D. Rosasco, B. C. Schardt, T. Solomun, D. Song, J. H. White, A. Wieckowski, J. Electroanal. Chem. Interfacial Electrochem. 168 (1984) 43-66.

[173]   M. P. Soriaga, ACS Symp. Ser. 378 (1988) 1-7.

[174]   A. Wieckowski, S. D. Rosasco, G. N. Salaita, A. Hubbard, B. E. Bent, F. Zaera, G. A. Somorjai, J. Am. Chem. Soc. 107 (1985) 5910-5920.

[175]   G. Jerkiewicz, ACS Symp. Ser. 656 (1997) 1-12.

[176]   R. Alkire, M. Verhoff, Electrochim. Acta 43 (1998) 2733-2741.

[177]   R. Cabrera-Sierra, M. Miranda-Hernandez, E. Sosa, T. Oropeza, I. Gonzalez, Corros. Sci. 43 (2001) 2305-2324.

[178]   Y.-H. Fang, Z.-P. Liu, J. Phys. Chem. C 114 (2010) 4057-4062.

[179]   E. Gileadi, E. Kirowa-Eisner, Corros. Sci. 47 (2005) 3068-3085.

[180]   G. Horanyi, Interface Science and Technology 3 (2004) 39-97.

[181]   J. Kelber, G. Seshadri, T.-C. Lin, Official Proceedings - International Water Conference 57th (1996) 324-327.

[182]   R. D. Leggett, H. W. Paxton, Corros. Sci. 2 (1962) 217-223.

[183]   W. J. Lorenz, G. Staikov, Proceedings - Electrochem. Soc. 98-17 (1999) 303-318.

[184]   J. V. Macpherson, P. R. Unwin, Scanning Electrochemical Microscopy (2001) 521-592.

[185] S. Ningshen, U. K. Mudali, R. K. Dayal, British Corrosion Journal 36 (2001) 36-41.

[186] O. Teschke, J. Electrochem. Soc. 134 (1987) 1865-1866.

[187] I. T. Vargas, M. A. Alsina, P. A. Pasten, G. E. Pizarro, Corros. Sci. 51 (2009) 1030-1037.

[188] O. A. Sadik, S. K. Mwilu, A. Aluoch, Electrochim. Acta 55 (2010) 4287-4295.

[189] O. A. Sadik, A. O. Aluoch, A. Zhou, Biosens. Bioelectron. 24 (2009) 2749-2765.

[190] A. T. Hubbard, V. K. F. Chia, D. G. Frank, J. Y. Katekaru, S. D. Rosasco, G. N. Salaita, B. C. Schardt, D. Song, M. P. Soriaga, et al., New Directions in Chemical Analysis: Proceedings of the Third Symposium of the Industry-University Cooperative Chemisty Program of the Department of Chemistry, Texas A&M University, 1985, pp. 135-160.

[191] F. Reniers, Journal of Physics D: Applied Physics 35 (2002) R169-R188.

[192] G. A. Somorjai, J. Y. Park, Surf. Sci. 603 (2009) 1293-1300.

[193] G. A. Somorjai, Chemistry in Two Dimensions: Surfaces, Cornell University Press, Ithaca, 1981.

[194] D. Briggs, M. P. Seah, Eds., Practical Surface Analysis by Auger and X-ray Photoelectron Spectroscopy, John Wiley & Sons, New York, 1983.

[195] B. Schardt, R. Thiehsen, Computation LEED patterns, Electrochemical Surface Science Laboratory, Department of Chemistry, Texas A&M University, College Station, TX.

[196] E. A. Wood, J. Appl. Phys. 35 (1964).

[197]   T. Abe, G. M. Swain, K. Sashikata, K. Itaya, J. Electroanal. Chem. 382 (1995) 73-83.

[198]   J. Clavilier, J. Electroanal. Chem. 107 (1980) 211-216.

[199]   A. T. Hubbard, R. M. Ishikawa, J. Katekaru, J. Electroanal. Chem. 86 (1978) 271-288.

[200]   M. Nakamura, Y. Sakurai, M. Ito, J. Electroanal. Chem. 563 (2004) 63-69.

[201]   R. Gomez, J. M. Feliu, H. D. Abruna, J. Phys. Chem. 98 (1994) 5514-5521.

[202]   Z.-L. Wu, Z.-H. Zang, S.-L. Yau, Langmuir 16 (2000) 3522-3528.

[203]   A. Al-Akl, G. A. Attard, J. Phys. Chem. B 101 (1997) 4597-4606.

[204]   H. Ogasawara, J. Inukai, M. Ito, Surf. Sci. 311 (1994) L665-L670.

[205]   N. M. Markovic, H. A. Gasteiger, P. N. Ross, Jr., Langmuir 11 (1995) 4098-4108.

[206]   K. Sashikata, N. Furuya, K. Itaya, J. Electroanal. Chem. 316 (1991) 361-368.

[207]   Y. Shingaya, H. Matsumoto, H. Ogasawara, M. Ito, Surf. Sci. 335 (1995) 23-31.

[208]   G. M. Berry, J. R. McBride, J. A. Schimpf, M. P. Soriaga, J. Electroanal. Chem. 353 (1993) 281-287.

[209]   J. R. McBride, J. A. Schimpf, M. P. Soriaga, J. Am. Chem. Soc. 114 (1992) 10950-10952.

[210]   J. R. McBride, J. A. Schimpf, M. P. Soriaga, J. Electroanal. Chem. 350 (1993) 317-320.

[211] J. A. Schimpf, J. B. Abreu, A. Carrasquillo, M. P. Soriaga, Surf. Sci. 314 (1994) L909-L912.

[212] J. A. Schimpf, J. B. Abreu, M. P. Soriaga, Langmuir 9 (1993) 3331-3333.

[213] J. A. Schimpf, J. B. Abreu, M. P. Soriaga, Electrochim. Acta 39 (1994) 2445-2448.

[214] J. A. Schimpf, J. B. Abreu, M. P. Soriaga, J. Electroanal. Chem. 364 (1994) 247-249.

[215] J. A. Schimpf, J. B. Abreu, M. P. Soriaga, K. Sashikata, K. Itaya, Proceedings - Electrochem. Soc. 96-8 (1996) 180-188.

[216] J. A. Schimpf, J. R. McBride, M. P. Soriaga, J. Phys. Chem. 97 (1993) 10518-10520.

[217] E. A. Lafferty, Y.-G. Kim, M. P. Soriaga, Electrochim. Acta 44 (1998) 1031-1036.

[218] L. E. Davis, N. C. MacDonald, P. W. Palmberg, G. E. Riach, R. E. Weber, Handbook of Auger Electron Spectroscopy, Second ed., Physical Electronics Division, Perkin-Elmer Corp., Eden Prairie, 1978.

[219] T. E. Felter, A. T. Hubbard, J. Electroanal. Chem. 100 (1979) 473-491.

[220] M. Wasberg, L. Palaikis, S. Wallen, M. Kamrath, A. Wieckowski, J. Electroanal. Chem. 256 (1988) 51-63.

[221] J. Okada, J. Inukai, K. Itaya, Phys.Chem. Chem. Phys. 3 (2001) 3297-3302.

[222] R. Vasilic, L. T. Viyannalage, N. Dimitrov, J. Electrochem. Soc. 153 (2006) C648-C655.

[223]   M. J. Lundwall, S. M. McClure, D. W. Goodman, J.Phys. Chem. C 114 (2010) 7904-7912.

VITA

Name: Mohammad Akhtar Hossain

Address: Department of Chemistry, Texas A&M University
                 3255 TAMU
                 College Station, TX 77842-3255

Email Address: mohammad.a.hossain@gmail.com

Education: B.S., Chemistry, University of Dhaka, Dhaka, Bangladesh, 1997
                 M.S., Chemistry, University of Dhaka, Dhaka, Bangladesh, 1999
                 M.S., Chemistry, Lamar University, Beaumont, Texas, 2002